# SYNTHESIS AND EXPLORATIONS OF INDENOFLUORENES AND RELATED MOLECULES

by

BRADLEY D. ROSE

A DISSERTATION

Presented to the Department of Chemistry and Biochemistry
and the Graduate School of the University of Oregon
in partial fulfillment of the requirements
for the degree of
Doctor of Philosophy

June 2014

DISSERTATION APPROVAL PAGE

Student: Bradley D. Rose

Title: Synthesis and Explorations of Indenofluorenes and Related Molecules

This dissertation has been accepted and approved in partial fulfillment of the requirements for the Doctor of Philosophy degree in the Department of Chemistry and Biochemistry by:

| | |
|---|---|
| Michael D. Pluth | Chairperson |
| Michael M. Haley | Advisor |
| Darren W. Johnson | Core Member |
| John Halliwill | Institutional Representative |

and

| | |
|---|---|
| Kimberly Andrews Espy | Vice President for Research and Innovation;<br>Dean of the Graduate School |

Original approval signatures are on file with the University of Oregon Graduate School.

Degree awarded June 2014

DISSERTATION ABSTRACT

Bradley D. Rose

Doctor of Philosophy

Department of Chemistry and Biochemistry

June 2014

Title: Synthesis and Explorations of Indenofluorenes and Related Molecules

Small perturbations upon the bonding of polycyclic conjugated hydrocarbons (PCH) lead to drastic changes of the properties. Despite being extensively studied for decades, there are numerous variants that remain unknown. Many PCHs are of interest for application in organic electronics; namely organic photovoltaics, organic field effect transistors and non-linear optics. Although many properties of these compounds can routinely be calculated to within desired accuracy, their morphology in the solid state remains in the experimentalists' realm. The solid state morphology of these compounds dictates how easily charge moves, a very important parameter for devices. Organic compounds can range from insulators to conductors, and making organic compounds that are semiconductors is a difficult task. This dissertation covers my progress in research in the synthesis and calculations of some of new PCHs.

Chapter I serves as an overview of the progress in our laboratory working with indenofluorenes and structurally related motifs. Chapter II covers the first report of a well characterized atmospherically stable indeno[1,2-*b*]fluorene which was the groundwork for all further research. Chapter III discloses the synthetic advances that have been made in regards to the indeno[1,2-*b*]fluorene diones and a number of derivatives synthesized. Chapter IV encompasses fundamental studies of the reduced states of the indeno[1,2-

*b*]fluorene scaffold. Chapter V details the observations of the photo excited state of indenofluorene and related molecules, providing a rationale why these are non-emissive molecules. Chapter VI discusses the synthesis and electronic properties of the expanded indenofluorene scaffold, fluoreno[4,3-*c*]fluorene.

This dissertation includes previously published and unpublished co-authored material.

CURRICULUM VITAE

NAME OF AUTHOR: Bradley D. Rose

GRADUATE AND UNDERGRADUATE SCHOOLS ATTENDED:

University of Oregon, Eugene
Illinois State University, Normal
Illinois Central College, East Peoria

DEGREES AWARDED:

Doctor of Philosophy, Chemistry, 2014, University of Oregon
Bachelor of Science, Chemistry, 2009, Illinois State University
Associate of Arts, Chemistry, 2009, Illinois Central College

AREAS OF SPECIAL INTEREST:

Physical Organic Chemistry
Computational Chemistry

GRANTS, AWARDS, AND HONORS:

American Chemical Society Division of Organic Chemistry Fellowship, 2012-2013

National Science Foundation Graduate STEM Fellow in K-12 Education, University of Oregon, 2011 – 2012 and 2013 - 2014

Henry V. Howe Scholarship, University of Oregon, 2013-2014

Science Literacy Program Fellow, University of Oregon, Spring 2011

Graduate Teaching Fellow, University of Oregon, 2009 - 2010

PUBLICATIONS:

"Experimental and Computational Studies of the Neutral and Reduced States of Indeno[1,2-*b*]fluorene," B. D. Rose, N. J. Sumner, A. S. Filatov, S. J. Peters, L. N. Zakharov, M. A. Petrukhina, M. M. Haley, *Journal of the American Chemical Society* **2014**, Accepted.

"6,12-Bis[(tricyclohexylsilyl)ethynyl]indeno[1,2-*b*]fluorene," B. D. Rose, L. N. Zakharov, M. M. Haley, *Acta Crystallographica Section E* **2013**, *69*, o890. doi: 10.1107/S160053681301218X.

"Indeno[2,1-*c*]fluorene: A New Electron-Accepting Scaffold for Organic Electronics," A. G. Fix, P. E. Deal, C. L. Vonnegut, B. D. Rose, L. N. Zakharov, M. M. Haley, *Organic Letters* **2013**, *15*, 1362–1365. doi: 10.1021/ol400318z.

"Formation of the Donor-Acceptor Charge Transfer Exciton and its Contribution to Charge Photogeneration and Recombination in Small-Molecule Bulk Heterojunctions," M. J. Kendrick, A. Neunzert, M. M. Payne, B. Purushothaman, B. D. Rose, J. E. Anthony, M. M. Haley, O. Ostroverkhova, *Journal of Physical Chemistry C*, **2012**, *116*, 18108–18116. doi: 10.1021/jp305913s.

"6,12-Diarylindeno[1,2-*b*]fluorenes: Syntheses, Photophysics, and Ambipolar OFETs," D. T. Chase, A. G. Fix, S. J. Kang, B. D. Rose, C. D. Weber, Y. Zhong, L. N. Zakharov, M. C. Lonergan, C. Nuckolls, M. M. Haley, *Journal of the American Chemical Society* **2012**, *134*, 10349–10352. doi: 10.1021/ja303402p.

"Fluoreno[4,3-*c*]fluorene: A Closed-Shell, Fully Conjugated Hydrocarbon", B. D. Rose, C. L. Vonnegut, L. N. Zakharov, M. M. Haley, *Organic Letters* **2012**, *14*, 2426–2429. doi: 10.1021/ol300942z.

"Electron-Accepting 6,12-Diethynylindeno[1,2-*b*]fluorenes: Synthesis, Crystal Structures, and Photophysical Properties," D. T. Chase, A. G. Fix, B. D. Rose, C. D. Weber, S. Nobusue, C. E. Stockwell, L. N. Zakharov, M. C. Lonergan, M. M. Haley, *Angewandte Chemie International Edition* **2011**, *50*, 11103–11106. doi: 10.1002/anie.201104797.

"Synthesis, Crystal Structures, and Photophysical Properties of Electron-Accepting Diethynylindenofluorenediones," B. D. Rose, D. T. Chase, C. D. Weber, L. N. Zakharov, M. C. Lonergan, M. M. Haley, *Organic Letters* **2011**, *13*, 2106–2109. doi: 10.1021/ol200525g.

"Indeno[1,2-*b*]fluorenes: Fully Conjugated Antiaromatic Analogues of Acenes," D. T. Chase, B. D. Rose, S. P. McClintock, L. N. Zakharov, M. M. Haley, *Angewandte Chemie International Edition* **2011**, *50*, 1127–1130. doi: 10.1002/anie.201006312.

"Reduction of an Hexamethylphosphoramide Degradation Product: A Diazabutadiene," B. D. Rose, S. J. Peters, R. C. Reiter, C. D. Stevenson, *Organic Letters* **2009**, *11*, 4564-4567. doi: 10.1021/ol901798s.

"The Isomers of [12]Annulyne and their Reactive Relationships to Heptalene and Biphenyl," B. D. Rose, S. J. Peters, R. C. Reiter and C. D. Stevenson, *Angewandte Chemie International Edition*, **2008**, *47*, 8842–8846. doi: 10.1002/anie.200803863.

ACKNOWLEDGMENTS

I wish to thank Michael Haley and the rest of my committee for assistance in preparing this manuscript. This research was supported by the National Science Foundation through research grants (CHE-1013032, CHE-1301485). I was supported by an American Chemical Society Division of Organic Chemistry Graduate Fellowship and a National Science Foundation STEM Fellowship in K-12 Education.

TABLE OF CONTENTS

LIST OF FIGURES

Figure Page



CHAPTER VI

LIST OF TABLES

Table Page

CHAPTER VI

LIST OF SCHEMES

# CHAPTER I

# EXPLORATIONS OF INDENOFLUORENES

This chapter was co-authored with Michael M. Haley who provided editorial and content advice. It is in preparation for publication in *Accounts of Chemical Research*.

## Conspectus

Small highly conjugated hydrocarbons have attracted interest for use as active materials in electronic devices such as organic field effect transistors (OFET) and organic photovoltaics (OPV). In this account we review our progress in making small organic molecules for use as organic semiconductors. This idea originated from our prior research on dehydrobenzannulenes; the octadehydrodibenz[12]annulene system could undergo double transannular cyclization to yield the indeno[1,2-*b*]fluorene skeleton, which could then be functionalized. Gratifyingly, this initial strategy worked leading to the first well characterized and stable indeno[1,2-*b*]fluorene derivatives. The synthesis of indeno[1,2-*b*]fluorenes has since been optimized—the new synthetic routes utilize inexpensive starting materials and are amenable to larger scale reaction, whereas the transannular method was only amenable to producing small amounts (tens of milligrams) of compound. We have since researched the chemical space of indeno[1,2-*b*]fluorenes and related quinoidal structures by substitution with a number of functional groups.

Knowing that the synthesis of these formally antiaromatic compounds was possible, we explored permutations to the indeno[1,2-*b*]fluorene scaffold. This has been accomplished by including of additional rings as part of the fully conjugated skeleton, exchanging carbocyclces for heterocycles, and altering the ring fusion pattern. The effects of these modifications are reflected in altered electronic properties and solid-state interactions.

## Project Origins

As an incoming graduate student the junior author (B.D.R.) asked to work on a project involving strange and unusual aromatic molecules. The senior author (M.M.H.) had just the project for him, one that had mulled around in the back of his mind for many years but had never been explored in the group. Swager et al. had reported back in 1994 that treatment of octadehydrodibenz[12]annulene (**1,** Scheme 1) with elemental iodine led to the "collapse" of the 12-membered ring to form a 6-5-6-5-6 fused ring system known

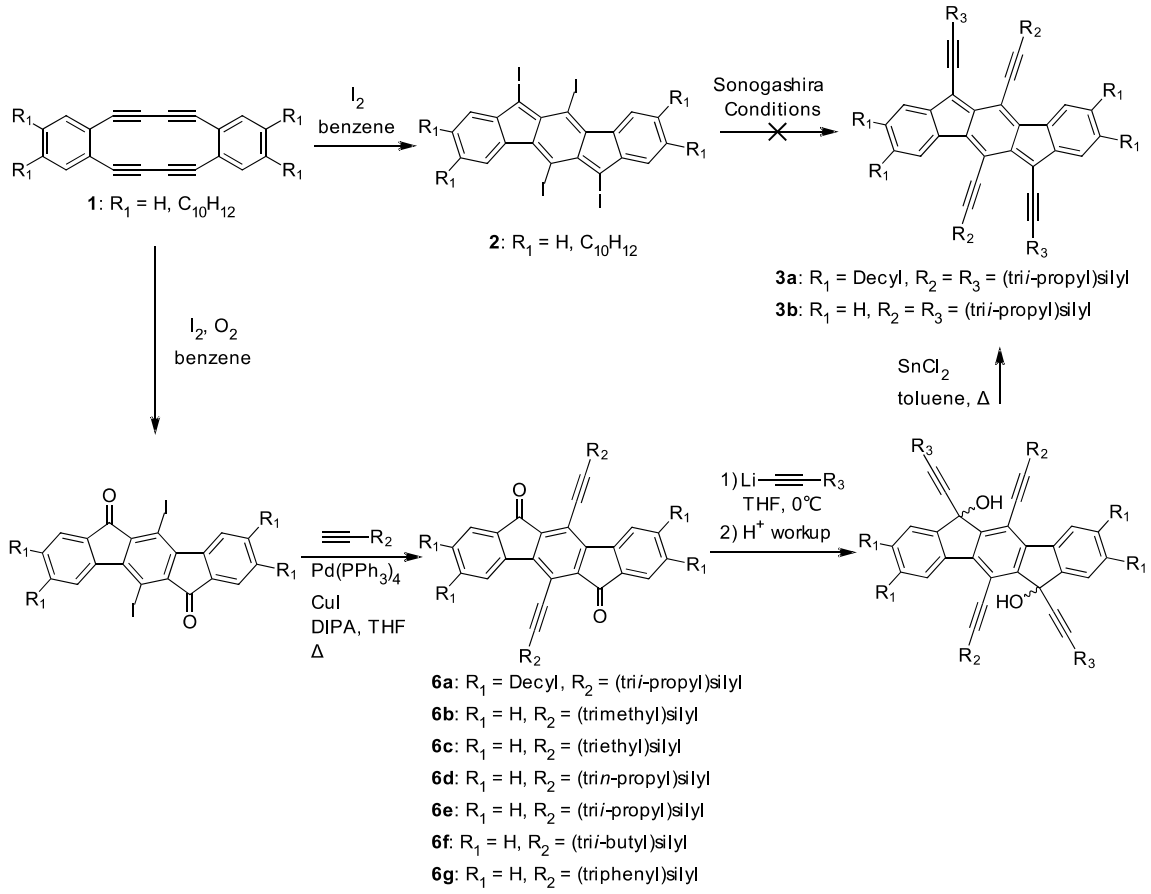


**Figure 1**. Original synthetic route.

as indeno[1,2-*b*]fluorene.[1] The resultant tetraiodo species **2** could then undergo a reaction our lab was very familiar with: Sonogashira cross-coupling to install ethynyl moieties. We chose trialkylsilylethynyl groups since Anthony and many other groups have successfully utilized these in increasing the solubility, improving solution stability, and altering the molecular packing of acenes.[2] Between our copious annulene studies[3] and myriad Sonogashira reactions to prepare such carbon-rich molecules, we were confident we could synthesize tetrayne **3**.

Up to this point there were only two reports of indenofluorenes in the literature, compound **2** and **4d** the latter of which was poorly described. The paucity of these molecules is likely due to the fact that simple arguments can lead one to believe that indeno[1,2-*b*]fluorenes may be too reactive to isolate, beyond transient characterization under inert conditions. One could easily imagine aromatizing the central benzene ring,

resulting in a biradicaloid species as a major resonance contributor. The subunit of indeno[1,2-*b*]fluorene, *s*-indacene **5**, required substitution with four bulky *tert*-butyl groups to permit isolatation and charaterization due to its high reactivity. Another subunit of indeno[1,2-*b*]fluorene, *p*-xylylene (**6**), is a well-known reactive intermediate that readily undergoes oligo/polymerizations. Despite this body of evidence pointing to the potential high reactivity of indeno[1,2-*b*]fluorene, we pushed forward.

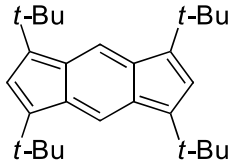


**5**

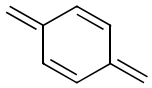

**6**

Our confidence in generating **3** was shaken as multiple attempts to cross-couple to **2** failed, likely due to the instability of the unprotected indeno[1,2-*b*]fluorene core. All we isolated was an uncharacterisable mess. As the end of the term approached, we decided to pursue an alternate route. If the transannular cyclization of **2** with iodine was performed under oxygen, the reaction produced a diiododiketone. This molecule was much more amenable to Sonogashira cross-coupling and yielded diyne **6** in modest to good yield. Taking a page from the Anthony playbook, we then attempted nucleophilic attack of the acetylide on the carbonyls of **6** followed by a reductive aromatization (formally a de-aromatization) with Sn(II) to ideally generate **3**. The first time the Sn(II) reduction was done in our lab, however, the reaction nearly failed, which would have resulted in the end of this project. In the case of ethynylated acenes, treatment of the dihydroxy intermediate with $SnCl_2$ results in a very fast color change, indicating that acene formation is occurring rapidly.[4] After an hour or two of stirring the dihydroxyindenofluorene, the solution color was still the pale yellow and we decided to examine what, if anything, had become of the starting material. Removing the solvent by rotary evaporation involved heating the water bath. Gratifyingly, upon heating the color of the solution changed to a deep blue originating from **3a**. Purposeful treatment of the dihydroxide with $SnCl_2$ in toluene at 80 °C gave modest to good yields of tetraethylindenofluorenes **3**. Though this route is seemingly less elegant than direct

coupling to **2**, it still afforded the desired product **3** as the first well characterized indeno[1,2-*b*]fluorene derivatives.[5]

Improved Synthesis

It was clear at this point that if compounds like **3** and **6** were to become useful as materials, similar to the acenes, we needed short, scalable synthetic routes to be able to make more than a few milligrams of the final compounds. It did not take long to find that this could be achieved in five steps from relatively inexpensive starting material utilizing a synthetic route to the key precursor of indeno[1,2-*b*]fluorene-5,11-dione (**7**) found in the literature as shown in Figure 2.[6] The new route also gave easier access to substitution on the peripheral benzene rings. We synthesized several derivatives with functional groups at the 2,8 positions (**8a-i**). Unfortunately, we found that many of the electronic properties were relatively unchanged and computations reveal carbons 2 and 8 have little to no LUMO and HOMO density, relegating these effects to be through weaker inductive interactions (Figure 3). Instead, the calculations suggested we should be focused on positions 5/11 and 6/12.

Now that we had access to large quantities of the dione precursor **7** we began to explore using groups other than [(triisopropyl)silyl]ethynyl at the 6 and 12 position. In principle most nucleophiles will work, but the reactivity of the core requires use of relatively bulky substituents. For example, the solution half-life of the **4a** is approximately on the order of a few hours, while that of the bulkier substituents such as **4c** or **8a** is on the order of several weeks. Despite the instabilities we were able to synthesize and characterize a number of arylated indeno[1,2-*b*]fluorenes (Figure 2).[7]

The most recent synthetic breakthrough in the synthesis of indeno[1,2-*b*]fluorenes was gaining functionality at the 5 and 11 position, which was discussed in Chapter III. This has been a difficult position to functionalize and retrosynthetic analysis of one route from the desired dione **9** leads to the simple looking building block **10**, which surprisingly has not been reported in the literature. An iodination of 2,5-dibromo-*p*-xylene leads to **10.** Subsequent Suzuki cross-coupling installs the peripheral phenyls and then an intramolecular Friedel-Crafts reaction gives **9**. This route allowed the synthesis of material bearing substitution on the 6 and 12 position on a larger scale.

We have also been interested in the precursors to the indeno[1,2-*b*]fluorenes, the indeno[1,2-*b*]fluorene diones (**6**). These were found to be soluble and stable when substituted with a number of (trialkylsilyl)ethynyl groups. Our initial study explored substitution of the electron-poor scaffold.[8] The new synthetic route utilizing **9** allowed

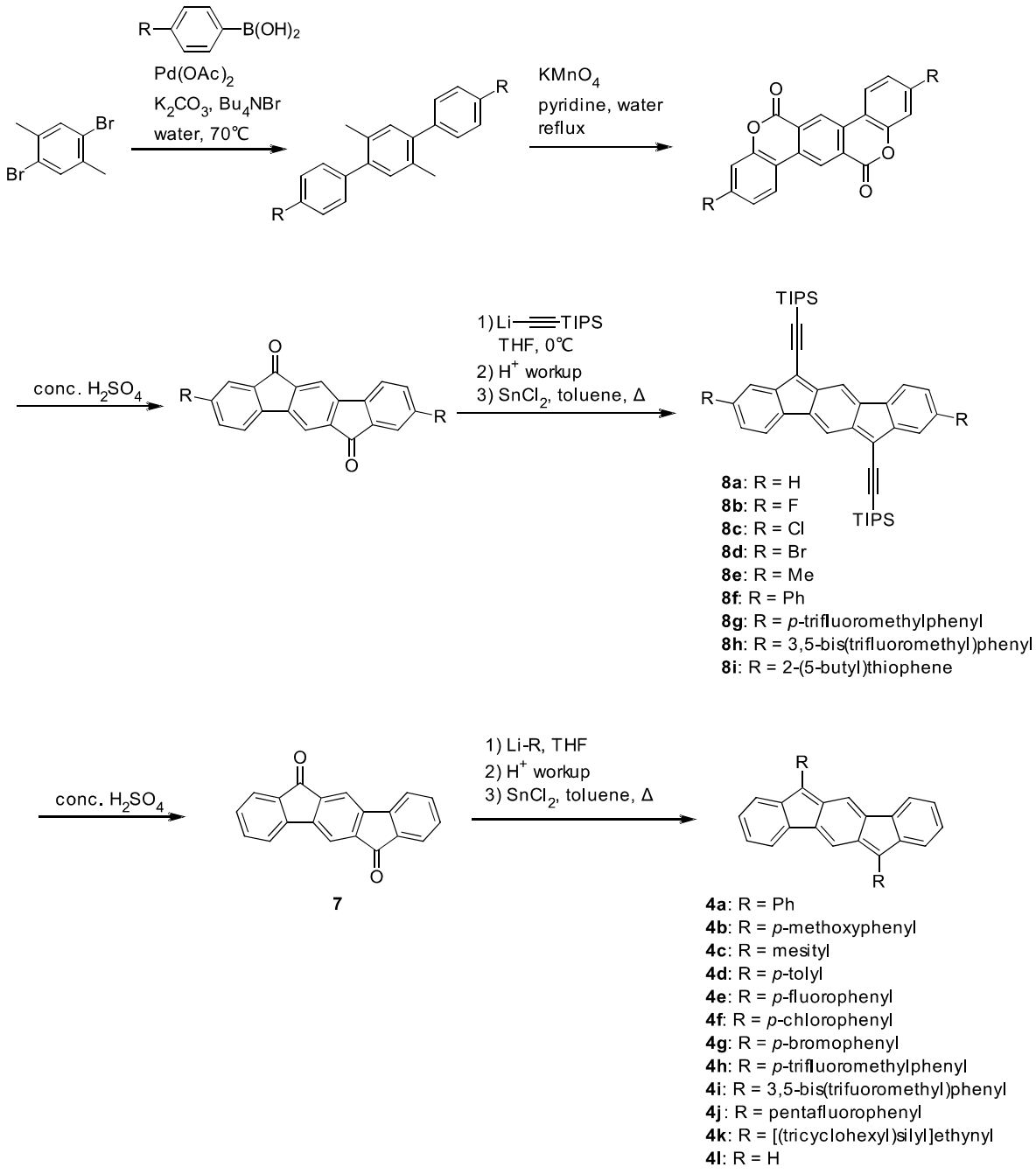


**Figure 2**. 2nd generation synthesis & arylated derivatives.

easy access to 5,11-substitution and the (trialkylsilyl)ethynyl groups were varied further. Unfortunately, analysis of a variety of [(trialkyl)silyl]ethynyl groups (**6a-k**) in the solid state yielded no guiding parameters for engineering the solid state interactions to increase intermolecular electronic coupling.

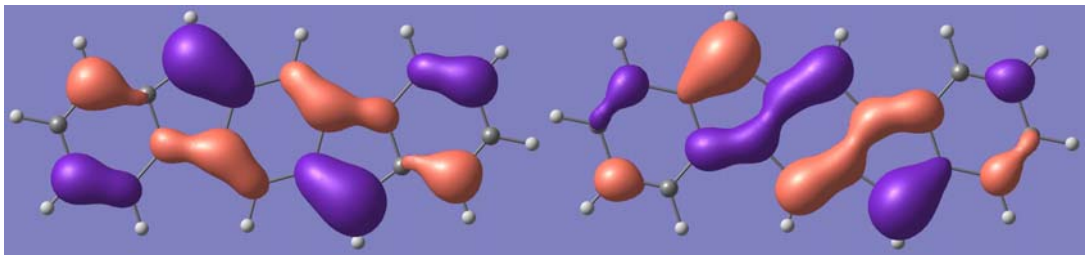

**Figure 3**. B3LYP/6-311+G(d,p) HOMO (left) and LUMO (right) density plots.

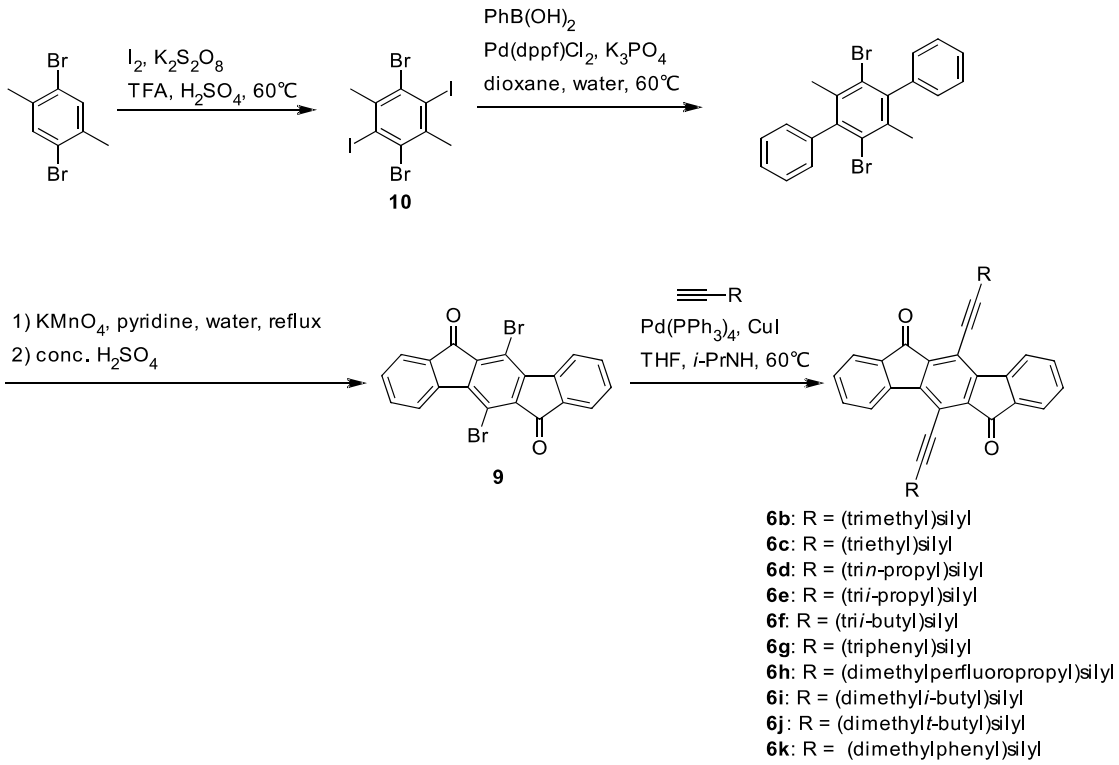


**Figure 4**. 3rd generation synthesis

Other Isomeric Structures

With a firm grasp on the synthesis of stable indeno[1,2-*b*]fluorenes, the door was now open to explore other structural isomers and heterocyclic analogues. It should be

noted that other groups have also been working on indenofluorenes and related isomers.[9–11] The first isomer that we worked on was indeno[2,1-*c*]fluorene (**11**).[12] Akin to the newer indeno[1,2-*b*]fluorene synthetic methodologies, the synthesis of **11** was through simple chemistry and done in relatively few steps. The notable difference between **11** and indeno[1,2-*b*]fluorene is that the **11** contains an *as*-indacene (**12**) subunit, unlike the *s*-indacene subunit of the indeno[1,2-*b*]fluorenes. X-ray analysis and computational studies reveal that **11** possess axial chirality with a very low energetic barrier to inversion. The *as*-indacene core of **11** was found to contain localized bonds and the peripheral benzenes retained aromaticity, just like the indeno[1,2-*b*]fluorenes. Also similar to the indeno[1,2-*b*]fluorenes, **11a-c** possess high electron affinities.

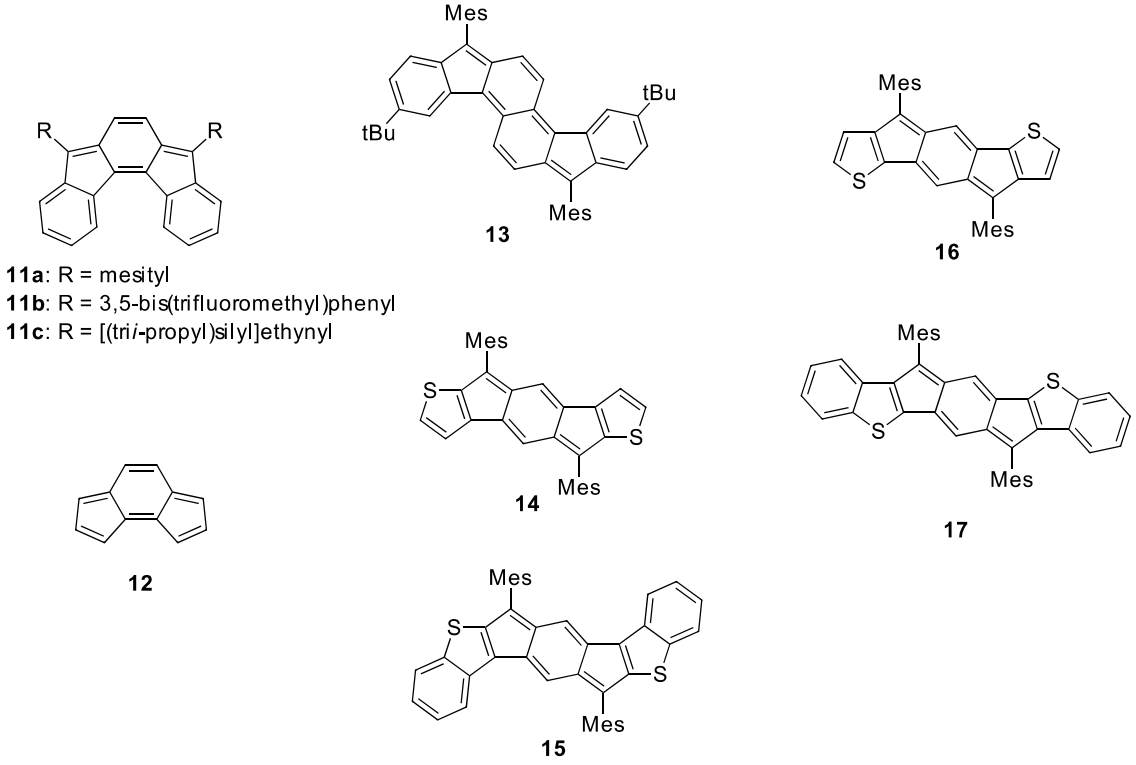


**Figure 5**. Indenofluorene **11** and related structures **13-17** prepared by the Haley group, along with model **12**.

During studies of the indeno[1,2-*b*]fluorene scaffold the desire arose to expanded the core systems to address several questions: Will the reductive aromatization work (since the mechanism for this reaction is unknown)? Would the expanded systems be stable? Thus the target of a naphthalene containing core formed in the shape of

fluoreno[4,3-*c*]fluorene (**13**).[13] The synthesis was reported up to the dione precursor and reacting it with a nucleophile and reductively dearomatizing with tin(II)chloride yielded the desired product **13**. The reductive aromatization worked much better than anticipated giving higher isolated yields for tin reduction than in the smaller systems of **3**, **4**, and **8**. Compound **13** was a blue solid which was surprisingly stable upon heating and exhibited no measurable biradical character.

Heteroatom substitution was also explored, in the form of thiophene rings (**14-17**).[14] These were found to possess high electron affinities, very similar to the indeno[1,2-*b*]fluorene parent. Thiophene fusion also increased the antiaromatic character relative to indeno[1,2-*b*]fluorene. The increased localized nature of this scaffold relative to others discussed here is evidenced by the upfield shift of the two hydrogens on the central benzene ring. The $^{1}$H chemical shift for this hydrogen 6.85 ppm in **4c** is while it is 6.06 ppm for **14** and 6.05 ppm for **16**.

Intrinsic Properties

Our interest has been held by the classes of molecules discussed above due to the fascinating properties inherent in these systems. One feature of note is that the many of these compounds (i.e., **3**, **4**, **6**, **8**) have high electron affinities accompanied by low LUMO energies (Table 1). The high electron affinity can be rationalized in simple terms; upon forming the dianion we are left with five aromatic rings, three benzene rings and two cyclopentadiene anions. This is in contrast to many purely hydrocarbon polycyclic aromatics which typically have much lower electron affinities.

Another interesting aspect is the bonding. This has been assessed through X-ray diffraction studies of single crystals of some of the compounds (Figure 6). In **4c**, **13** and **11a** the bonds are localized in the *p*-xylylene motif while the outer benzene rings remain delocalized. Molecules **14-17** pose an interesting case where the antiaromatic character reasserts itself as a result of the thiophene substitution. This is reflected in even more pronounced bond length alternation for the *p*-xylylene motif as compared to **4c**.

Another noteworthy feature is that the fully conjugated compounds (i.e., **4**, **11**, **14**) absorb in the visible region of the electromagnetic spectrum. Thus these are highly colored molecules and representative absorbance spectra are shown in Figure 7. The molar absorptivity for some derivatives, such as **4k**, is as high as ca. 70000 $M^{-1}$ $cm^{-1}$. The

absorption profile clearly shows vibronic coupling akin to acenes and other polycyclic hydrocarbons.

**Table 1**. Electronic properties of selected systems in solution.[6–8,13,14]

| compound | first reduction potentials (V vs. SCE) | second reduction potential (V vs. SCE) | LUMO Energies (eV) | optical gap (eV) |
|---|---|---|---|---|
| **3b** | –0.62 | –1.16 | –4.07 | 1.98 |
| **4a** | –0.96 | –1.49 | –3.72 | 2.17 |
| **4b** | –1.01 | –1.53 | –3.68 | 2.05 |
| **4c** | –1.12 | –1.73 | –3.56 | 2.29 |
| **4d** | –0.99 | –1.50 | –3.69 | 2.12 |
| **4e** | –0.93 | –1.41 | –3.76 | 2.16 |
| **4f** | –0.88 | –1.34 | –3.81 | 2.14 |
| **4g** | –0.89 | –1.35 | –3.80 | 2.12 |
| **4h** | –0.84 | –1.12 | –3.85 | 2.16 |
| **4i** | –0.73 | –1.07 | –3.97 | 2.16 |
| **4j** | –0.68 | –1.17 | –4.00 | 2.20 |
| **6a-k** | –0.77 to –0.84 | –1.18 to –1.26 | –3.85 to –3.90 | 2.36 to 2.40 |
| **8a** | –0.69 | –1.20 | –4.00 | 2.12 |
| **8b** | –0.60 | –1.07 | –4.08 | 2.15 |
| **8c** | –0.59 | –1.07 | –4.09 | 2.13 |
| **8d** | –0.60 | –1.10 | –4.09 | 2.13 |
| **8e** | –0.69 | –1.27 | –3.99 | 2.11 |
| **8f** | –0.66 | –1.20 | –4.03 | 2.10 |
| **8g** | –0.62 | –1.11 | –4.06 | 2.11 |
| **8h** | –0.52 | –1.00 | –4.16 | 2.11 |
| **11a** | –1.05 | –1.51 | –3.63 | 1.60 |
| **11b** | –0.71 | –1.02 | –3.97 | 1.54 |
| **11c** | –0.66 | –1.11 | –4.02 | 1.48 |
| **13** | –0.87 | –1.29 | –3.77 | 1.79 |
| **14** | –0.94 | –1.59 | –3.70 | 1.96 |
| **15** | –0.61 | –1.24 | –4.03 | 1.59 |
| **16** | –0.92 | –1.69 | –3.72 | 2.07 |
| **17** | –0.80 | –1.62 | –3.84 | 1.88 |

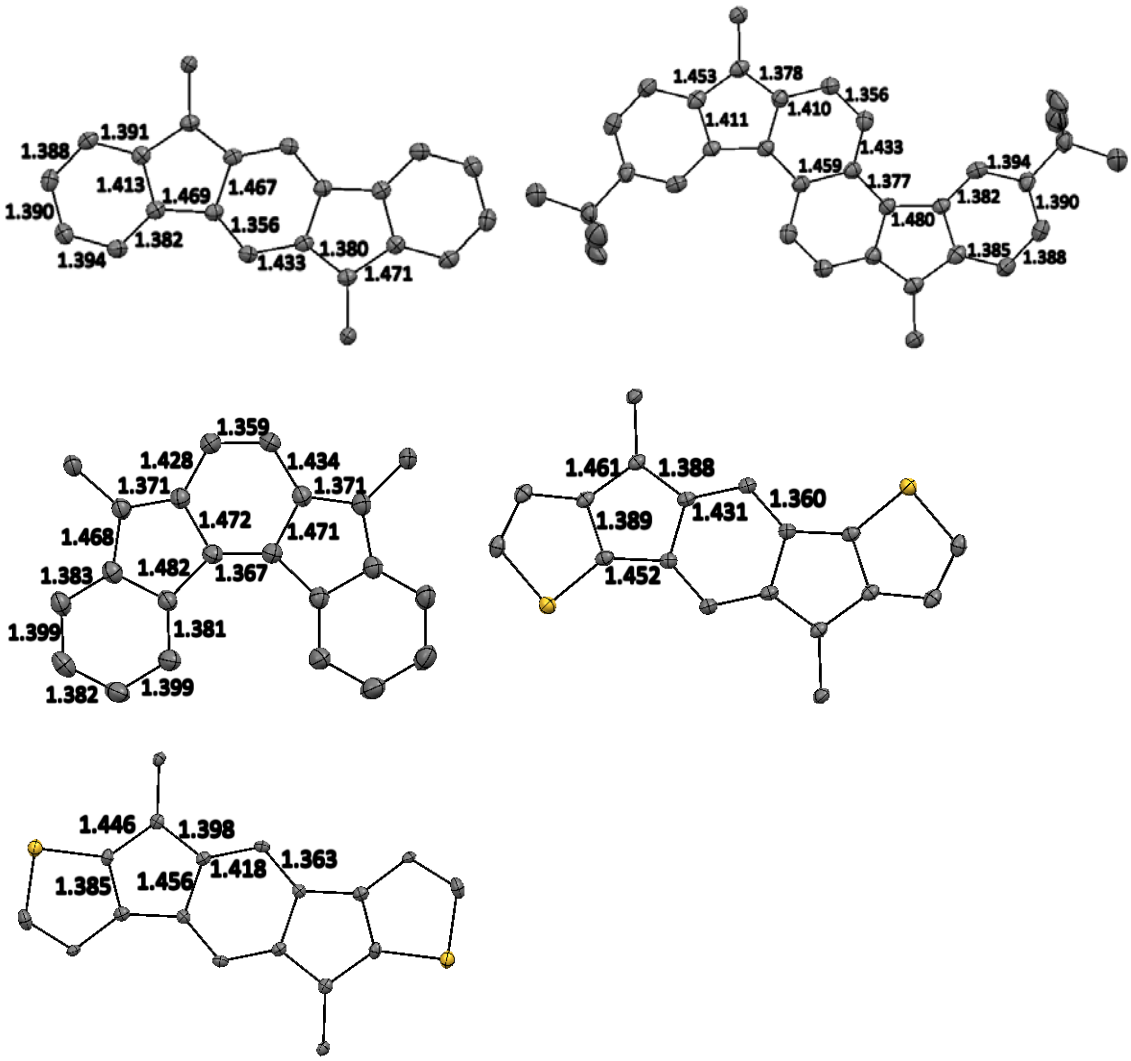


**Figure 6**. X-ray data for **4c**, **13**, **11a** (P-isomer), **14**, and **16** showing select bond lengths. Thermal ellipsoids are drawn at 40% probability, hydrogens and mesityl groups removed for clarity.

Some of these compounds made in our laboratory have been used in devices. Derivatives **8a** and **4k** were used as electron accepting material to explore the effects of LUMO offset and bulk around the acceptor on the exciton generation in OPVs.[15] An OFET was also fabricated using a single crystal of **4j** on $Si/SiO_2$ with a passivation layer of octadecyltrichlorosilane and thermally deposited gold as the source and drain electrodes.[7] The OFET exhibited ambipolar charge transport, albeit with relatively low field effect mobilities of $7x10^{-4}$ and $3x10^{-3}$ $cm^2V^{-1}s^{-1}$ for electrons and holes respectively.

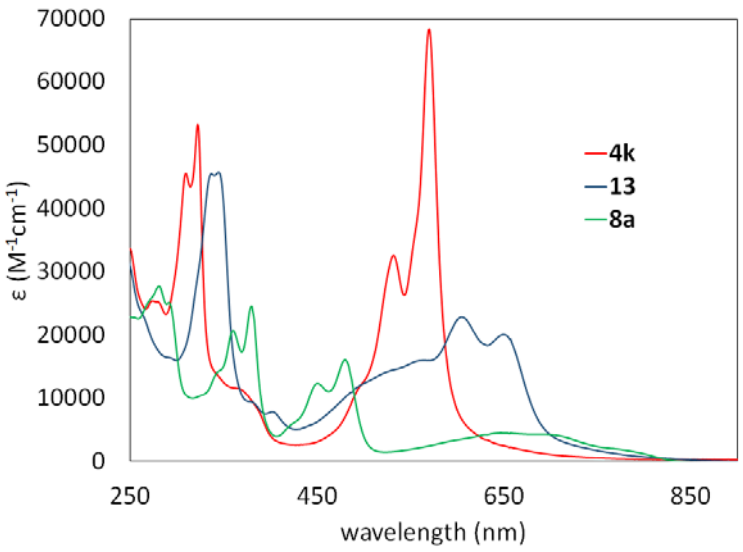


**Figure 7**. Absorbance spectrum of representative compounds.

Reduced States

The indeno[1,2-*b*]fluorene scaffold has an unusually high electron affinity and we studied the reduced states for model systems **8a** and **4k**, this is discussed in Chapter IV. In the singly reduced species $\mathbf{8a}^{\cdot-}$ the electron density is higher on the *p*-xyxylene motif and ethynyl group relative to the peripheral benzene rings as determined by EPR spectroscopy and DFT calculations. $^{1}$H NMR experiments on dianion $\mathbf{8a}^{2-}$ show the aromatic character of the system through a 1 ppm downfield shift of the hydrogens at the 5 and 11 position relative to the antiaromatic **8a**. X-ray analysis of a single crystal of the dianion $\mathbf{4k}^{2-}$ revealed that the scaffold remains planar and the changes in the bond lengths are representative of an aromatic periphery relative to neutral **4k**. The absorbance spectrum shows that the low energy absorption red shifts from 2.19 eV for **8a** to 1.11 eV for $\mathbf{8a}^{\cdot-}$ and 1.82 eV for $\mathbf{8a}^{2-}$ (Figure 8). The intensity of this absorption is about half for upon reducing to $\mathbf{8a}^{\cdot-}$ and the molar absorptivity is only a small amount of for $\mathbf{8a}^{2-}$. Interestingly, **8a**, $\mathbf{8a}^{\cdot-}$, and $\mathbf{8a}^{2-}$ all show vibronic coupling in the absorbance spectrum.

Photophysics

Intriguingly the fully conjugated indenofluorene and related systems are all non-emissive molecules. Similar to **5**, we found this to be the result of an easily accessible potential energy surface crossing between the first excited singlet state ($S_1$) and ground electronic state ($S_0$). This allows efficient internal conversion to the ground state.

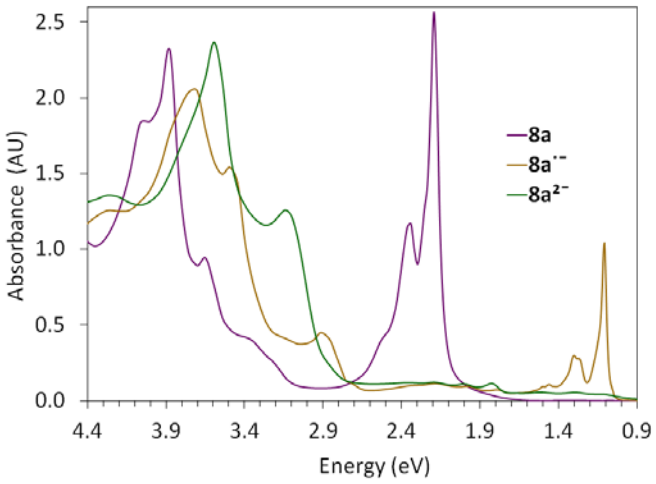


**Figure 8**. Absorbance spectrum of **8a**, **8a**$^{\cdot-}$, and **8a**$^{2-}$.

Experimentally this manifested in excited state lifetimes of only a few picoseconds as measured by femtosecond transient absorption spectroscopy for **8a**, **11c**, and **13**, thus rendering emissive processes, typically occurring with lifetimes of greater than $10^{-9}$ s, non-competitive. Also we found that compounds with a symmetry inversion center have a symmetry forbidden $S_0 \rightarrow S_1$ transition (i. e. **8**) and for compounds possessing no symmetry inversion center (i. e. **11**) the $S_0 \rightarrow S_1$ transition is allowed.

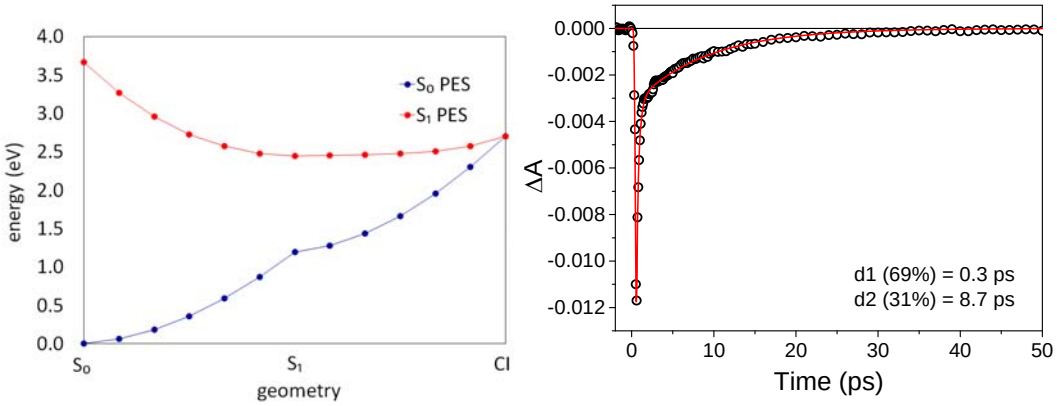


**Figure 9**. Left: FORS(4,4)/cc-pVDZ interpolated energies for $S_0$ and $S_1$ potential energy surfaces in vacuum (right) for **4l**. Right: Femtosecond transient absorption kinetics traces from the ground state bleach in a toluene solution of **8a** at 529 nm showing recovery corresponding to rapid excited state decay pathways.

The improved accessibility of indenofluorenes and related molecules discussed above has opened the door to polycyclic anti-aromatic systems containing *p*-xylylene like motifs. These scaffolds have been interesting for studying the unique photophysical and redox properties they possess. However, there still remain challenges for indenofluorenes to be a useful material in organic electronic devices. A major issue limiting the usefulness of these compounds is increasing charge mobilities. It is clear that many indenofluorenes and related molecules are now synthetically feasible, where not long ago this was not the case. Now having a good grasp of their synthesis they offer plenty of opportunity for functionalization to tailor the molecules to specific applications.

Bridge to Chapter II

Chapter I serves as an overview of the research in the laboratory over the past five years. Now Chapter II provides a look at the beginnings of the project in more details by examining the first derivatives of indenofluorenes synthesized.

Chapter II through Chapter VI contain co-authored material. Chapter II co-authors include Daniel T. Chase, Sean P. McClintock, Lev N. Zakharov, and Michael M. Haley. Chapter III co-authors include Peter J. Santa Maria, Aaron G. Fix, Chris L. Vonnegut, Lev N. Zakharov, and Michael M. Haley. Chapter IV co-authors include Natalie Sumner, Alexander S. Filatov, Lev N. Zakharov. Steven J. Peters, Marina Petrukhina, and Michael M. Haley. Chapter V co-authors include Leah E. Shoer, Aaron G. Fix , Michael R. Wasielewski, and Michael M. Haley. Chapter VI co-authors include Chris L. Vonnegut, Lev N. Zakharov, and Michael M. Haley.

# CHAPTER II

# INDENO[1,2-*b*]FLUORENES: FULLY CONJUGATED ANTIAROMATIC ANALOGUES OF ACENES

This chapter was co-authored with Daniel T. Chase who did the writing and experimental, Sean P. McClintock who did computations, Lev N. Zakharov who gathered and solved X-ray data, and Michael M. Haley who provided editorial and content advice. This work was originally published in *Angewandte Chemie International Edition* volume 50 pages 1127–1130.

## Discussion

Conjugated hydrocarbons with extended polycyclic frameworks have fascinated chemists for more than a century.[1] Originally studied because of interest in the fundamental, intrinsic properties associated with such aesthetically appealing structures, more recent investigations have focused on utilization of these π-electron-rich compounds as materials in optical and electronic device applications.[2] Acenes such as pentacene and its derivatives (e.g., **1**)[3] have received the bulk of the renewed attention,[1c,d] but they unfortunately are prone toward oxidative degradation;[4] hence, there is demand for alternative, acene-like topologies. While incorporation of heteroatoms is one possibility,[5] very recent studies by the groups of Saito, Kawase, and Tilley have reported improved syntheses of derivatives of dibenzopentalene (**2**), in which two five-membered rings have replaced the more traditional six-membered rings, as potential acene analogues.[6]

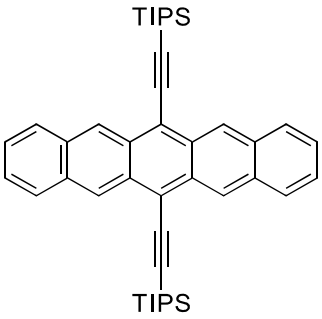


**1**

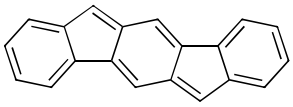

**3**

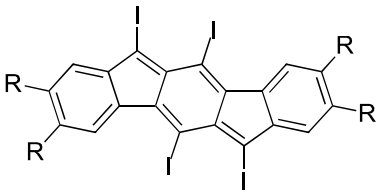


**6**, R = H, Dec, Dodec

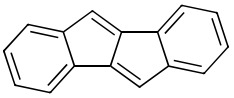

**2**

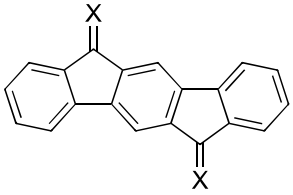


**4**, X = O
**5**, X = $C(CN)_2$

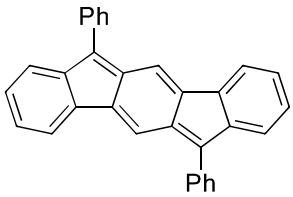


**7**

The indeno[1,2-b]fluorene skeleton (**3**), a 6-5-6-5-6 fused ring system also known as dibenzo[a,g]-*s*-indacene,[7] is an attractive structural motif in this regard. A fully conjugated indenofluorene (IF) should possess some remarkable characteristics: (i) Compounds like **3** have two fewer carbons than pentacene and thus two fewer π-electrons, making **3** formally anti-aromatic (20 π-electrons). (ii) Such molecules host a *para*-xylylene (*p*-quinodimethane) core, a reactive moiety that typically cannot be isolated because of its tendency to oligomerize/polymerize.[8] (iii) The bonding picture of **3** should be interesting as the IF core can be viewed several possible ways (e.g., a [20]annulene, a dibenzo-fused [12]annulene). (iv) IFs do not possess any internal *s*-*cis* diene linkages, which could make them more resistant to the cycloaddition pathways that degrade acenes.

Although a number of molecules incorporate the indenofluorene core, nearly all bear substituents on positions 5 and 11 that either result in cross-conjugation (ketones **4**, olefins **5**)[9] or disrupt conjugation altogether (disubstitution, spiro-fusion).[10] Examples of fully conjugated species are extremely rare, as only four compounds have been reported to date. In 1994 Swager et al. prepared and characterized tetraiodides **6** but these rapidly oxidized to the corresponding diones upon exposure to air.[11] Very little is known

about IF **7** prepared by Scherf as the synthesis has not been disclosed; the only spectroscopic feature mentioned is a UV-vis $\lambda_{max}$ absorption of 543 nm.[12] Recently Kubo and co-workers prepared naphthalene-fused IFs. These molecules exhibited singlet biradical behavior, however, meaning that the dominant resonance structure has a benzene unit as the central six-membered ring; thus, the molecules cannot be considered fully delocalized.[13] In this communication, we disclose the synthesis of stable indenofluorenes **8a–b**. We also report the X-ray crystal structure of **8a**, which unambiguously confirms the planar, fully conjugated state and provides a rare glimpse into the *p*-xylylene core. Also discussed are the optoelectronic profiles of **8a–b**, as well as a cursory examination of their stability to photooxidative conditions in comparison to **1**.

Initial attempts to access the tetraethynylated derivatives via Sonogashira cross-coupling of **6b** (prepared as previously described from the corresponding dehydrobenzo[12]annulene, Scheme 1),[11] with either phenylacetylene or (triisopropylsilyl)acetylene (TIPSA) proved to be problematic, affording complex mixtures of products. Instead, the syntheses of IFs **8a-b** introduced the alkynes in a stepwise manner. Starting with known diiododiones **9a-b,** again prepared from the dehydrobenzo[12]annulene,[11] cross-coupling with TIPSA afforded diynes **10a-b**. Addition of the lithiated acetylide of TIPSA and subsequent reduction of the intermediate diols **11a-b** overnight using $SnCl_2$ in toluene at 80 °C provided **8a-b** in modest overall yield. While red in the solid state, solutions of IFs **8a-b** exhibit a brilliant blue-purple color.

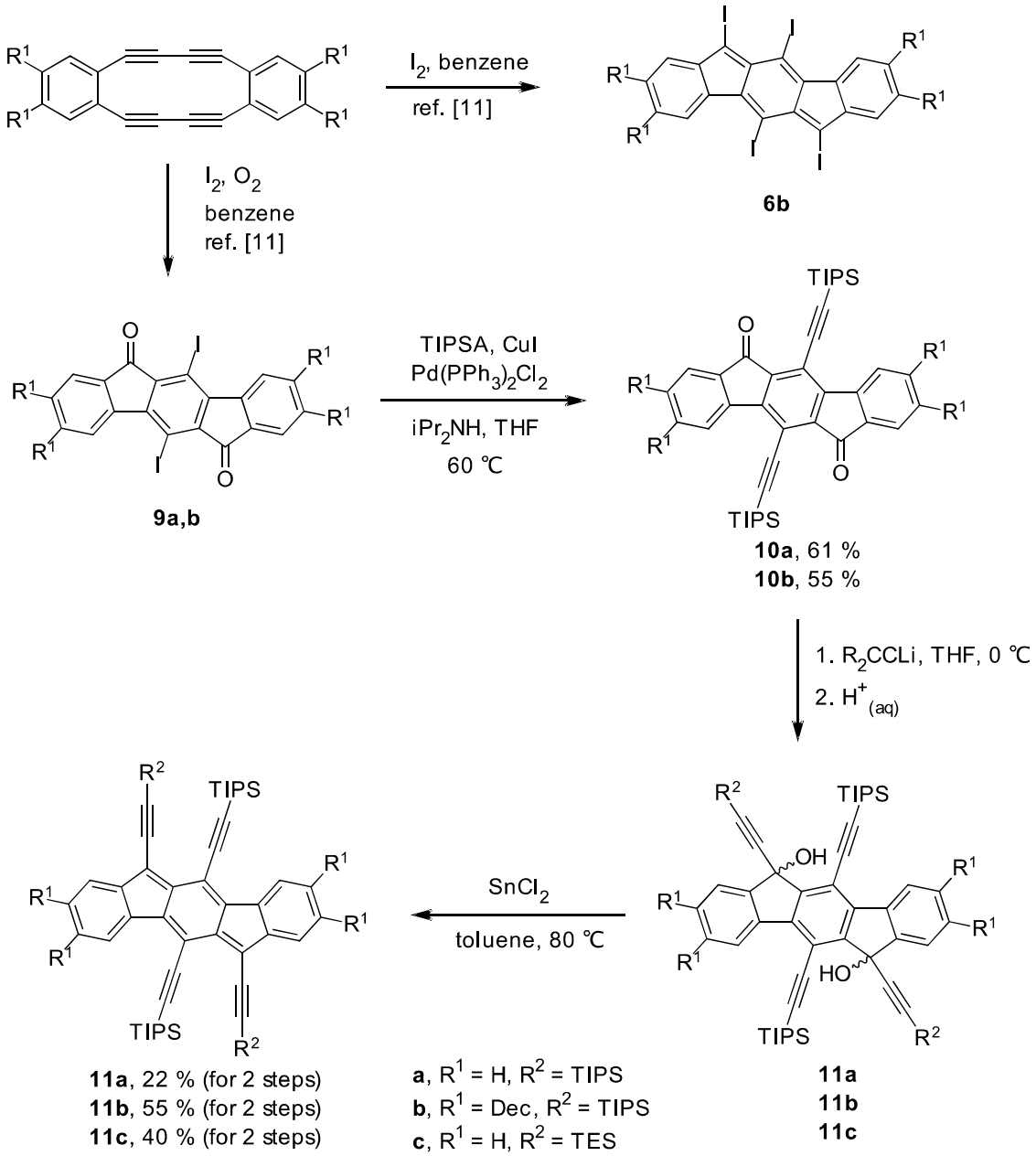


**Scheme 1.** Synthesis of **8a-c**.

Single crystals of **8a** suitable for x-ray diffraction were obtained by slow evaporation of a solution in hexanes. The molecular structure (Figure 1) reveals that the fused ring system is essentially planar (deviation rms = 0.013 Å). The bulky TIPS-capped acetylenes are bent away from one another by 4-11° and are also bent out the plane of the

20-carbon core by 3.5-4.0°. Our initial hypothesis regarding bond lengths consisted of two possibilities: (1) the overall anti-aromaticity of the molecule would dominate, resulting in alternating long and short bonds throughout the entire ring system, i.e., a [20]annulene; or (2) the benzene rings would stay fully delocalized and the *p*-xylylene unit would possess long and short bond lengths as typical for non-aromatic single and double bonds, i.e., a dibenzo[12]annulene. Examination of the C–C bond lengths (Table 1) indicates that indeed there are alternating long (1.438(3) and 1.457(3) Å for C1–C2 and C2–C3, respectively) and short (1.374(3) and 1.390(3) Å for C1–C3A and C2–C4, respectively) bonds in the central *p*-xylylene core but the peripheral benzene bond lengths are relatively homogenized (1.392-1.412 Å). Interestingly, this bonding situation closely resembles the x-ray data analyses of Thiele's and Chichibabin's hydrocarbons, two previously reported molecules containing crystallographically determined *p*-xylylene cores.[14]

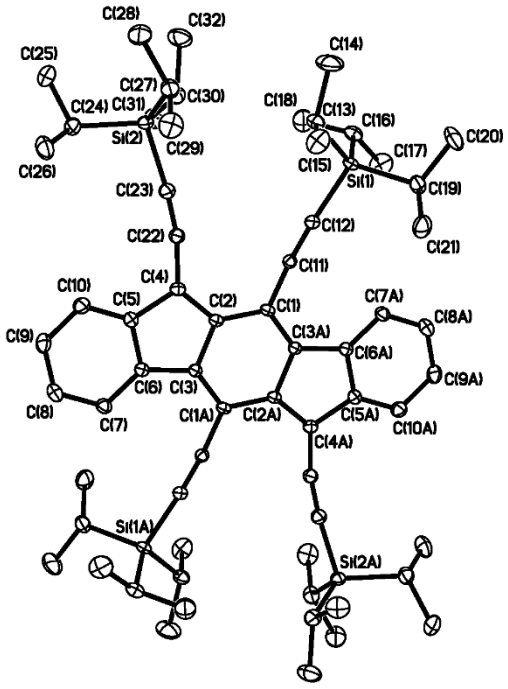


**Figure 1.** Molecular structure of indenofluorene **8a**; ellipsoids drawn at 30% probability level.

**Table 1.** Experimental and calculated bond lengths of indenofluorene **8a** and a structurally related *p*-xylylene molecule.

| Bond | X-Ray | DFT Calcs[a] | SCF MO Calcs[b] | Thiele's Hydrocarbon[c,d] |
|---|---|---|---|---|
| C1-C3A | 1.374(3) | 1.379 | 1.365 | 1.346 |
| C1-C2 | 1.438(3) | 1.444 | 1.457 | 1.449 |
| C2-C3 | 1.457(3) | 1.457 | 1.462 | 1.449 |
| C2-C4 | 1.390(3) | 1.396 | 1.371 | 1.381 |
| C3-C6 | 1.470(3) | 1.466 | 1.470 | [e] |
| C4-C5 | 1.470(3) | 1.463 | 1.456 | 1.482 |
| C5-C6 | 1.412(3) | 1.417 | 1.411 | [e] |
| Benzene (avg) | 1.389(3) | 1.398 | 1.402 | [e] |

[a] Performed using Gaussian 03 at the B3LYP/6-311+G** level of theory. [b] Ref. [16]. [c] Ref. [14a]. [d] A more descriptive name is 3,6-bis(diphenylmethylene)-1,4-cyclohexadiene. [e] Not applicable.

To shed additional light, NICS(1) calculations for the desilylated analogue of **8a** afforded NICS values for the peripheral, five-membered, and central rings to be –7.12, 1.84, and 0.02, respectively. The B3LYP/6-311+G**-optimized geometry of desilylated **8a** (Table 1) using Gaussian 03[15] provided bond lengths of 1.444, 1.457, and 1.379 Å for C1-C2, C2-C3, and C1-C3A, respectively, and 1.393 to 1.418 Å for bond lengths of the peripheral arene rings, values which nearly coincide with the crystallographic data. Lower level semi-empirical calculations by Kataoka and Toyota also confirm these findings.[16] Such good agreement between the experimental and computational data suggests that neither hypothesis is correct. Instead, **8a** should be considered a fully conjugated 20 π-electron hydrocarbon with fused *s-trans* 1,3-diene linkages across both the top and bottom portions of the carbon skeleton. The 1,4-diphenyl-1,3-butadiene bonding picture is also consistent in solution, as the $^3J$ values of the arene protons are within a narrow range of 7.44-7.55 Hz. As initially described by Günther[17] and used extensively by Mitchell,[18] one can utilize these coupling constants to determine the bond alternance parameter, *Q*, which equals the ratio of the bond orders of the benzene C7-C8

and C8-C9 bonds (as shown in Figure 1) and thus reveals the nature of the ring current in the fused ring. As such, we obtain a *Q* value of 1.01, which is indicative of a nonaromatic fused ring, analogous to the NICS results.

The crystal packing of **8a** (Figure 2) loosely resembles the herringbone pattern often found in unsubstituted acenes such as pentacene. The presence of four interdigitated TIPS groups per indenofluorene expands this basic motif, yet the packing is sufficiently tight that no solvent molecules co-crystallize with **8a**. The major contacts in the unit cell are between the TIPS groups and the central IF ring with an average distance of 3.93 Å.

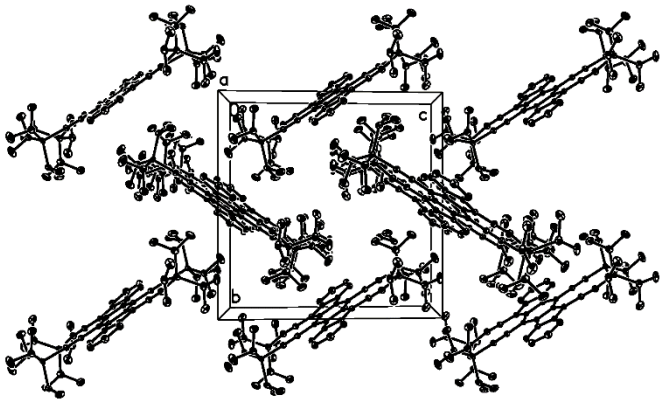


**Figure 2.** Crystal packing of **8a**.

The optoelectronic spectra of **8a-b** are shown along with pentacene **1** in Figure 3. Similar to **1**, IFs **8a** and **8b** exhibit three low energy absorptions ($\lambda_{max}$: 594 and 614 nm, respectively) but are blue-shifted ca. 50 and 30 nm, respectively, compared to **1**. These optical data correspond to estimated HOMO-LUMO gaps of 1.98 and 1.91 eV for **8a** and **8b**, respectively, compared to 1.85 eV for **1**, which agree quite well with the B3LYP/6-311+G**-calculated gap of 1.97 eV for the desilylated analog of **8a**. Unlike **1**, both **8a** and **8b** are non-emissive, which is usually the case with [4*n*] π-electron systems.

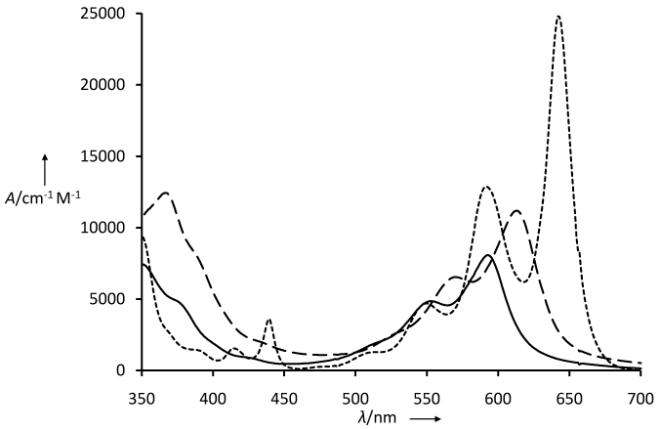


**Figure 3.** Electronic absorption spectra of **1** (- - -), **8a** (——), and **8b** (– –) in $CH_2Cl_2$.

The relative stabilities of **8a** and **8b** were also briefly examined. Initial testing via UV-vis spectroscopy was performed under similar conditions as reported by Miller et al. but no degradation was observed in the traditional time frame used for their pentacene studies (<12 h).[4c] Instead, samples of **8a** and **8b** were allowed to stand in loosely capped volumetric flasks under air in the light, and periodic $^1$H NMR measurements were made. While it was found that samples of **8a** and **8b** were stable on the order of a few weeks, the molecules eventually did degrade over the course of 2-3 months.

In summary, we have demonstrated the feasibility of fully conjugated, formally anti-aromatic indenofluorenes. Through x-ray crystallography, we have also captured a rare glimpse of the *p*-xylylene core and confirmed the structure of **8a** with comparison to the other known molecules that contain this moiety. Examination of the optoelectronic properties of IFs **8a** and **8b** unambiguously confirm that a clear comparison of fully conjugated indenofluorenes to pentacenes can be made with potentially superior stabilities. Future work will consist of exploring more efficient methodologies to generate the conjugated indenofluorene core along with investigating a larger variety of substitution motifs to better improve packing in the solid state as well as to provide a greater opportunity for detailed study of structure-property-relationships.

Bridge to Chapter III

Chapter II was the first report of a well characterized fully conjugated indeno[1,2-*b*]fluorene. Chapter III covers the subsequent work on the precursor indeno[1,2-*b*]fluorene-5,11-diones also of interest for use in organic electronics.

# CHAPTER III

# A SCALABLE SYNTHESIS OF 5,11 DISUBSTITUTED INDENO[1,2-*b*]FLUORENE-6,12-DIONES AND EXPLORATION OF THEIR SOLID STATE PACKING

This chapter was co-authored with Peter J. Santa Maria, Aaron G. Fix, Chris L. Vonnegut, Lev N. Zakharov providing experimental results. Michael M. Haley provided editorial and content advice.

## Discussion

Polycyclic conjugated hydrocarbons (PCHs) have been studied extensively due to the wide variety of physical properties that can be accessed by appropriate manipulation or "tuning" of a molecular scaffold (e.g., installation of donor/acceptor groups, inclusion of heteroatoms, etc.).[1] Recently there has been resurging interest in PCHs for use as active materials in organic electronic devices. Some popular examples of devices undergoing extensive exploration are organic field effect transistors (OFET),[2] organic photovoltaics (OPV),[3] and organic light emitting devices (OLED).[4] For such devices to operate properly, these must include materials that conduct holes (electron donating) and that conduct electrons (electron accepting).[5] While there are many systems that display good hole mobilities, those that exhibit good electron mobilities are far fewer.

Our laboratory has been exploring a new class of PCHs based on the five structural isomers of indenofluorene.[6] In particular, the indeno[1,2-*b*]fluorene (IF, **1**) skeleton is similar to linear oilgoacenes, with the notable exception that the molecule contains two five-membered carbocycles. This modest alteration imparts an inherent propensity of the IF scaffold to be electron accepting.[7] A simple explanation for the high electron affinity of the IF is that to make all five rings formally aromatic two electrons must be added to the system, effectively making two cyclopentadiene anions.[8] The result of the IFs high electron affinity is nearly balanced ambipolar charge transport in OFETs.[7b,9]

The synthetic precursors to **1**, the indeno[1,2-*b*]fluorene-6,12-diones (IF-diones, **2**) have also been explored as the active layer in OFETs. The first reported IF-dione OFET utilized **3**. While its solid state structure showed several sub van der Waals contact distances, the n-type mobility of **3** was very low ($2 \times 10^{-5}$ cm$^2$ V$^{-1}$ s$^{-1}$).[10] On the other hand, an OFET utilizing **4** (X=F) had measured electron mobilities of 0.17 cm$^2$ V$^{-1}$ s$^{-1}$,

and its X-ray crystal structure revealed 1-dimensional pi-stacking with a close interplanar distance of 3.30 Å.[11] Due to the inherent insolubility of compounds **3** and **4**, however, they needed to be vapor deposited under vacuum. More recently IF-diones **5**–**7** were reported (along with polymeric and other derivatives) with **5** and **6** exhibiting both n- and p-channel behavior in OFETs.[12] Notably, **6** showed balanced hole and electron mobilities when vapor or solution processed. Molecule/polymer solubility is desirable because it offers the benefit of being solution processable, which could allow for the inexpensive large area printing of electronic devices.

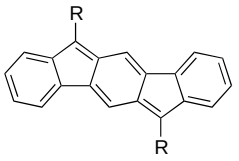


**1** (R=Ar, CCSi*i*-Pr$_3$)

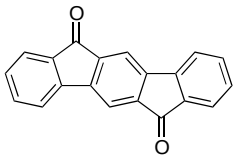


**2**

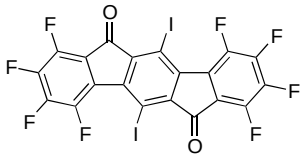


**3**

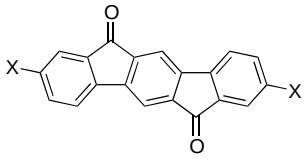


**4** (X=F, Cl, Br)

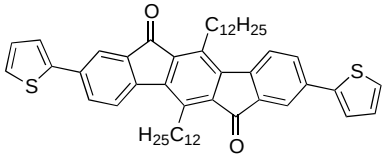


**5**

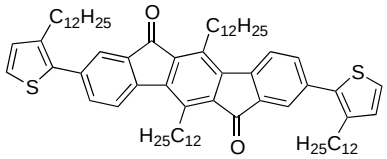


**6**

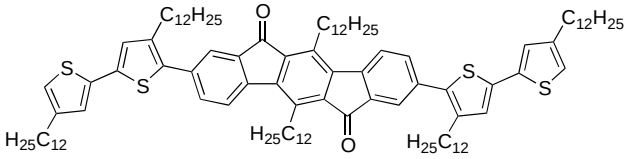


**7**

We report herein the preparation of a variety of diethynylated IF-diones **8** that are readily soluble in common organic solvents and the exploration of their packing in the solid-state by X-ray crystallography. The prototypical molecule that served as inspiration for our studies was pentacene, as it along with numerous other acene derivatives have been substituted with trialkylsilylethynyl groups of varying size to study the effect on the solid state packing in single crystals.[13] This was shown to have a large effect on the OFET performance as slight changes in the geometry can dramatically alter the

intermolecular electronic coupling, which is what ultimately dictates performance of the device.[14]

Synthesis

Our initial studies[15] toward **8** (Scheme 1) focused on the Sonogashira cross-coupling of known diiodo intermediate **9**, which was prepared by double transannular cyclization of **10** using elemental iodine under air.[16] Dehydrobenzo[12]annulene **10** in turn was synthesized via Glaser homocoupling of 1,2-diethynylbenzene.[17] While in theory this route permitted relatively easy access to diethynyldiones **8**, in practice it was fraught with problems: (1) the formation of **10** was very sensitive to the reaction conditions and thus typically gave low yields (approx. 10 %) upon scale-up. The reaction must be run in very dilute solution to minimize the formation of larger cyclooligomers as well as polymer. (2) Pure **10** in the solid state is known to be shock sensitive,[17] a fact that we can readily reaffirm. (3) The iodine atoms on **9** are quite labile as we often observed formation of elemental iodine if solutions of **9** were exposed to heat or sunlight. If we wanted to obtain quantities of diones **8** beyond 20-30 milligrams at a time, we had to overcome the synthetic roadblock that Scheme 1 represented.

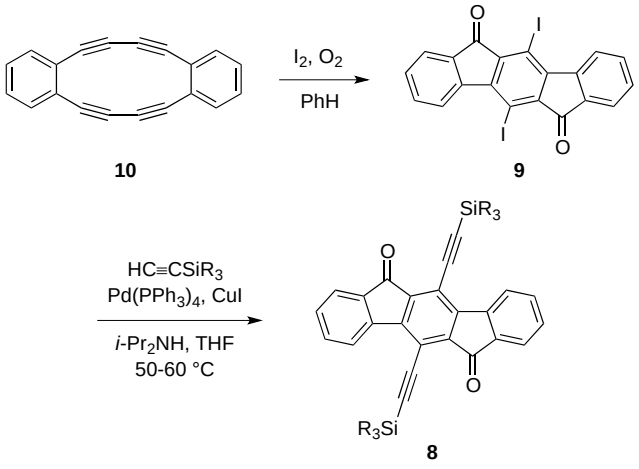


**Scheme 1**. Transannular cyclization route to diethyny[1,2-*b*]IF-diones **8**.

The improved synthetic route to **8** arises from a retrosynthetic analysis of the current method to prepare IF derivatives.[7,9] The needed modification must include halogens at the 5 and 11 positions for subsequent functionalization, such as the more robust bromines in **11**, yet avoid annulene transannualr synthesis. Instead, the route we

decided on involved key precursor **12**, which surprisingly is an unknown compound. Starting with commercially available 1,4-dibromo-*p*-xylene (**13**), iodination using the robust method reported by Kitamura gave tetrahalide **12** in good yield on 10+ g scale.[17] Suzuki cross-coupling with **12** furnished *p*-terphenyl **13**, followed by oxidation of the methyl groups to produce diacid **14**. Intramolecular Friedel–Crafts acylation then afforded 5,11-dibromo-IF-dione **11**. The yields for the Sonogashira cross-coupling of a variety of trialkylsilylacetylenes to either **9** or **11** were modest to very good (Table 1) but were not optimized.

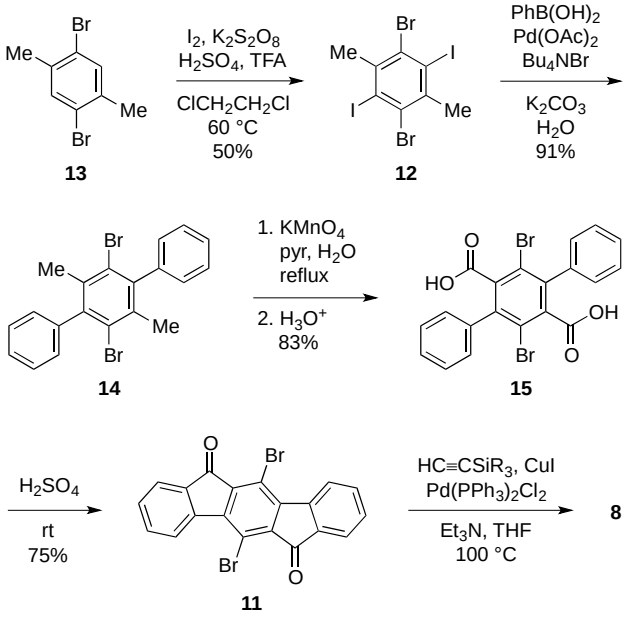


**Scheme 2**. Suzuki/Friedel-Crafts route to diethyny[1,2-*b*]IF-diones **8**.

Optical and electronic properties

Shown in Figure 1 are the UV/Vis spectrum and cyclic voltammogram of **8c**, data which are representative of all the 5,11-diethynyl-[1,2b]IF-diones. As anticipated, altering the trialkylsilyl group has very little effect on the optoelectronic properties of the conjugated scaffold (Table 2). All molecules have two strong absorptions around 310 and 330 nm, with a much weaker, broad absorption in the 450-550 nm range. Electrochemistry shows two reversible reductions with potentials of –0.78 to –0.84 V for the first reduction and –1.18 to –1.26 V for the second reduction. The small differences in the absorbance and cyclic voltammetry fall within is essentially due to experimental error.

**Table 1**. Diethyny[1,2-*b*]IF-diones Synthesized and Yields for Sonogashira Cross-Coupling

| | trialkylsilyl group | | | isolated yield | |
|---|---|---|---|---|---|
| | $R^1$ | $R^2$ | $R^3$ | from **9** | from **11** |
| **8a** | Me | Me | Me | 40 | --- |
| **8b** | Et | Et | Et | 8 | 27 |
| **8c** | *n*Pr | *n*Pr | *n*Pr | --- | 72 |
| **8d** | *i*Pr | *i*Pr | *i*Pr | 61 | 48 |
| **8e** | *i*Bu | *i*Bu | *i*Bu | 7 | --- |
| **8f** | Ph | Ph | Ph | 15 | --- |
| **8g** | Me | Me | $CF_3(CH_2)_2$ | --- | 20 |
| **8h** | Me | Me | *i*Bu | --- | 35 |
| **8i** | Me | Me | *t*Bu | 17 | --- |
| **8j** | Me | Me | Ph | --- | 24 |

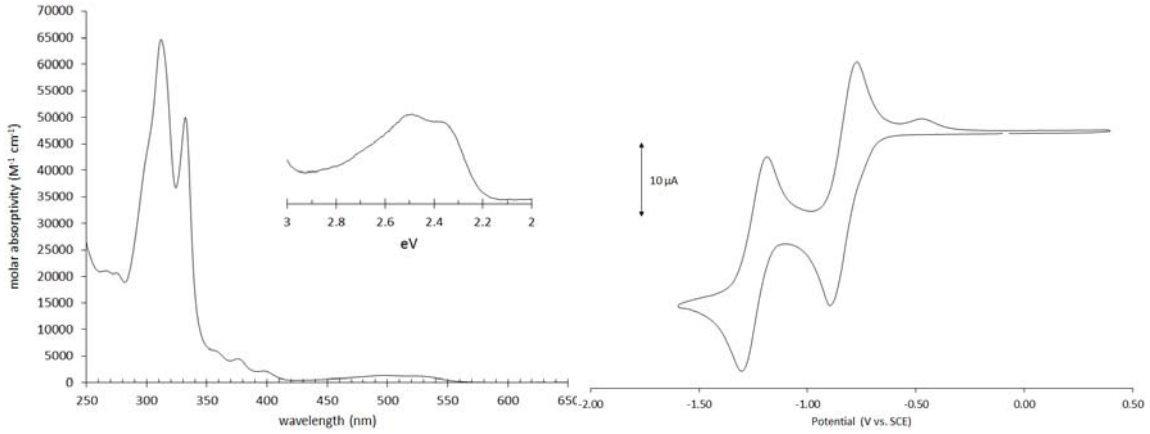


**Figure 1**. UV/Vis spectrum (left) and cyclic voltammogram (right) of dione **8c**.

**Table 2**. Electrochemical and Optical data for ID-diones **8a-8j**.

| | electrochemical | | | | optical | |
|---|---|---|---|---|---|---|
| compd | $E_{red}^1$ (V) | $E_{red}^2$ (V) | $E_{LUMO}$ (eV)[c] | $E_{HOMO}$ (eV)[d] | $\lambda_{abs}$ (nm) | gap (eV)[e] |
| **8a** | –0.80[a] | –1.21[a] | –3.89 | –6.26 | 310, 330, 524 | 2.37 |
| **8b** | –0.79[a] | –1.23[a] | –3.90 | –6.28 | 311, 332, 522 | 2.38 |
| **8c** | –0.83[b] | –1.24[b] | –3.86 | –6.23 | 312, 332, 524 | 2.37 |
| **8d** | –0.82[a] | –1.24[a] | –3.87 | –6.23 | 313, 333, 525 | 2.36 |
| **8e** | –0.84[a] | –1.26[a] | –3.85 | –6.22 | 314, 333, 524 | 2.37 |
| **8f** | –0.78[a] | –1.18[a] | –3.90 | –6.29 | 312, 333, 520 | 2.39 |
| **8g** | –0.77[b] | –1.18[b] | –3.87 | –6.27 | 308, 330, 516 | 2.40 |
| **8h** | –0.78[b] | –1.21[b] | –3.86 | –6.24 | 310, 331, 521 | 2.38 |
| **8i** | –0.81[a] | –1.25[a] | –3.87 | –6.23 | 312, 331, 526 | 2.36 |
| **8j** | –0.78[b] | –1.20[b] | –3.86 | –6.24 | 310, 331, 521 | 2.38 |

a: CV recorded using 1–5 mM of analyte in 0.1 M solution of $Bu_4NOTf$ in $CH_2Cl_2$. Values reported as the half-wave potential (vs. SCE) using the Fc/Fc+ couple (0.46 V) as an internal standard. See SI for details. b: Electrolyte solutions (0.1 M) were prepared from HPLC-grade $CH_2Cl_2$ and anhydrous $Bu_4NBF_4$. Values reported as the half-wave potential (vs. SCE) using the Fc/Fc+ couple (0.46 V) as an internal standard. See SI for details. c: LUMO energy levels were approximated using SCE = –4.68 eV vs. vacuum.[18] d: Estimated by subtracting the optical bandgap from $E_{LUMO}$. e: Estimated from the $\lambda_{max}$ of the lowest energy UV-Vis peak.

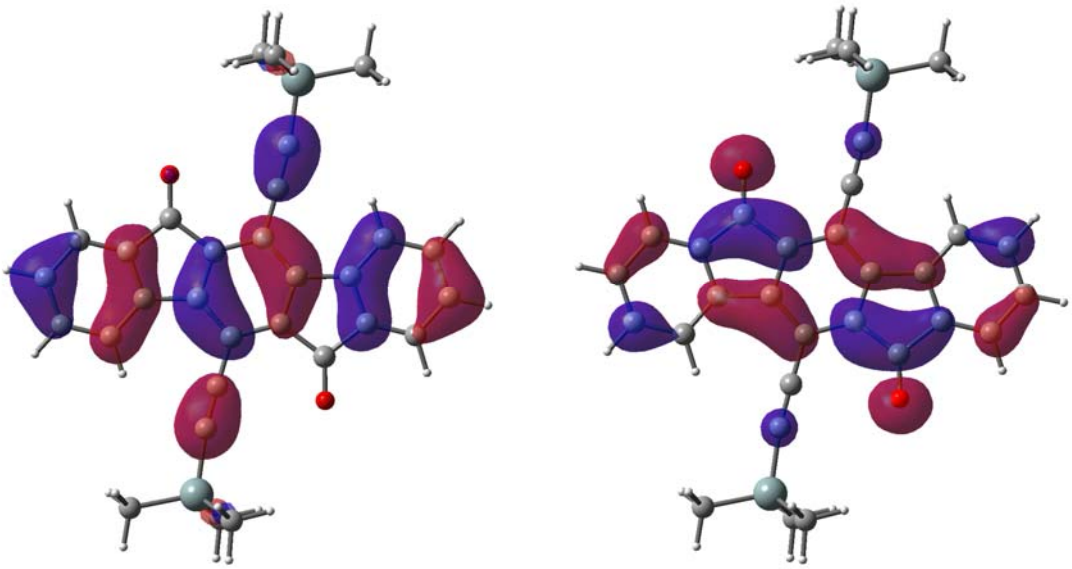

**Figure 2**. Plot of Kohn-Sham HOMO (left) and LUMO (right) spectrum of **8a** showing calculated transitions.[22]

**Table 3**. Calculated transitions for **8a**, showing only the main contribution to each excitation. Calculated using TD-B3LYP/6-311+G(d,p)//B3LYP/6-31G(d).

| transition | molecular orbitals | contribution to excitation, % | oscillator strength | energy, eV (nm) |
|---|---|---|---|---|
| $S_0 \rightarrow S_1$ | HOMO→LUMO | 97 | 0.0295 | 2.35 (527) |
| $S_0 \rightarrow S_2$ | HOMO-2→LUMO | 89 | 0.0000 | 2.71 (458) |
| $S_0 \rightarrow S_3$ | HOMO-3→LUMO | 80 | 0.0000 | 2.86 (434) |
| $S_0 \rightarrow S_4$ | HOMO-1→LUMO | 88 | 0.0486 | 2.95 (420) |

Interestingly these compounds have a low energy $S_0 \rightarrow S_1$ transition at ca. 500-525 nm which has previously been described as a n→π* transition; [12,15] however, TD-DFT calculations predict this to be π→ π* (Figure 2). The n→π* transition was calculated to have a slightly higher energy transition with an oscillator strength of 0, predicting that it should not be visible in the UV-Vis spectrum (Table 3).[19] To see if this was a computational artifact, the same calculations were performed for fluorenone and benzophenone, where it has previously been established that the $S_0 \rightarrow S_1$ transition

corresponds to $\pi \rightarrow \pi^*$and $n \rightarrow \pi^*$ respectively.[20,21] The calculations correctly predict the ordering of the states for fluorenone and benzophenone. To experimentally test this, UV/vis spectra were gathered in solvents of differing polarity. We anticipated that if the $S_0 \rightarrow S_1$ transition corresponds to a $n \rightarrow \pi^*$transition, the energy separating the $S_0$ and $S_1$ states would be measurably different in polar solvents when compared to non-polar solvents, thus leading to an energy shift of this transition. Likewise if the $S_0 \rightarrow S_1$ transition was a $\pi \rightarrow \pi^*$ there should be essentially no change in the transition energy when changing solvent polarity. We found that the shift in the spectrum upon changing solvent polarity in going from n-hexane to acetone was 0.02 eV, supporting our hypothesis that the 450-550 nm absorption is indeed a $\pi \rightarrow \pi^*$ transition as indicated by calculations.

X-ray Crystallography

We explored the solid-state packing geometries resulting from altering the trialkylsilyl groups. The high crystallinity of the majority of the compounds examined allowed for the facile growth of large single crystals, of approximately several millimeters, from solution (typically hexanes). The molecular structures were then elucidated using x-ray diffraction. Single crystals for **8g** and **8j** were grown from chlorobenzene due to the low solubility and low crystallinity of these compounds.

There are three clear substitution patterns visible in the array of IF-diones synthesized—the three groups are n-alkyl chains with symmetry (three mirror symmetry planes about the silicon), bulky alkyl groups with symmetry, and dimethyl-substituted possessing only one mirror plane of symmetry about the silicon. When looking for trends we compared three parameters to see if any of them ultimately yielded packing motifs with close contacts between the carbons of the conjugated system. One parameter examined is the distance between the centroid of the planar system and its next nearest neighbor along the 1-dimensional π stack. The other parameter is the angle between the centroids of the nearest neighbor molecules and the normal to the plane of a molecule; thus, a system with perfect overlap would have $\theta=0°$ and $\theta=90°$ would result in no π orbital overlap. Using these two parameters a crude parameter for examining the possible intermolecular electronic coupling can be developed, this is pictorially represented in Figure 3.

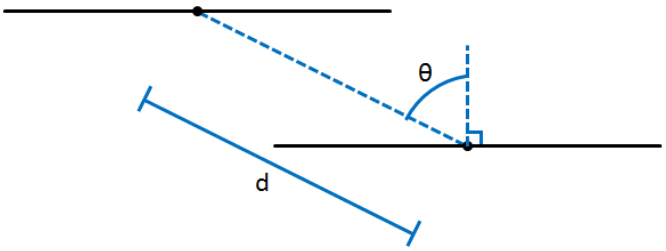


**Figure 3**. Schematic of the parameters used for comparing x-ray crystal structures, view is parallel to the molecular plane. Black lines represent the molecules with circles denoting the centroid.

Looking at Table 4 the only trend in the series is within the n-alkyl symmetric. The n-alkyl symmetric series has both the d and θ follow the trend of the alkyl group's radius. When examining symmetric and asymmetric series there is not a easily interpretable trend between the radii and d or θ. Pictorially the overlap between the molecular planes is clearly visible in Figure 4. For the n-alkyl symmetric series visual inspection reveals that the overlap between the planes of the molecules is greatest for the smallest group, **7a**, and least for the largest group, **7c**. Yet again, there is no clear visual trend in the overlap between the symmetric and asymmetric series. Considering that derivatives of **7** are most likely a n-channel material in OFETs the density and phase of the LUMO should be the most important since in a molecular orbital picture of charge transport this is the orbitals that the extra electron would occupy. The Kohn-Sham LUMO density in Figure 2 is predominately located on the indacene moiety and the oxygen. From this perspective the best candidates for n-channel OFET materials would have large overlap between the indacene moiety and oxygen. In **7a**-**7j** the oxygen is pointing away from the indacene moiety in the neighboring molecules along the stack and there is little to no overlap between the indacene moieties.

**Table 4**. Sizes of Trisubstituted-silylethynyl Groups in **8**.

| | | | | intermolecular close contacts | | | |
|---|---|---|---|---|---|---|---|
| | | radius (Å)[a] | radius (Å)[b] | contact | distance (Å) | d[c] | θ[d] |
| n-alkyl symmetric | **8a** | 2.69 | --- | --- | --- | 6.366 | 57.2 |
| | **8b** | 4.06 | --- | --- | --- | 6.439 | 57.5 |
| | **8c** | 5.26 | --- | --- | --- | 8.239 | 65.4 |
| symmetric | **8a** | 2.69 | --- | --- | --- | 6.366 | 57.2 |
| | **8b** | 4.06 | --- | --- | --- | 6.439 | 57.5 |
| | **8d** | 4.09 | --- | --- | --- | 9.550, 7.419[e] | 69.6, 62.7[e] |
| | **8c** | 5.26 | --- | --- | --- | 8.239 | 65.4 |
| | **8e** | 5.28 | --- | C9···C2, C6···C3, C6···C6 | 3.407, 3.562, 3.524 | 6.134 | 56.4 |
| | **8f** | 5.89 | --- | C10···C10, C17···C4 | 3.188, 3.369 | 10.984 | 74.7 |
| asymmetric | **8i** | 2.73 | 3.99 | C7···C3 | 3.348 | 6.356 | 58.0 |
| | **8h** | 2.68 | 5.26 | C9···C2, C10···C3 | 3.437, 3.409 | 5.976 | 55.3 |
| | **8g** | 2.67 | 5.74 | C6···C10, C3···C17 | 3.361, 3.361 | 6.096 | 56.5 |
| | **8j** | 2.68 | 5.94 | --- | --- | 6.292 | 57.3 |

a: Si…X distance where X is the farthest atom from Si with the covalent radii of X added to the distance.[25] b: radius for other axis of lower symmetry trialkylsilanes. c: distance between the centroid of two molecules in the 1-D stack. d: angle between the centroid of each of two molecules of the pi stack and the normal to the average plane. e: there are two symmetrically independent 1-D stacks.

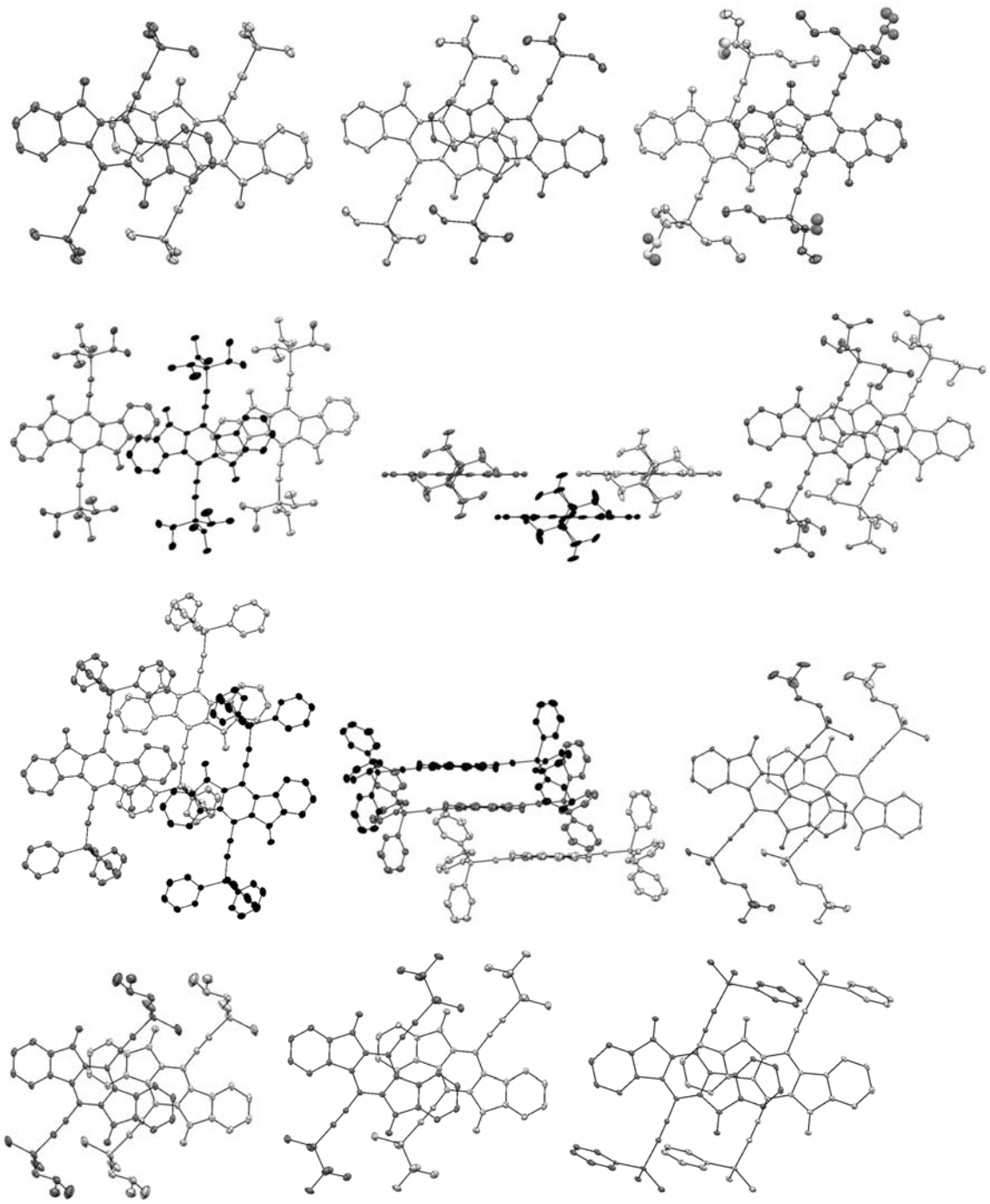

**Figure 4**. Views perpendicular to the average plane of the pi stack. 1st row left to right **7a**, **7b**, **7c**, **7d**. 2nd row left to right **7d**, **7d**, **7e**. 3rd row **7f**, **7f**, **7g**. 4th row **7h**, **7i**, **7j**. Hydrogens omitted for clarity, ellipsoids were drawn at the 30 % probability, individual molecules were colored the same to identify overlap easier.

We have described the new synthetic route to 5,11 functionalized IF. This importantly allows for the scalable synthesis of larger amounts of IF. With reasonable quantities of starting material we were able to further explore the solid state packing motifs that result from altering the bulkiness as well as directionality of the trialkylsilyl groups. X-ray analysis of solution grown single crystals reveals several promising motifs. Device studies of the on the single derivatives of interest are ongoing. These compounds may also be useful in make ambipolar OFETS when blended with p-type materials, for example 6,12-bis[(triisopropylsilyl)ethynyl]pentacene.

Bridge to Chapter IV

Chapter III discusses our findings with the precursors to the indeno[1,2-*b*]fluorenes. Next, attention is given back to the fully conjugated indenofluorenes which reversibly accept up to two electrons. Chapter IV describes the characterization of the one and two electron reduced species.

# CHAPTER IV

# EXPERIMENTAL AND COMPUTATIONAL STUDIES OF THE NEUTRAL AND REDUCED STATES OF INDENO[1,2-*b*]FLUORENE

This chapter was co-authored with Natalie Sumner, Alexander S. Filatov, Lev N. Zakharov providing experimental results. Steven J. Peters, Marina Petrukhina, and Michael M. Haley provided editorial and content advice.

## Discussion

### Introduction

Polycyclic conjugated hydrocarbons (PCH) have intrigued chemists for decades because of their interesting and varied physical properties, which are a result of the specific electronic structure of each unique scaffold.[1] Renewed interest in the optical and magnetic properties of PCHs in recent years has arisen from their application as electronic materials in devices.[2] This is due to the fact that charge is transported easier through π orbitals as compared to their exclusively σ bonded counterparts. A driving force for research into organic electronics is to develop materials for use in inexpensive electronic devices that are easily mass produced, for example, by roll to roll printing.[3] One widely studied, π-electron-rich compound is pentacene (**1**, Figure 1). This molecule and its numerous derivatives display relatively high performance in organic field effect

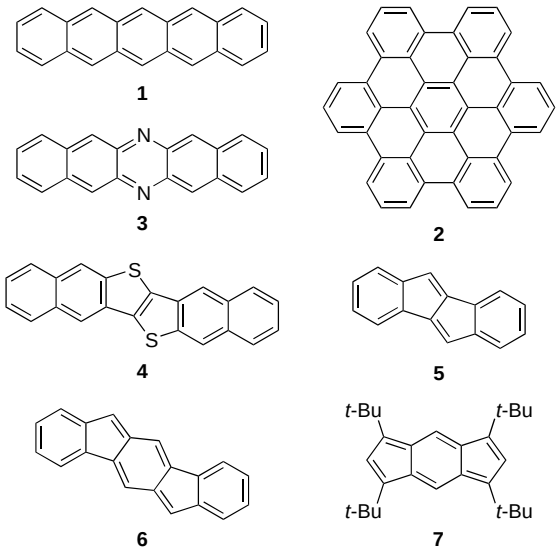


**Figure 1.** Representative examples of π-electron-rich polycyclic conjugated hydrocarbons.

transistors (OFET) and organic photovoltaics (OPV).[3] The larger acenes, however, are inherently prone to degradation via cycloaddition pathways of the "locked" *s*-cis diene(s) within the acene core.

A tremendous variety of additional π-electron-rich motifs (Figure 1) have been explored over the last decade, such as larger condensed aromatics (e.g., hexabenzocoronene, **2**),[4] heteroatomic acenes (e.g., **3**)[5] and heteroatomic acene-like structures (e.g., **4**).[6] It is worth noting that in the last example one or more of the six-membered rings was replaced with a five-membered heterocycle. Only recently has this same modification been examined for five-membered carbocycles; the most prevalent examples are molecules based on benzo- and dibenzopentalenes (e.g., **5**).[7] Studies have shown that a vast majority of these new PCH structures are electron-donating and thus exhibit p-type semiconducting behavior in devices. Far fewer molecules are electron-accepting and thus exhibit n-type semiconducting behavior in devices; therefore, there is need to develop new organic molecules that possess electron-accepting properties so that they are available in the toolbox of materials chemists.

A PCH scaffold that is structurally similar to pentacene is indeno[1,2-*b*]fluorene (IF, **6**).[8] Replacement of two six-membered rings in **1** with five-membered carbocycles means two less π-electrons and thus a formally anti-aromatic 20 π-electron skeleton. This class of hydrocarbons has been rarely studied; prior to 2011, the four known examples were either unstable or poorly characterized.[9,10] Such instability might be anticipated since *s*-indacene, a molecule too reactive to be isolated, is a structural subunit of the IF scaffold; however, *s*-indacene could be kinetically stabilized by inclusion of four *tert*-butyl groups (e.g., **7**).[11]

Over the last three years our group[12-15] and others[16] have developed or adapted synthetic methods that permit the preparation of indeno[1,2-*b*]fluorene derivatives on the gram scale, which in turn should allow IFs to be further explored for use as organic electronic materials.[14,15] A key discovery in our research has been the high electron affinity that is inherent to the IF scaffold, a result of the inclusion of the five-membered carbocycles. A simple explanation for the ease of reduction is that upon accepting two extra electrons, all five rings become aromatic and a 22 π-electron species is generated. In

a similar manner, *s*-indacene **7** could be reduced and the resultant anion radical[17] and dianion[18] characterized. This information is useful to detail the electron accepting and/or transporting behavior of an organic material. To this extent we sought to characterize the reduced states of the IF scaffold to determine the location and effects on the molecular structure. This in turn should afford better insight and understanding when designing materials for electron transporting and/or accepting applications, as the phase and overlap of the relevant molecular orbitals are critically important for applications in devices.[19] One goal in the design of new organic materials is to be able to easily screen possible structures using computational methods to find molecules predicted to have a desirable property(ies).[20] Density functional theory (DFT) has opened the door for routine calculations to be completed in the timeframe of a few days on desktop computers to inexpensively probe some of the basic properties that influence whether or not a compound is worthy of synthesis; however, with the plethora of DFT methods available, we decided to obtain data for a model electron-accepting PCH, i.e., **6**. We wanted to find a method that gave reasonable results and is accessible to a broad audience. This inherently excludes very specialized techniques or complicated correlations and very high levels of theory, since many systems of interest consist of dozens of atoms. With that in mind the limiting factors were that we wanted (1) to utilize readily available DFT methods, (2) minimal manipulation of data and (3) methods that can be easily applied by a using a desktop computer with minimal training.

There are numerous benchmark studies for DFT as well as other post Hartree-Fock methods. Some well-known examples include atomization energies, enthalpies of reactions, ligand binding energies, ionization potentials and electron affinities, to name a few.[21,22] We sought to assess a selection of DFT methods based on spectroscopic properties. Considerable theoretical groundwork has been done to enable the "routine" computation of these spectral parameters and somewhat surprisingly there lacks, to the best of our knowledge, a broad assessment of DFT functionals for the prediction of NMR chemical shifts of neutral and the more difficult case of charged states.[23-25] Likewise, most of the studies exploring DFT prediction of isotropic hyperfine coupling constants (HFCC) for free radicals survey few DFT methods.[26,27] Studies have also been performed that explore the energies predicted by time dependent DFT (TD-DFT); however, none

have examined the predictions for reduced PCHs.[22,28,29] This study is not a comprehensive test bed consisting of dozens of molecules, but instead we use it as an entry point for investigating the feasibility for PCHs and their negatively charged species, which is important for the development of electron accepting and/or transporting materials from theory.

Herein we report the formation and characterization of the accessible redox states of 6,12-bis[(trialkylsilyl)eth-ynyl]indeno[1,2-*b*]fluorenes **6a** and **6b**. The IF scaffold is convenient for this study since there are no major geometric or symmetry changes for the different redox states, as is the case in, for example, cyclooctatetraene.[30] We compare the experimental data with that derived for computational analog **6c** utilizing twenty DFT methods to determine their performance for predicting spectroscopic properties for the states considered. The functionals are assessed by calculating the $^{1}$H and $^{13}$C NMR spectra of neutral **6c** and its corresponding dianion, the hyperfine coupling constants (HFCC) for the anion radical, and the low energy transitions in the absorbance spectra of the neutral molecule, anion radical and dianion. To our knowledge this study represents one of the first broad assessments comparing predictive properties of varying DFT methods for differing redox states of a PCH.

## Results and Discussion

### Experimental.

IF derivatives **6a** and **6b** were synthesized by previously reported procedures.[13,14] The EPR spectrum of the anion radical **6a**$^{\bullet-}$ was obtained by reducing the neutral compound with 1 equiv. of K in THF to give the light yellow anion radical (Scheme 1), in contrast to the deep purple color of **6a**. The NMR spectra of the dark green solution of the dianion was obtained by reducing **6a** with 2 equiv. of K in the presence of 18-crown-6 to help solubilize **6a**$^{2-}$. The absorbance spectra were obtained by controlled reduction of **6a** in THF with K in the presence of 18-crown-6 in a quartz cuvette sealed with a screw cap. Single crystals of dianion **6b**$^{2-}$ were prepared by reduction in THF with excess Rb in the presence of 18-crown-6; see the SI for complete experimental details.

The DFT functionals utilized in this study were chosen from a variety of ones that are readily available and popular in the literature, i.e., the 2012 DFT poll list.[31] The

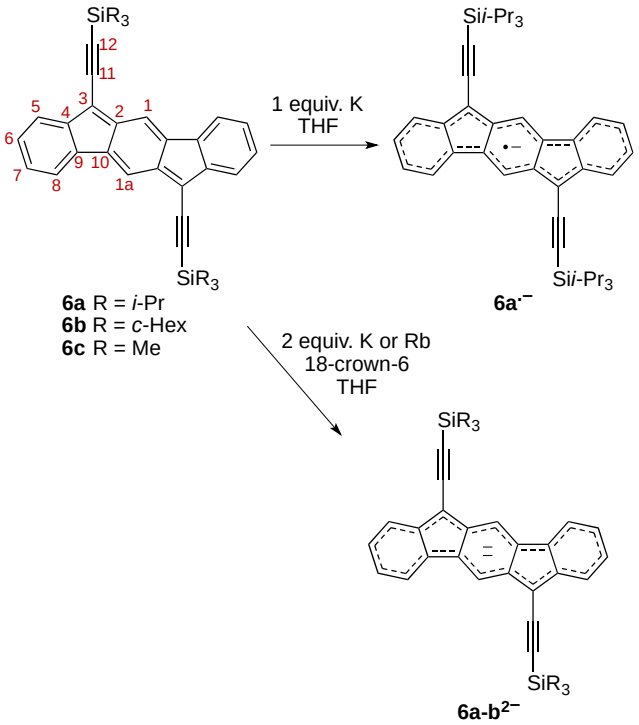


**Scheme 1**. Synthesis of Indeno[1,2-*b*]fluorene Anion Radical (**6a**$^{\bullet-}$) and Dianion (**6a-b**$^{2-}$). Atom numbering scheme used throughout this chapter shown in red.

functionals considered are the generalized gradient approximation functionals (GGA) BP86,[32,33] BLYP,[32] PBE[34] and PW91.[35] The hybrid GGA functionals used are BHandHLYP,[36] B3PW91,[37] B3LYP,[38] HSE06,[39–41] PBE0[42–44] and mPW1PW91.[45] The hybrid meta GGA functionals used are M06,[46] M06-2X,[46] M06-L,[47] M05,[48] M05-2X[49] and τ-HCTH.[50] Dispersion corrected functionals used are B97-D[51] and ωB97X-D.[52,53] Range separated functionals used are LC-ωPBE[54–56] and CAM-B3LYP.[57] Hartree-Fock (HF) provides a reference as a simple *ab initio* method alongside the DFT methods. All calculations were restricted to $C_2$ symmetry and positions will only be referred to by the lowest numbering with the knowledge that it also refers to the other symmetrically equivalent position. These methods were used as implemented in Gaussian 09 Revision C.01 and all calculations were done for the gas phase molecules.[58] For computational ease the trialkylsilyl groups of **6a-b** were truncated as a trimethylsilyl group (**6c**) since we have shown previously that altering the trialkylsilyl functionality has very little effect on the electronics, which are dominated by the π system.[59]

**Experimental and calculated structures for the neutral and dianion IF 6.**

Single crystals of **6a** suitable for X-ray diffraction study were obtained from $CHCl_3$; the molecular structure and crystal packing are shown in Figure 2. The bond lengths, along with those previously reported for the structure of **6b**,[60] are compiled in Table 1. Unlike most other bisethynylated IF derivatives,[8] both **6a** and **6b** pack in such a way that the bulky trialkylsilyl groups are situated over the IF core unit of neighboring molecules (CH···π contacts start at ca. 2.69 Å), effectively preventing any π-π stacking within the crystal lattice (closest π-π contacts >3.7 Å).

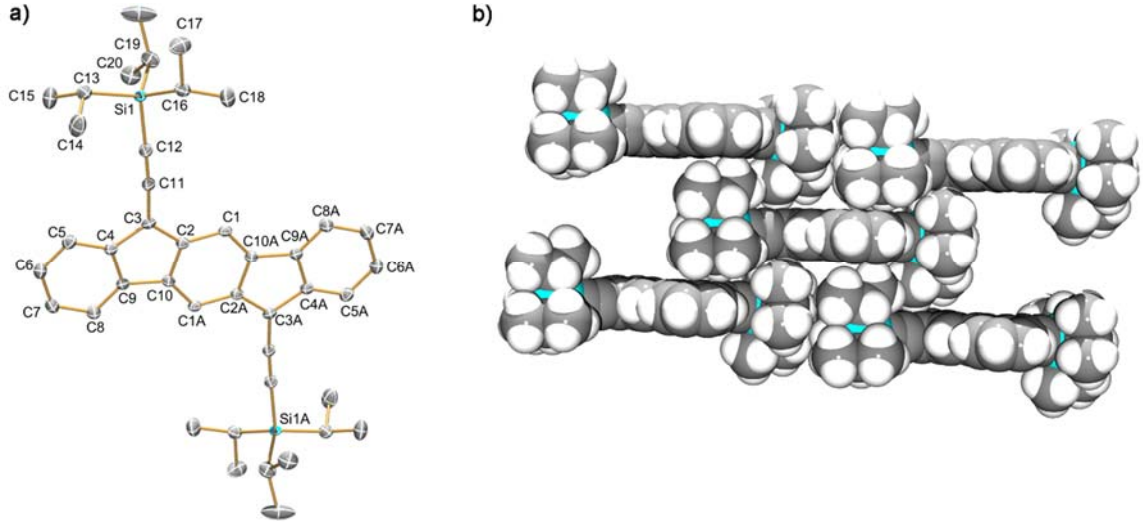


**Figure 2.** Molecular structure (left) and crystal packing (right) of IF **6a**; hydrogen atoms in molecular structure omitted for clarity. Ellipsoids drawn at the 30% probability level.

Fortunately, we were able to obtain single crystals suitable for X-ray diffraction of dianion $\mathbf{6b^{2-}}$ via reduction with Rb in the presence of 18-crown-6, whereas analogous reaction conditions did not afford suitable crystals of $\mathbf{6a^{2-}}$. As depicted in Figure 3, two crystallographically independent molecules were found in the solved structure, where the two Rb atoms exhibit either $\eta^6$-coordination (left) or $\eta^2$-coordination (right), illustrating flexibility of the dianion in alkali metal binding.

A close-up view of the indenofluorene core of $\mathbf{6b^{2-}}$ with the alkynes and crown ethers removed (Figure 4, Table 1) clearly shows the two different coordination motifs, where both $Rb^+$ cations are either $\eta^6$-coordinated to the central six-membered ring

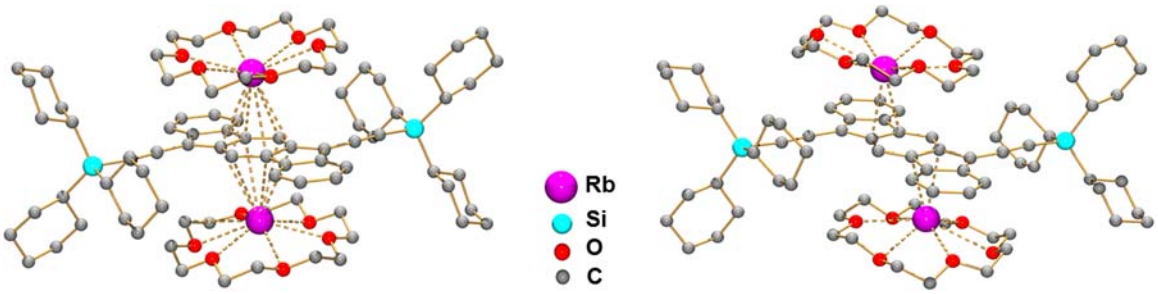


**Figure 3.** Molecular structure of **6b**$^{2-}$ exhibiting $\eta^6$-coordination (left) and $\eta^2$-coordination (right) of the $Rb^+$ cations; hydrogen atoms are omitted for clarity. Same atom color-coding scheme is used in Figure 4.

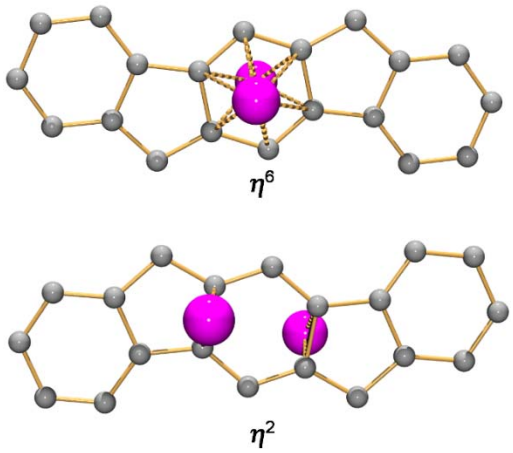


**Figure 4.** Close-up view of indenofluorene core of **6b**$^{2-}$ with both $Rb^+$ ions either (top) $\eta^6$-coordinated to the central six-membered ring or (bottom) $\eta^2$-side-coordinated to the central six-membered ring.

(3.216(7)–3.370(7) Å) or side-coordinated on opposite ends of the central six-membered ring (3.048(6)–3.133(6) Å) with additional longer contacts to the adjacent C-atoms of five- and six-membered rings (3.364(6)–3.637(7) Å). The corresponding Rb···C distances are comparable with those measured in the π-adducts of rubidium(I) with planar and non-planar polyaromatic hydrocarbons.[61,62,63] In contrast, the X-ray structures of both the $[(Li^+)_2(OEt_2)_2]$ and $[(K^+)_2(18\text{-crown-}6)_2]$ complexes of **7**$^{2-}$ show the alkali metals to be $\eta^5$-coordinated to the five-membered rings.[18] The differences in the X-ray determined bond lengths between the $\eta^2$ and $\eta^6$ isomers of **6b**$^{2-}$ are minimal and lie below the error in the data.

In the solid-state structure, additional intramolecular interactions can be identified between the crown ether and the planar surface of the dianion. In the case of $\eta^2$-bound complex, short CH···π contacts are observed with the 5-membered rings (2.379(9) Å to the centroid of 5-membered ring). Slightly longer CH···π contacts are found with the peripheral benzene rings of the $\eta^6$-bound complex (2.706(9) Å to the centroid of 6-membered ring). While alkali metal cations are generally considered to be good electrostatic probes of electron density distribution over the hydrocarbon surface[64-66] the crown ether interactions with the π-system also play a crucial role and may be responsible for specific positioning of the cationic units over the negatively charged hydrocarbon surfaces.[62,67] The observation of two different coordination modes in $\mathbf{6b}^{2-}$ is a result of such interplay between $Rb^+$···π and CH···π interactions with the negatively charged surface of the indenofluorene core.

Unlike the structure of **7**, which was discovered to be a rare example of a nonalternant (i.e., delocalized) antiaromatic compound,[68] benzo-fusion to the indacene core affords the alternant *p*-xylylene motif found experimentally (X-ray) and reproduced computationally (B3LYP) in the indeno[1,2-*b*]fluorenes.[12,13,15] Typically, bonds 1-10a and 2-3 are short (1.35–1.39 Å) and bond 1-2 is long (1.42–1.43 Å). Upon two-fold reduction of **6b**, the lengths of bonds 1-2 and 1-10a in $\mathbf{6b}^{2-}$ become nearly homogenous (1.386–1.396 Å), suggesting regeneration of a benzenoid configuration within the central six-membered ring. In addition, bond 2-3 is lengthened and bonds 3-4 and 9-10 are significantly shortened, implicating the formation of a cyclopentadiene-like aromatic anion in each five-membered ring. As a result, the entire hydrocarbon now obeys Hückel's rule with a total of 22 π-electrons within the pentacyclic structure. In comparison, the geometrical changes upon reduction of **7** to $\mathbf{7}^{2-}$ were much more modest, where the bridging bond (bond 2-10 in the case of **6**) increased by 0.023 Å and all other bond lengths possessed differences less than 0.011 Å;[18,68] the length of bond 2-10 is essentially unchanged in the case for **6b** to $\mathbf{6b}^{2-}$. Notably, the planarity of the ligand skeleton has not changed upon addition of 2 electrons and binding of $Rb^+$ ions. The average deviation of C-atoms from the least-squares plane passing through all atoms of the ligand is less than 0.02 Å in both the neutral and charged states.

**Table 1**. Comparison of the Bond Distances (Å) of **6a**, **6b** and **6b**$^{2-}$ from X-ray Data and B3LYP/6-31++G(d,p) Calculated Structures of **6c**, **6c**$^{\bullet-}$ and **6c**$^{2-}$.

| bond | neutral | | | | | radical anion | dianion | | | | |
|---|---|---|---|---|---|---|---|---|---|---|---|
| | X-ray (**6a**) | X-ray (**6b**) | avg X-ray | calc | UE | calc | X-ray ($\eta^6$) | X-ray ($\eta^2$) | avg X-ray | calc | UE |
| 1-10a | 1.354(6) | 1.364(5) | 1.359 | 1.369 | 0.010 | 1.387 | 1.386(9) | 1.391(9) | 1.389 | 1.401 | 0.013 |
| 1-2 | 1.424(6) | 1.423(5) | 1.424 | 1.428 | 0.004 | 1.412 | 1.396(9) | 1.392(9) | 1.394 | 1.402 | 0.008 |
| 2-3 | 1.382(6) | 1.395(5) | 1.389 | 1.399 | 0.011 | 1.431 | 1.439(9) | 1.407(9) | 1.423 | 1.459 | 0.036 |
| 3-4 | 1.472(6) | 1.469(5) | 1.471 | 1.468 | 0.002 | 1.452 | 1.414(9) | 1.446(9) | 1.430 | 1.439 | 0.009 |
| 4-5 | 1.379(6) | 1.372(5) | 1.376 | 1.392 | 0.016 | 1.403 | 1.394(9) | 1.405(10) | 1.400 | 1.399 | 0.000 |
| 5-6 | 1.384(6) | 1.394(5) | 1.389 | 1.400 | 0.011 | 1.397 | 1.369(9) | 1.380(10) | 1.375 | 1.396 | 0.022 |
| 6-7 | 1.374(7) | 1.370(5) | 1.372 | 1.401 | 0.029 | 1.408 | 1.397(9) | 1.413(9) | 1.405 | 1.412 | 0.007 |
| 7-8 | 1.389(6) | 1.394(5) | 1.392 | 1.403 | 0.012 | 1.399 | 1.387(9) | 1.367(9) | 1.377 | 1.401 | 0.024 |
| 8-9 | 1.373(6) | 1.370(5) | 1.372 | 1.392 | 0.020 | 1.397 | 1.392(8) | 1.388(9) | 1.390 | 1.399 | 0.009 |
| 9-10 | 1.481(6) | 1.465(5) | 1.473 | 1.467 | 0.006 | 1.458 | 1.439(9) | 1.449(9) | 1.444 | 1.453 | 0.009 |
| 4-9 | 1.410(6) | 1.406(5) | 1.408 | 1.422 | 0.014 | 1.432 | 1.434(9) | 1.433(9) | 1.434 | 1.443 | 0.010 |
| 2-10 | 1.456(5) | 1.437(5) | 1.447 | 1.458 | 0.012 | 1.447 | 1.442(9) | 1.454(9) | 1.448 | 1.442 | 0.006 |
| 3-11 | 1.411(6) | 1.411(5) | 1.411 | 1.407 | 0.004 | 1.398 | 1.441(10) | 1.425(10) | 1.433 | 1.385 | 0.048 |
| 11-12 | 1.206(6) | 1.211(5) | 1.209 | 1.227 | 0.019 | 1.234 | 1.210(9) | 1.220(9) | 1.215 | 1.245 | 0.030 |
| 12-Si | 1.843(4) | 1.845(4) | 1.844 | 1.846 | 0.002 | 1.816 | 1.821(8) | 1.821(8) | 1.821 | 1.786 | 0.035 |
| MUE | | | | | 0.011 | | | | | | 0.018 |

For the broader picture of this study, comparison of the bond lengths in the X-ray data and the gas phase computed structures in Table 1 reveals no notable discrepancies, and as expected, packing forces slightly alter the bond lengths from the gas phase calculated structures. IFs **6a** and **6b** demonstrate the effects of the packing forces have on the scaffold, with the largest effected bond difference of 0.019 Å for the 2-10 bond. In comparison, the largest error discrepancy between the calculated structure and the X-ray data for the neutral molecule is 0.029 Å with a mean unsigned error (MUE) of 0.011 Å. The calculated structure of $\mathbf{6c}^{2-}$ omitted explicit inclusion of the metal, and for the comparison with $\mathbf{6b}^{2-}$ the largest discrepancy is 0.048 Å with a MUE of 0.018 Å. The low MUE indicates that the geometries determined using B3LYP/6-31++G(d,p) are reasonable for further use in this study.

**EPR Spectrum of Anion Radical $\mathbf{6a}^{\bullet-}$.**

To probe the location of the electron density within an IF skeleton that is reduced with a single electron, we generated and characterized the anion radical $\mathbf{6a}^{\bullet-}$. Upon single electron reduction with K, the color of the solution changes from the deep purple of **6a** to a clear yellow of $\mathbf{6a}^{\bullet-}$. The experimental EPR spectrum of $\mathbf{6a}^{\bullet-}$ along with the simulated spectrum are shown in Figure 5; the hyperfine coupling present in the EPR spectrum was simulated with the EasySpin[69] package utilizing MATLAB code.[70] The close agreement between simulation and experiment is demonstrated by an $R^2$ value of 0.987.

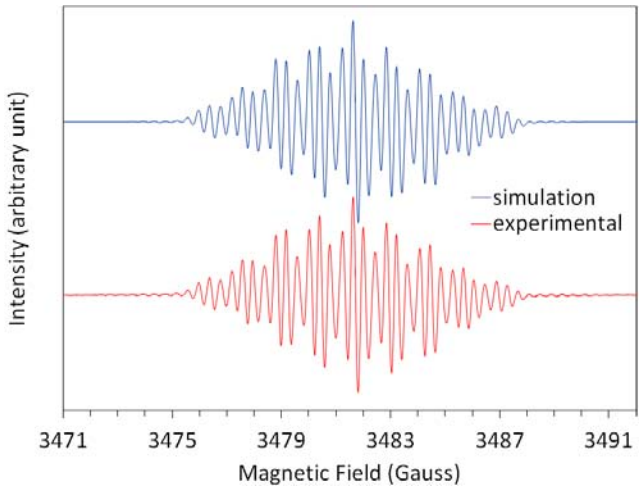


**Figure 5.** Experimental and simulated EPR spectrum of $\mathbf{6a}^{\bullet-}$ and using two of each of the HFCCs listed in Table 2.

**Table 2.** Calculated HFCCs for **6c**$^{\bullet-}$ Using 6-311++G(2df,2pd) Basis Set.

| method | position | | | | | | MUE[a] | MSE |
|---|---|---|---|---|---|---|---|---|
| | 1 | 5 | 6 | 7 | 8 | 12 | | |
| HF | -11.26 | -19.94 | 18.78 | -19.50 | 18.69 | 17.24 | 15.89 | 15.89 |
| M05 | -4.70 | -2.67 | 1.44 | -2.97 | 1.54 | 2.76 | 1.43 | 1.00 |
| LC-ωPBE | -3.41 | -2.45 | 1.72 | -2.63 | 1.77 | 3.72 | 1.04 | 0.94 |
| BHandHLYP | -3.44 | -2.36 | 1.57 | -2.56 | 1.61 | 4.18 | 0.94 | 0.94 |
| M06 | -3.83 | -1.90 | 0.73 | -2.26 | 0.80 | 2.22 | 0.89 | 0.28 |
| M06-L | -3.53 | -1.77 | 0.52 | -2.26 | 0.63 | 2.90 | 0.64 | 0.26 |
| BLYP | -1.90 | -0.90 | 0.17 | -1.15 | 0.24 | 1.95 | 0.63 | -0.63 |
| BP86 | -1.91 | -0.92 | 0.19 | -1.19 | 0.26 | 2.04 | 0.60 | -0.60 |
| PBE | -1.96 | -0.95 | 0.19 | -1.22 | 0.26 | 2.07 | 0.57 | -0.57 |
| PW91 | -1.97 | -0.95 | 0.19 | -1.22 | 0.27 | 2.09 | 0.57 | -0.57 |
| ωB97X-D | -2.89 | -1.50 | 0.76 | -1.66 | 0.80 | 2.56 | 0.51 | 0.01 |
| CAM-B3LYP | -2.76 | -1.57 | 0.85 | -1.75 | 0.90 | 3.03 | 0.47 | 0.13 |
| mPW1PW91 | -2.71 | -1.52 | 0.73 | -1.76 | 0.80 | 3.18 | 0.39 | 0.10 |
| τ-HCTH | -2.76 | -1.39 | 0.39 | -1.68 | 0.48 | 2.53 | 0.37 | -0.14 |
| PBE0 | -2.66 | -1.47 | 0.69 | -1.72 | 0.76 | 3.10 | 0.37 | 0.06 |
| M06-2X | -2.72 | -1.21 | 0.33 | -1.43 | 0.40 | 2.35 | 0.36 | -0.27 |
| M05-2X | -2.65 | -1.30 | 0.54 | -1.44 | 0.62 | 2.60 | 0.36 | -0.15 |
| HSE06 | -2.62 | -1.47 | 0.68 | -1.72 | 0.75 | 3.11 | 0.36 | 0.04 |
| B97-D | -2.52 | -1.24 | 0.30 | -1.53 | 0.39 | 2.26 | 0.32 | -0.31 |
| B3LYP | -2.35 | -1.21 | 0.47 | -1.44 | 0.53 | 2.64 | 0.32 | -0.24 |
| B3PW91 | -2.50 | -1.33 | 0.56 | -1.58 | 0.63 | 2.88 | 0.29 | -0.10 |
| expt[b] | 2.48 | 1.26 | 0.37 | 1.53 | 0.40 | 4.05 | | |

[a] Descending order with respect to MUE. [b] Experimental values are for **6a**$^{\bullet-}$.

**Table 3**. Spin Densities of **6a**$^{\bullet-}$ ($\rho_C$) as Related to the Experimental HFCC ($a_H$) and DFT Calculated Values of **6c**$^{\bullet-}$.

| position | $a_H$ | Q | $\rho_C$ | B3PW91 Mulliken spin density |
|---|---|---|---|---|
| 1 | 2.48 | | 0.102 | 0.101 |
| 5 | 1.26 | 24.2 | 0.052 | 0.052 |
| 6 | 0.37 | | 0.015 | -0.027 |
| 7 | 1.53 | | 0.063 | 0.070 |
| 8 | 0.40 | | 0.017 | -0.029 |
| | $a_{Si}$ | | | |
| 12 | 4.05 | 24.4 | 0.166 | 0.166 |

Interestingly, when the reduction was attempted using HMPA as the solvent, **6a** was reduced to **6a**$^{\bullet-}$ by the HMPA as it was distilled into the apparatus, illustrating the high electron affinity of **6a**.

We next compared the experimental hyperfine coupling constants (HFCCs) of **6a**$^{\bullet-}$ with calculated values for **6c**$^{\bullet-}$ to assess the ability of various DFT functionals to determine these numbers. The geometry used for calculating HFCCs was optimized using UB3LYP/6-31++G(d,p). Single point energies were then calculated with each method using a relatively large 6-311++G(2df,2pd) balanced Pople basis set of triple zeta quality and diffuse functions on all atoms, since it is known that the HFCC is critically dependent on the description of the Kohn-Sham wavefunction close to the nucleus and the size of the basis set.[71] The absolute sign of the HFCCs was not experimentally determined but for comparison purposes the sign was assumed to be the same as the calculated value. The MUE and mean signed error (MSE) were used for analyzing the agreement between the computed values and experimentally determined values. The data reveals the best three performing functionals were B3PW91, B3LYP, and B97-D with several others performing quite well. It is also clear that HF does a poor job describing the HFCCs for this hydrocarbon.

Unfortunately, there are many sites on **6a**$^{\bullet-}$ that are not measurable using EPR due to the relatively few spin active nuclei acting as electron density probes around the scaffold. Nevertheless the location of the spin densities for the measured sites can be used to determine the unpaired electrons spin density in parts of the π-system. Experimental spin densities can be determined by applying the McConnell equation (Eq. 1)

Eq 1. $$a_X = Q\rho_X$$

where the experimental HFCC ($a_X$) is related to the spin density ($\rho_X$) using the proportionality factor (Q). Using $Q_H = 24.2$ and $Q_{Si} = 24.4$ was found to give spin densities that agree well with the B3PW91 results as shown in Table 3. This good agreement lends credence to the use of the B3PW91 method as a computational tool to evaluate spin density. The resulting spin density plot (Figure 6) reveals that the spin density has slightly higher density on the central indacene motif and on the ethynyl π-system than the peripheral benzene rings. Interestingly, this is consistent with the Rb-binding sites observed also in the X-ray crystal structure of **6b**. The LUMO density map of the neutral species is nearly identical to the SOMO density plot and slightly reminiscent of the spin density plot, and thus seems a reasonable first approximation to the location of the unpaired electron as shown in Figure 6.

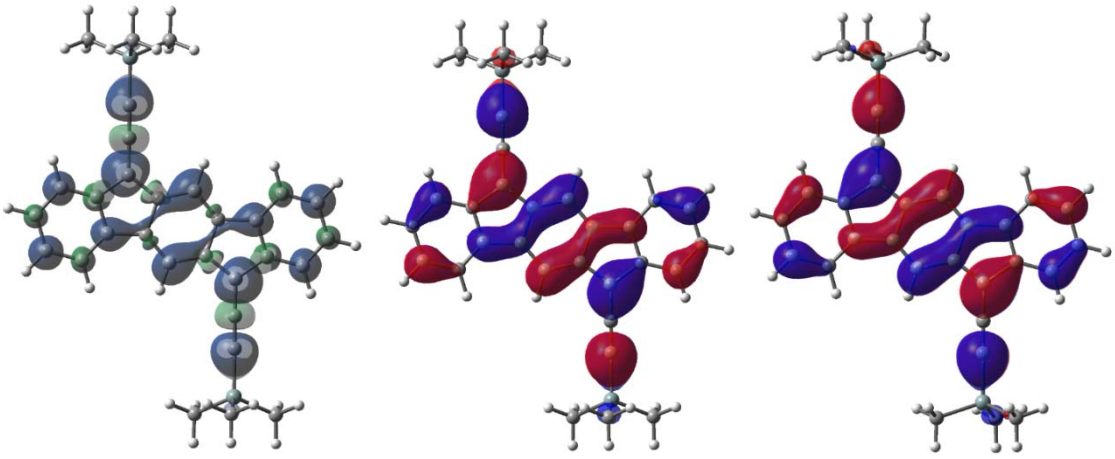

**Figure 6.** B3PW91 spin density plot (left) and SOMO density plot (center) for **6c**$^{\bullet-}$ and LUMO density plot (right) for **6c**.

**NMR Spectra of Neutral and Dianion IF 6**.

We successfully obtained $^{1}H$ and $^{13}C$ NMR data for dianion **6a**$^{2-}$, which was generated by reduction of **6a** with K in THF-d$_8$ in the presence of 18-crown-6. Comparison of the methine protons of the neutral species to those in the dianion (Figure 7) clearly shows that the most affected hydrogen atom is located on position 1. The deshielded hydrogen shifts downfield by ca. 1 ppm, which is indicative of the newly introduced diatropic ring current that results from the addition of 2 electrons to make a 22 π-electron species. An even greater downfield shift of the analogous protons was observed upon reduction of **7** to **7**$^{2-}$ ($\Delta\delta$ ~1.4 ppm).[18] This diatropic ring current also deshields H8 and H5 upon two-electron reduction from **6a** to **6a**$^{2-}$ as indicated by ca. 0.5 and 0.3 ppm shifts downfield, respectively. In contrast, H6 and H7 become shielded and shift upfield by 0.2 and 0.6 ppm respectively.

As one might expect, most of the $^{13}C$ NMR peaks of **6a**$^{2-}$ are significantly shielded in comparison to the corresponding peaks in **6a**, attributable to the increased electron density (Tables 6 and 7). This effect is most evident in carbon 3 of the pentacyclic skeleton, which shifts upfield by more than 50 ppm, suggesting considerable anionic character. Interestingly, alkyne carbons 11 and 12 are deshielded ($\Delta\delta$ ~23.5 ppm) and shielded ($\Delta\delta$ ~21.4 ppm), respectively, suggesting some delocalization of the negative charge out onto C12 that could be stabilized by the alpha-silicon atom; however, the solid state data for both the $\eta^2$ and $\eta^6$ isomers of **6b**$^{2-}$ indicate such a contribution is minimal.

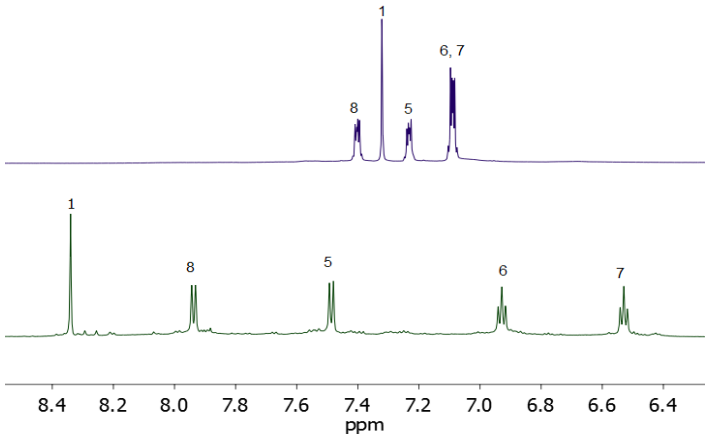


**Figure 7.** Partial $^{1}H$ NMR spectra of the methine protons of neutral **6a** (top) and dianion **6a**$^{2-}$ (bottom) in THF-d$_8$ with assigned hydrogen position listed above peaks.

**Table 4**. Calculated $^{1}$H NMR Chemical Shifts for 6c Using 6-311++G(2df,2pd)//B3LYP/6-31++G(d,p) Basis Set.

| method | position | | | | | MUE[a] | MSE |
|---|---|---|---|---|---|---|---|
| | 1 | 5 | 6 | 7 | 8 | | |
| HF | 7.82 | 7.65 | 7.42 | 7.39 | 7.82 | 0.39 | 0.39 |
| M06-2X | 8.18 | 8.02 | 7.91 | 7.71 | 8.16 | 0.77 | 0.77 |
| M05-2X | 8.05 | 8.06 | 7.59 | 7.77 | 8.08 | 0.68 | 0.68 |
| LC-ωPBE | 7.80 | 7.70 | 7.57 | 7.56 | 7.89 | 0.48 | 0.48 |
| M05 | 7.78 | 7.46 | 7.48 | 7.37 | 7.98 | 0.39 | 0.39 |
| ωB97X-D | 7.62 | 7.47 | 7.33 | 7.30 | 7.70 | 0.26 | 0.26 |
| CAM-B3LYP | 7.56 | 7.49 | 7.31 | 7.30 | 7.62 | 0.23 | 0.23 |
| BHandHLYP | 7.53 | 7.47 | 7.25 | 7.24 | 7.58 | 0.19 | 0.19 |
| M06-L | 7.04 | 7.01 | 7.03 | 7.03 | 7.22 | 0.16 | -0.16 |
| τ-HCTH | 7.11 | 7.16 | 6.97 | 6.95 | 7.19 | 0.15 | -0.15 |
| M06 | 7.40 | 7.25 | 7.34 | 7.24 | 7.61 | 0.14 | 0.14 |
| PBE0 | 7.44 | 7.42 | 7.24 | 7.23 | 7.52 | 0.14 | 0.14 |
| B97-D | 7.13 | 7.16 | 6.98 | 6.96 | 7.22 | 0.14 | -0.14 |
| mPW1PW91 | 7.41 | 7.40 | 7.22 | 7.21 | 7.50 | 0.12 | 0.12 |
| BLYP | 7.15 | 7.16 | 6.98 | 6.97 | 7.26 | 0.12 | -0.12 |
| HSE06 | 7.41 | 7.38 | 7.20 | 7.19 | 7.51 | 0.11 | 0.11 |
| B3PW91 | 7.37 | 7.36 | 7.18 | 7.17 | 7.46 | 0.08 | 0.08 |
| BP86 | 7.22 | 7.24 | 7.06 | 7.04 | 7.32 | 0.05 | -0.05 |
| PW91 | 7.23 | 7.23 | 7.08 | 7.07 | 7.33 | 0.04 | -0.04 |
| PBE | 7.25 | 7.26 | 7.10 | 7.08 | 7.35 | 0.03 | -0.02 |
| B3LYP | 7.32 | 7.30 | 7.11 | 7.09 | 7.40 | 0.02 | 0.02 |
| expt[b] | 7.32 | 7.23 | 7.09 | 7.09 | 7.40 | | |

To further test the DFT functionals under consideration, we calculated the $^{1}$H and $^{13}$C NMR chemical shifts and compared these with the experimental data. Since the structure in question is a PCH, solvent effects should have minimal influence on the NMR chemical shifts.[13] The geometry of **6c**$^{2-}$ was minimized using RB3LYP/6-31++G(d,p) and values were referenced to tetramethylsilane (0 ppm) using the same method. Here again in order to minimize basis set effects, the relatively large 6-311++G(2df,2pd) basis set was used to assess the various methods without having to worry about fortuitous error cancellation using a smaller basis set. The calculations were performed using the Gauge-Independent Atomic Orbital (GIAO) method and the complete data are compiled in Tables 4-7.

**Table 5**. Calculated $^{1}$H NMR Chemical Shifts for **6c**$^{2-}$ Using 6-311++G(2df,2pd)//B3LYP/6-31++G(d,p) Basis Set.

| method | position | | | | | MUE[a] | MSE |
|---|---|---|---|---|---|---|---|
| | 1 | 5 | 6 | 7 | 8 | | |
| HF | 8.72 | 7.71 | 7.18 | 6.52 | 8.56 | 0.30 | 0.29 |
| M06-2X | 9.28 | 8.22 | 7.65 | 6.98 | 8.89 | 0.76 | 0.76 |
| M05-2X | 9.20 | 8.34 | 7.27 | 7.15 | 8.81 | 0.71 | 0.71 |
| M05 | 8.91 | 7.62 | 7.25 | 6.68 | 8.74 | 0.40 | 0.40 |
| LC-ωPBE | 8.72 | 7.79 | 7.22 | 6.70 | 8.52 | 0.34 | 0.34 |
| PBE0 | 8.60 | 7.67 | 7.01 | 6.65 | 8.29 | 0.20 | 0.20 |
| ωB97X-D | 8.66 | 7.64 | 7.07 | 6.58 | 8.39 | 0.22 | 0.22 |
| CAM-B3LYP | 8.58 | 7.65 | 7.05 | 6.60 | 8.34 | 0.20 | 0.20 |
| BHandHLYP | 8.59 | 7.64 | 7.02 | 6.57 | 8.34 | 0.19 | 0.19 |
| HSE06 | 8.59 | 7.63 | 6.98 | 6.64 | 8.28 | 0.18 | 0.18 |
| M06-L | 8.16 | 7.23 | 6.69 | 6.33 | 7.97 | 0.18 | -0.17 |
| mPW1PW91 | 8.57 | 7.64 | 6.99 | 6.64 | 8.26 | 0.17 | 0.17 |
| M06 | 8.52 | 7.49 | 7.06 | 6.50 | 8.31 | 0.14 | 0.13 |
| B3PW91 | 8.53 | 7.61 | 6.94 | 6.60 | 8.21 | 0.13 | 0.13 |
| PBE | 8.46 | 7.55 | 6.91 | 6.63 | 8.12 | 0.10 | 0.09 |
| PW91 | 8.44 | 7.53 | 6.91 | 6.64 | 8.10 | 0.09 | 0.08 |
| B3LYP | 8.47 | 7.54 | 6.91 | 6.56 | 8.18 | 0.09 | 0.08 |
| BP86 | 8.44 | 7.52 | 6.86 | 6.57 | 8.08 | 0.08 | 0.05 |
| τ-HCTH | 8.32 | 7.45 | 6.78 | 6.51 | 7.97 | 0.05 | -0.04 |
| B97-D | 8.36 | 7.46 | 6.80 | 6.53 | 7.99 | 0.05 | -0.02 |
| BLYP | 8.35 | 7.44 | 6.82 | 6.54 | 8.03 | 0.05 | -0.01 |
| expt[b] | 8.34 | 7.49 | 6.93 | 6.53 | 7.94 | | |

[a] Descending order with respect to MUE. [b] Experimental values are for **6a**$^{2-}$.

The computational data clearly show there are several methods that perform well in predicting the chemical shift of the $^{1}$H NMR spectrum. Notably B3LYP, PBE, PW91 and BP86 had MSE and MUE of within 0.1 ppm of the measured $^{1}$H chemical shifts for both the dianion and neutral compound. The $^{13}$C NMR spectral prediction had three functionals with MSE and MUE below 5 ppm: B3LYP, B97-D and τ-HCTH. Interestingly in both cases, if a functional did a poor job predicting the chemical shift of the neutral species it typically performed equally poor for predicting the dianion data and vice versa.

Unfortunately, unambiguous assignment of the $^{13}$C NMR spectrum was not possible when interpreting COSY, HSQC, and HMBC spectra. This is due to the carbons located on the cyclopentadiene moiety lacking spin active nuclei to assist with clear

**Table 6**. Calculated $^{13}C$ NMR Chemical Shifts of Neutral **6c** Using 6-311++G(2df,2pd)//B3LYP/6-31++G(d,p) Basis Set.

| method | position | | | | | | | | | | | | MUE[a] | MSE |
|---|---|---|---|---|---|---|---|---|---|---|---|---|---|---|
| | 1 | 2 | 3 | 4 | 5 | 6 | 7 | 8 | 9 | 10 | 11 | 12 | | |
| HF | 129.25 | 150.30 | 134.78 | 151.13 | 129.74 | 135.62 | 135.44 | 128.58 | 145.24 | 142.36 | 96.09 | 119.38 | 7.77 | 6.87 |
| M05-2X | 146.55 | 169.03 | 155.62 | 173.05 | 147.30 | 155.91 | 154.62 | 144.72 | 164.21 | 158.42 | 114.97 | 142.49 | 25.95 | 25.95 |
| M06-2X | 141.90 | 165.96 | 154.88 | 170.15 | 143.91 | 148.33 | 149.81 | 142.92 | 161.65 | 160.24 | 114.49 | 140.31 | 23.26 | 23.26 |
| M05 | 128.27 | 151.90 | 138.02 | 151.84 | 131.38 | 134.65 | 138.30 | 129.59 | 150.20 | 150.33 | 116.86 | 133.80 | 11.64 | 11.64 |
| LC-ωPBE | 133.06 | 153.17 | 140.11 | 154.99 | 133.27 | 139.23 | 139.13 | 131.92 | 131.92 | 147.61 | 105.41 | 121.59 | 10.80 | 9.66 |
| CAM-B3LYP | 130.06 | 152.03 | 138.15 | 154.64 | 131.34 | 137.25 | 137.66 | 129.11 | 148.84 | 147.04 | 104.58 | 121.54 | 9.73 | 9.73 |
| BHandHLYP | 129.10 | 150.79 | 136.48 | 153.10 | 130.46 | 136.03 | 136.57 | 128.15 | 147.51 | 145.29 | 102.52 | 121.50 | 8.50 | 8.50 |
| HSE06 | 126.46 | 148.36 | 134.57 | 151.14 | 128.76 | 134.12 | 134.86 | 126.03 | 145.84 | 144.34 | 107.27 | 124.82 | 7.59 | 7.59 |
| B3PW91 | 126.32 | 148.07 | 134.39 | 151.00 | 128.33 | 133.80 | 134.54 | 125.73 | 145.54 | 144.07 | 107.34 | 124.01 | 7.31 | 7.31 |
| M06 | 124.38 | 147.75 | 135.07 | 150.58 | 128.48 | 129.03 | 133.14 | 126.07 | 145.49 | 146.73 | 109.18 | 127.14 | 7.30 | 7.30 |
| PBE0 | 126.49 | 148.02 | 134.43 | 150.77 | 128.48 | 133.98 | 134.64 | 125.88 | 145.39 | 143.81 | 106.82 | 124.03 | 7.28 | 7.28 |
| mPW1PW91 | 126.47 | 148.02 | 134.37 | 150.90 | 128.59 | 134.00 | 134.71 | 126.04 | 145.44 | 143.51 | 106.60 | 123.66 | 7.24 | 7.24 |
| ωB97X-D | 128.26 | 149.07 | 135.98 | 151.27 | 128.89 | 134.15 | 135.18 | 126.79 | 145.86 | 144.78 | 103.28 | 118.44 | 7.21 | 7.21 |
| BLYP | 122.80 | 147.54 | 132.48 | 150.89 | 126.32 | 132.21 | 133.15 | 123.16 | 145.51 | 144.41 | 109.09 | 124.20 | 6.36 | 6.36 |
| PW91 | 122.66 | 146.49 | 131.95 | 149.74 | 126.44 | 132.10 | 133.04 | 123.40 | 144.47 | 143.05 | 110.24 | 125.97 | 6.18 | 6.18 |
| PBE | 122.66 | 146.12 | 131.79 | 149.33 | 126.06 | 131.81 | 132.62 | 123.03 | 144.09 | 143.03 | 110.41 | 126.07 | 5.97 | 5.97 |
| BP86 | 122.63 | 145.95 | 131.75 | 149.31 | 125.78 | 131.43 | 132.29 | 122.78 | 143.96 | 142.99 | 110.00 | 125.26 | 5.72 | 5.72 |
| M06-L | 115.05 | 136.41 | 121.72 | 139.10 | 118.46 | 119.03 | 121.85 | 115.52 | 134.12 | 136.50 | 106.56 | 117.09 | 4.78 | -2.83 |
| B3LYP | 122.70 | 145.84 | 131.38 | 148.82 | 125.13 | 130.81 | 131.61 | 122.30 | 143.35 | 141.75 | 102.91 | 119.56 | 4.23 | 4.23 |
| τ-HCTH | 117.45 | 139.27 | 125.46 | 142.26 | 120.40 | 125.86 | 126.68 | 117.51 | 137.17 | 136.04 | 103.68 | 118.14 | 2.10 | -0.46 |
| B97D | 119.03 | 142.14 | 127.90 | 145.28 | 122.28 | 127.73 | 128.67 | 119.26 | 140.10 | 138.95 | 105.32 | 119.63 | 2.00 | 1.74 |
| expt[b] | 120.36 | 140.31 | 128.14 | 143.04 | 122.23 | 126.47 | 128.34 | 118.76 | 138.73 | 137.10 | 101.48 | 110.47 | | |

[a] Descending order with respect to MUE. [b] Experimental values are for **6a**.

**Table 7**. Calculated $^{13}C$ NMR Chemical Shifts of **6c**$^{2-}$ Using 6-311++G(2df,2pd)//B3LYP/6-31++G(d,p) Basis Set.

| neutral | | | anion | | | dianion | | |
|---|---|---|---|---|---|---|---|---|
| method | eV (nm) | UE (eV) | method | eV (nm) | UE (eV) | method | eV (nm) | UE (eV) |
| HF | 2.37 (523) | 0.179 | HF | 0.746 (1660) | 0.363 | HF | 2.03 (611) | 0.207 |
| BLYP | 1.91 (651) | 0.285 | M06-L | 1.34 (923) | 0.235 | LC-ωPBE | 2.75 (451) | 0.925 |
| PW91 | 1.91 (650) | 0.283 | BP86 | 1.33 (933) | 0.221 | M06 | 1.10 (1130) | 0.728 |
| τ-HCTH | 1.91 (649) | 0.281 | PBE | 1.33 (934) | 0.218 | PW91 | 1.15 (1080) | 0.676 |
| B97-D | 1.91 (649) | 0.279 | BLYP | 1.33 (935) | 0.217 | BLYP | 1.16 (1070) | 0.668 |
| BP86 | 1.91 (649) | 0.279 | PW91 | 1.32 (938) | 0.213 | ωB97X-D | 2.35 (527) | 0.529 |
| PBE | 1.91 (648) | 0.278 | B97-D | 1.32 (943) | 0.206 | B97-D (1) | 1.31 (950) | 0.519 |
| M06-L | 2.00 (619) | 0.188 | M06-2X | 1.31 (946) | 0.202 | CAM-B3LYP | 2.33 (531) | 0.511 |
| M06 | 2.02 (613) | 0.168 | τ-HCTH | 1.30 (952) | 0.193 | τ-HCTH | 1.33 (932) | 0.493 |
| M05 | 2.03 (610) | 0.157 | B3LYP | 1.30 (954) | 0.191 | PBE | 1.34 (928) | 0.488 |
| B3LYP | 2.04 (609) | 0.155 | HSE06 | 1.30 (954) | 0.190 | B97-D (2) | 1.34 (923) | 0.480 |
| B3PW91 | 2.04 (607) | 0.148 | B3PW91 | 1.29 (958) | 0.185 | M05-2X | 2.29 (542) | 0.465 |
| HSE06 | 2.06 (601) | 0.128 | PBE0 | 1.28 (970) | 0.169 | M06-L | 1.46 (847) | 0.359 |
| LC-ωPBE | 2.31 (536) | 0.121 | mPW1PW91 | 1.27 (975) | 0.163 | BHandHLYP | 2.14 (579) | 0.315 |
| mPW1PW91 | 2.07 (598) | 0.119 | LC-ωPBE | 0.951 (1300) | 0.158 | BP86 (1) | 1.56 (795) | 0.263 |
| PBE0 | 2.07 (598) | 0.118 | M05-2X | 1.25 (996) | 0.136 | BP86 (2) | 1.59 (778) | 0.230 |
| ωB97X-D | 2.16 (575) | 0.036 | M06 | 1.22 (1010) | 0.115 | B3LYP (1) | 1.63 (763) | 0.198 |
| CAM-B3LYP | 2.17 (572) | 0.023 | CAM-B3LYP | 1.17 (1060) | 0.058 | M06-2X | 2.00 (619) | 0.179 |
| BHandHLYP | 2.20 (565) | 0.005 | BHandHLYP | 1.14 (1090) | 0.033 | B3LYP (2) | 1.66 (747) | 0.163 |
| M05-2X | 2.20 (565) | 0.004 | M05 | 1.13 (1100) | 0.023 | HSE06 (1) | 1.69 (734) | 0.135 |
| M06-2X | 2.19 (565) | 0.002 | ωB97X-D | 1.12 (1110) | 0.008 | mPW1PW91 (1) | 1.72 (721) | 0.103 |
| expt | 2.19 (566) | | expt | 1.11 (1120) | | HSE06 (2) | 1.72 (719) | 0.100 |
| | | | | | | mPW1PW91 (2) | 1.75 (709) | 0.074 |
| | | | | | | M05 (2) | 1.89 (655) | 0.071 |
| | | | | | | PBE0 | 1.89 (656) | 0.068 |
| | | | | | | B3PW91 (2) | 1.89 (657) | 0.065 |
| | | | | | | M05 (1) | 1.86 (668) | 0.034 |
| | | | | | | B3PW91 (1) | 1.86 (668) | 0.032 |
| | | | | | | expt | 1.82 (680) | |

interpretation. The lack of definitive NMR spectral assignment and little data comparing many readily available DFT methods for assisting with NMR spectral assignment was partial motivation for the undertaking of this study.

**Electronic absorption spectra.**

As a final test we examined the electronic absorption spectra of the neutral, anion radical, and dianion of IF **6a** as these should serve as representative spectroscopic handles for the reduced molecule in electronic devices such as OPVs.[72] Experimental data was gathered by reducing **6a** with potassium in a cuvette and monitoring the progress via absorbance spectrum from the UV to the near infrared (NIR) as shown in Figure 8. The reduction state was a visual feast as the starting purple color of **6a** faded upon exposure to K to the very light yellow of $\mathbf{6a}^{\bullet-}$ and then to the light green of $\mathbf{6a}^{2-}$. The green hue of the dianion suggests that the weak peak at ca. 500-700 nm is likely responsible for this transition. The absorbance spectrum shows vibronic coupling for the lowest energy transition indicative of a small geometry change upon excitation.[73]

Again, the DFT functionals were assessed in their ability for predicting the low energy electronics transitions using the model system of **6c**, $\mathbf{6c}^{\bullet-}$ and $\mathbf{6c}^{2-}$ (Table 8). TD-DFT calculations were performed omitting Franck-Condon effects. The exclusion of Franck-Condon effects will cause the spectra for low energy transitions to be incorrectly modeled as vibronic effects clearly play an important role; thus, no attempt was made to

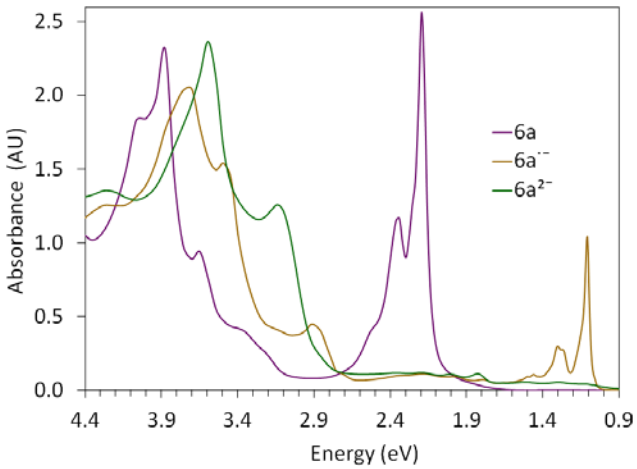


**Figure 8.** Electronic absorption spectra of **6a**, $\mathbf{6a}^{\bullet-}$ and $\mathbf{6a}^{2-}$.

assess the absorbance spectral prediction for the UV to the NIR and instead only the energy of the lowest energy transition is assessed.[29,74] The distribution of the vibronic coupling indicates that the lowest energy peak is likely the 0-0 peak and thus will be used as an estimate for the comparison with the calculated vertical excitation energy.[73]

In predicting the lowest energy transition in general, the functionals performed somewhat similarly for the neutral compound. A notable point is that the time-dependent calculations on **6c** find a triplet that is slightly lower in energy than the closed shell solution, contrary to experiment, for HF, BHandHLYP, PBE0, HSE06, LC-ωPBE, CAM-B3LYP, M05-2X, M05, M06, ωB97X-D and mPW1PW91. The lowest energy transition for the neutral molecule ωB97X-D, CAM-B3LYP, BHandHLYP, M05-2X, and M06-2X was found to be within 0.1 eV of the experimental value and for the anion radical CAM-B3LYP, BHandHLYP, M05, and ωB97X-D gave transition energies less than 0.1 eV from experiment.

The dianion proved to be a very challenging case for nearly all functionals with results varying significantly. Some of the results were without clear interpretation, so in cases where there were two absorbance energies that had similarly large oscillator strengths, both were listed and this is denoted by parenthesis and a number following the functionals that possessed this problem. From the data in Table 8, it is clear that mPW1PW91 (2), M05 (2), B3PW91 (2), M05 (1), B3PW91 (1), and HSE06 (2) gave results within 0.1 eV of the experimental values, but with ambiguity. The only functional that gave one result within 0.1 eV to the experimental value was PBE0.

**Conclusions**

We have synthesized and characterized derivatives of **6**, $\mathbf{6}^{\bullet-}$ and $\mathbf{6}^{2-}$ to explore the structure and electronics of the neutral and reduced indenofluorene scaffold. The NMR data reveal that reduction from the neutral to dianion introduces an aromatic ring current to the formerly antiaromatic indenofluorene, as evidenced by the nearly 1 ppm downfield shift of the proton at position 1. The X-ray data of $\mathbf{6b}^{2-}$ corroborate this finding, as the localized double bonds of the central indacene moiety in **6** become essentially delocalized. Interestingly, the specific coordination of rubidium ions plays a small role in

the bond lengths of **6b**$^{2-}$ as the $\eta^2$ and $\eta^6$ X-ray structures have RMSD difference of 0.03 Å when comparing only the carbons of the IF core.

The location of the unpaired electron of the anion radical is discerned from the EPR spectrum and interpreted with the aid of calculated DFT results. This information serves as a crude first approximation for the location of the unpaired electron in the singly reduced state of **6**, for example, in an OFET device behaving as an n-channel material. Likewise this can be a simple representation of the negatively charged IF in OPVs. Comparing the experimental results to twenty DFT methods reveals that there are several good functionals when predicting the HFCCs of the anion radical. Several functional performed well, with the three recommended functionals for HFCCs of PCHs are B97-D, B3LYP and B3PW91, all of which gave MUE of less than 0.32 Gauss. There is considerable room for improvement as errors in HFCCs of this magnitude strongly affect the appearance of the predicted spectrum. This could possibly be improved with basis sets that better describe the Kohn-Sham wavefunction close to the nucleus such as EPR-III, which is currently not available for silicon and thus not explored.[71] Additionally the NMR chemical shift prediction for the neutral and dianion revealed that B3PW91, BP86, PW91, PBE, and B3LYP gave MUE of less than 0.1 ppm for the neutral $^1$H NMR spectrum. The $^1$H NMR spectrum of the dianion had PBE, PW91, B3LYP, BP86, τ-HCTH, B97-D, and BLYP yield MUE within 0.1 ppm of the experimental values. The neutral $^{13}$C NMR spectrum had four functionals with MUE within 5 ppm of experimental values M06-L, B3LYP, τ-HCTH, and B97-D. The $^{13}$C spectrum of the dianion had PW91, PBE, BP86, B3LYP, B97-D, and τ-HCTH; thus, for NMR spectral prediction for PCHs, the recommendation would be either the B3LYP or τ-HCTH functional.

The absorbance transition energy prediction of the functionals was clear for the neutral and anion radical species; however, for the dianion the interpretation of calculated results was much more ambiguous with large disagreements between the functionals used. For the neutral species and anion radical ωB97X-D, CAM-B3LYP, and BH and HLYP all gave results with close agreement to experimental. The DFT calculated absorbance transition energies for the dianion were in general poor and the only

functional that seems the appropriate for this is PBE0, as the other functionals that were close to the experimental value gave unclear results.

Overall it is quite remarkable how close the computed values are considering that all of the calculations were completed for a single gas phase molecule. This study is an indicator that currently available DFT methods can be used for prediction of spectral properties of PCHs with reasonable accuracy and can thus be used for guiding synthesis in developing new PCHs with desired properties. Unfortunately, there does not appear to be one DFT method used in this study that gives results clearly in better agreement with experiment relative to the other methods considered and the DFT methods must be chosen on a case-by-case basis.

Bridge to Chapter V

Chapter IV represents the fundamental studies of the reduced states of indeno[1,2-*b*]fluorene. Chapter V expands on the fundamental studies by considering some of the photoexcited states and dynamics of the neutral systems providing rationale as to why these are non-emissive compounds.

CHAPTER V

# UNUSUALLY SHORT EXCITED STATE LIFETIMES OF INDENOFLUORENE AND FLUORENOFLUORENE DERIVATIVES VIA CONICAL INTERSECTION

This chapter was co-authored with Leah E. Shoer and Aaron G. Fix provided compound **3**. Michael R. Wasielewski and Michael M. Haley provided editorial and content advice.

## Discussion

There has been much interest in materials for organic electronics for the potential of easily-produced organic electronic devices.[1] Applications such as organic photovoltaics (OPVs) and field-effect transistors (OFETs) often require not only high efficiencies but also additional characteristics including processability, flexibility and photoactivity.[2–4] Numerous small-molecule systems have been developed toward this goal that employ extended conjugated centers.[5–9] One such molecular class of interest is

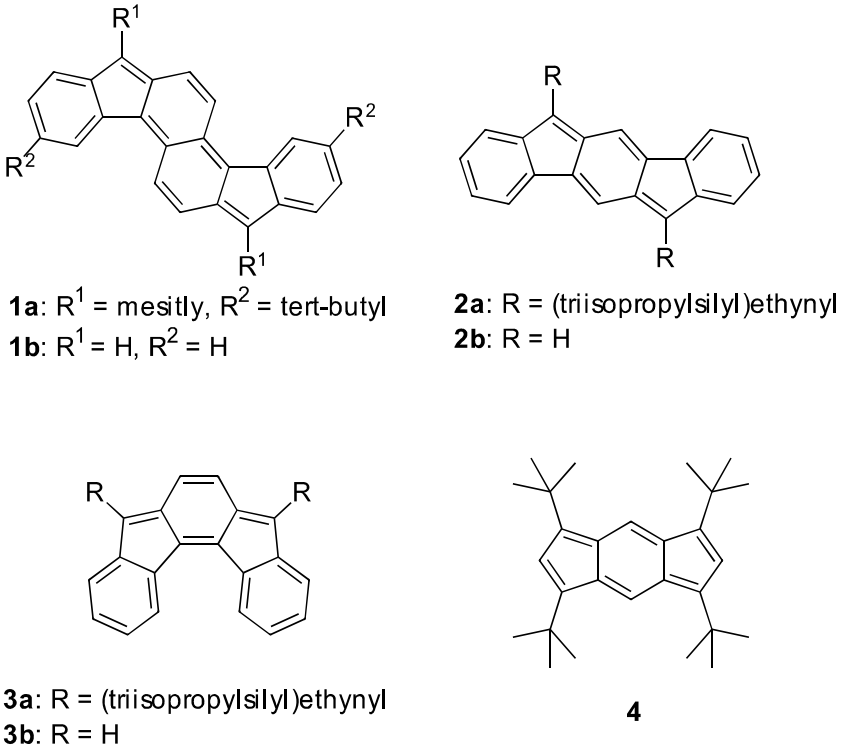


**Figure 1**. Structures of indenofluoene and fluorenofluorene derivatives investigated in this chapter (**1**-**3**) as well as that of related indenofluorene subunit, s-indacene (**4**).

the *p*-quinodimethane-containing indenofluorenes and related scaffolds (e.g., **1**–**3**, **Figure 1)**, which have recently been realized through synthesis.[10–16] Intriguingly, these compounds have been found to be non-emissive and thus we wished to examine their photoexcited states. One possible mechanism for non-emissive relaxation from a photoexcited state to the grounds state is singlet fission, proposed to be present in the expanded system fluorenofluorene (**1**), due to ideal state energies for singlet fission.[17] This process is particularly desirable in OPVs as it may boost the maximum power conversion efficiency and impede loss pathways from charge recombination.[18,19] Another plausible mechanism for the lack of emission is internal conversion through a conical intersection between the ground state, $S_0$, and the singlet first excited state, $S_1$. Such a mechanism is the cause for efficient internal conversion in **4**, a subunit of **2**.[20]

The first system explored using transient absorption spectroscopy in solution was fluoreno[4,3-*c*]fluorene derivative **1a**. The initial absorptive feature that appeared visible from approximately 675 nm to 800 nm (Figure S1a) is likely related to the $S_2$ state, as we have calculated the $S_0$ to $S_1$ transition is forbidden in this system (vide supra). Rapid internal conversion in less than a picosecond resulted in a blue-shifted absorptive feature corresponding to $S_1$, which significantly overlaps the ground state bleach from 470 nm to 650 nm. This lowest-lying excited state then decayed showing a remarkably short lifetime of $\tau = 14.0 \pm 5.7\times10^{-12}$ s (Figure 2a).

We also studied the related but smaller derivatives indeno[1,2-*b*]fluorene (**2a**) and indeno[2,1-*c*]fluorene (**3a**). Similar behavior in **2a** of sub-picosecond internal conversion from the $S_2$ state visible from 580 nm to 700 nm to the $S_1$ state followed by excited state decay was observed (Figure S2a). Once again, the lower excited state occupies a similar spectral region as the ground state bleach, from approximately 500 nm to 575 nm. The $S_1$ excited state lifetime of **2a** was $\tau = 9.7 \pm 0.9\times10^{-12}$ s (Figure 2b).

In **3a**, unlike **1a** and **2a**, the $S_0$ to $S_1$ transition is allowed. Instead of sub-picosecond intersystem crossing, a slower blue-shift in the region of 500 nm to 600 nm occurred in $\tau = 1.8$ ps (Figure S3a), which corresponds well to rates of intramolecular vibrational cooling to the lowest excited state observed in many systems.[21–23] This shift was followed by excited state decay in $\tau = 9.5 \pm 1.7\times10^{-12}$ s (Figure 2c). Thus, the same $S_1$ decay behavior was observed in solutions of **1a**, **2a** and **3a**, indicating picosecond

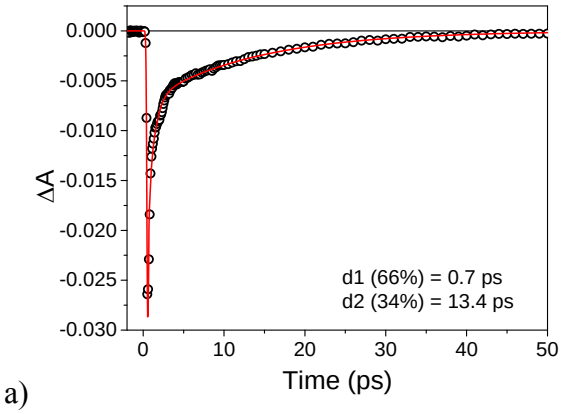


a)

b)

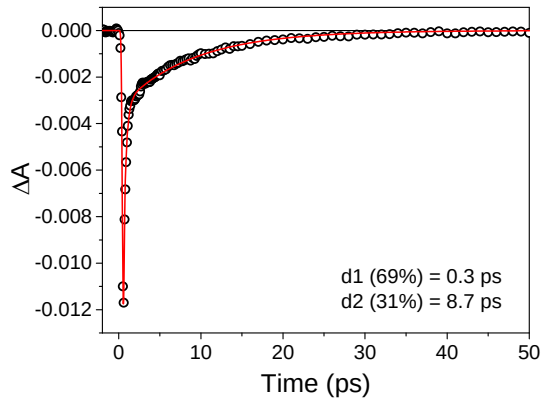


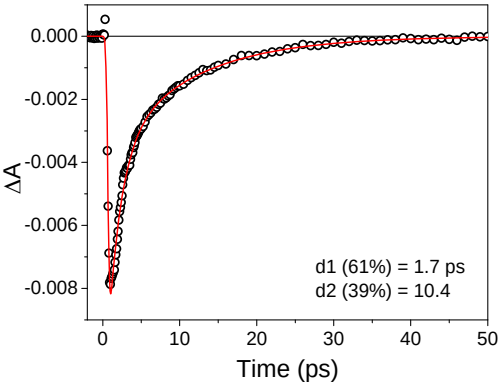


c)

**Figure 2**. Femtosecond transient absorption kinetics traces from the ground state bleach in a toluene solution of (a) **1a** at 653 nm, (b) **2a** at 529 nm, and (c) **3a** at 645 nm, showing recovery corresponding to rapid excited state decay pathways.

excited state decay is generic among these derivatives containing a de-aromatized core. The related subunit of indenofluorene, *s*-indacene derivative **4**, was found to have excited state lifetimes of $\tau = 18 \times 10^{-12}$ s and $\tau = 2.5 \times 10^{-12}$ s for the $S_1$ and $S_2$ states, respectively.

The lifetimes of **4** are similar to the excited states for the larger systems of this study, indicating a similar relaxation mechanism may be responsible.[24–26] The tens of picosecond excited state lifetimes explains why **1**-**4** are non-emissive, since fluorescence is not a competitive process at this time scale.[27]

To understand how rapid internal conversion of the excited state to the ground state takes place, we took inspiration from studies of **4**. It is believed **4** is able to efficiently return to the ground state through a potential energy surface crossing between $S_0$ and $S_1$ states.[20] Thus, we computationally searched for a conical intersection between the $S_0$ and $S_1$ states of **1–3**.

To locate a $S_0/S_1$ conical intersection, computations were carried out using the fully-optimized reaction space (FORS) method within the General Atomic and Molecular Electronic Structure System (GAMESS) package of programs.[28] This method can formally account for the static electronic correlation present in these systems. Further approximations are still needed to make this a manageable problem with presently available computational resources, so the functional groups were omitted and only a minimal active space was used—four electrons in four orbitals, denoted FORS(4,4). In the case of the excited states, state averaging was done with equal weights $S_0$ and $S_1$ states, denoted SA-FORS(4,4). The cc-pVDZ basis set[29] was used for all cases, except for TD-DFT where the 6-311G(2df,2p) basis set[30] was used. Considering the approximations used, the results obtained are only considered qualitatively correct as a larger active space, basis set and dynamic electron correlation would be needed for quantitatively correct results, but are beyond the scope and computational expense of this current study.

Interestingly, TD-DFT calculations using CAM-B3LYP[31,32] predict a symmetry forbidden $S_0 \rightarrow S_1$ transition for **1b** and **2b**, the compounds containing an inversion center, which is attributed to a HOMO-1→LUMO transition; however, the $S_0 \rightarrow S_1$ transition is allowed for **3b** which does not possess an inversion center (see supporting information). The smallest active space for exploring the conical intersection was therefore deemed to consist of 4 electrons and 4 orbitals to include the HOMO-1. The FORS(4,4) results for **1b**, **2b**, and **3b** show that the $S_1$ differs from the ground state in that the localized double bond character of the central rings becomes attenuated. Then, at the $S_1$ geometry, only a small perturbation is required to reach the geometry of the conical intersection. This

facile $S_1$-to-conical intersection rearrangement is reflected in the geometries as well as the potential energy surfaces. The energy difference for the $S_1$ potential energy surface going from the $S_1$ geometry to the conical intersection is 0.03 eV for **1b**, 0.26 eV for **2b**, and 0.05 eV for **3b**. While qualitative in nature, the small difference in energy and geometry between the $S_1$ and conical intersection geometry strongly implicates that the conical intersection is a likely mechanism for efficient non-radiative decay to the ground state, as has been found to be the case for **4**.

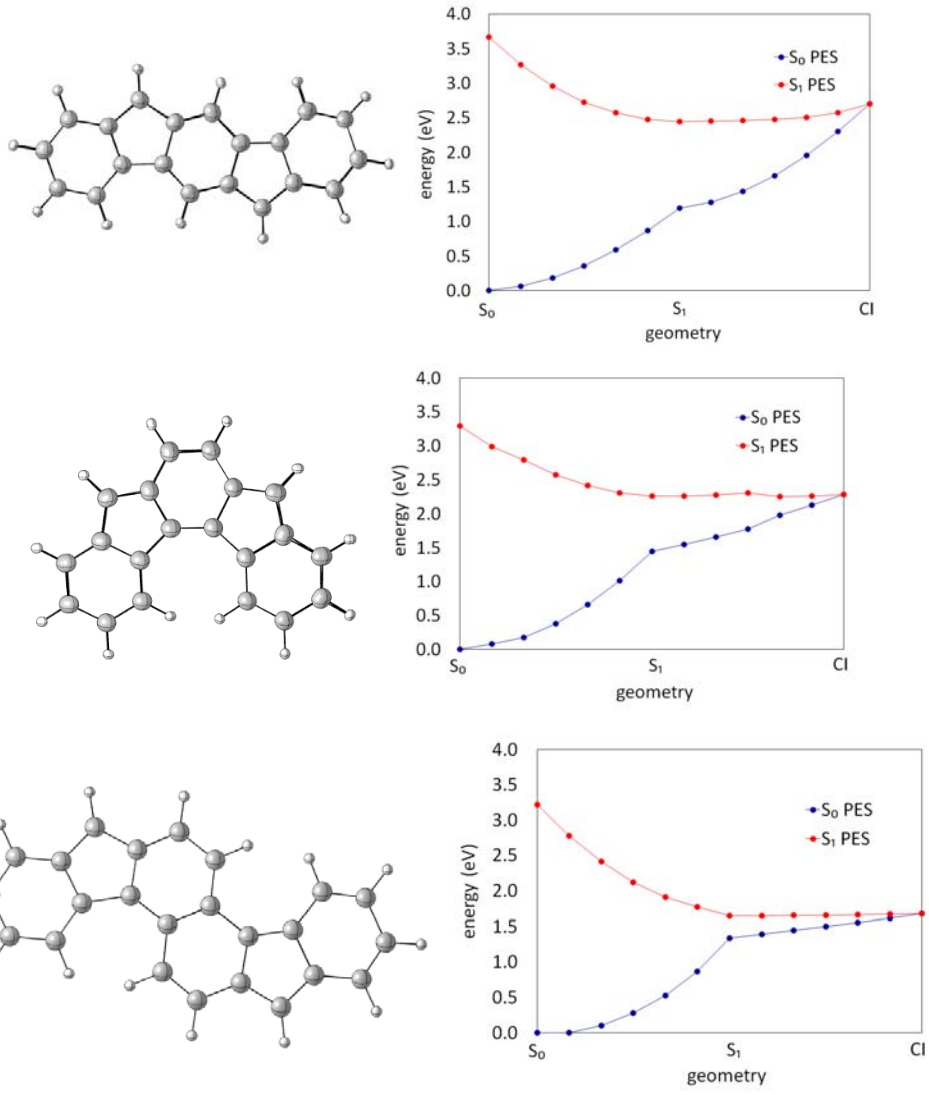

**Figure 3**. Overlay of SA-FORS(4,4) calculated $S_1$ and conical intersection geometries (left) and interpolated energies for $S_0$ and $S_1$ potential energy surfaces in vacuum (right) for **2b** (top), **3b** (middle), and **1b** (bottom).

In conclusion, we have reported the solution excited state lifetimes as measured by transient absorption spectroscopy and computationally explored the $S_0/S_1$ potential energy surface crossing for **1**–**3**. This series of quinoidal molecules was found to have relatively short $S_1$ excited state lifetimes, on the order or tens of picoseconds due to an easily accessible $S_0/S_1$ conical intersection. This work helps lay a foundation for future explorations on films of the compounds.

Bridge to Chapter VI

Thus far the main focus of the discussion has been the indenofluorene like molecules containing five fused rings in a row. Chapter VI describes the synthesis and properties of the expanded system containing six fused rings by adding an additional six membered ring to the center.

# CHAPTER VI

# FLUORENO[4,3-*c*]FLUORENE: A CLOSED-SHELL, FULLY CONJUGATED HYDROCARBON

This chapter was co-authored with Chris L. Vonnegut and Lev N. Zakharov providing experimental data. Michael M. Haley provided editorial and content advice. This work was published in *Organic Letters* volume 14 in pages 2426-2429.

## Discussion

Conjugated hydrocarbons with extended polycyclic frameworks have fascinated chemists for over 125 years.[1] Such molecules have undergone a resurgence in interest over the last two decades because of their utilization as materials in optical and electronic device applications such as organic field-effect transistors, photovoltaics, and light emitting diodes.[2] Large polycyclic aromatics have garnered considerable attention in this area due to π-orbital overlap of these electron-rich compounds in the solid-state, which facilitates charge transport.[3]

Recently the syntheses of derivatives of *o*- and *p*-quinodimethane-containing indeno[2,1-*a*]fluorene[4] and indeno[1,2-*b*]fluorene[5] (IF) have been reported. These acene-like molecules show promise as electron transporting materials due to their relatively low-lying LUMO energy levels.[6] In all cases generation of the IF skeleton utilized a Sn(II)-mediated reductive dearomatization to furnish the quinodimethane core. We set out to probe the limits of this dearomatization reaction in larger arenes such as naphthalene.

The feasibility of dearomatizing a larger system was first explored computationally by considering the energy required to form the product. We employed isodesmic reaction schemes and computationally determined the aromatic stabilization energies (ASE) of the basic indeno[1,2-*b*]fluorene and fluoreno[4,3-*c*]fluorene core structures (IF **1** and FF **2**, respectively in Figure 1).[7] The geometries were optimized with DFT using the B3LYP/6-31G(d) method[8] as utilized in Gaussian 09[9] and then single point energies and frequency calculations were performed with the same method using the larger 6-311+G(d,p) basis set. This method was verified against benzene, the usual standard, yielding a computed ASE value of –34.3 kcal $mol^{-1}$, whereas the experimentally determined ASE is –32.2 kcal $mol^{-1}$ from the enthalpies of formation

($\Delta H_f$).[10] The ASE of IF core **1** is surprisingly small at –13.4 kcal mol$^{-1}$, 38% the ASE of benzene. However, the ASE for the expanded FF core **2** is –19.4 kcal mol$^{-1}$, which is expected relative to **1** since naphthalene has about 1.7 times the ASE of benzene. These results indicated that the synthesis of **2** should be possible. Although **2** is formally antiaromatic with a total 24 of π-electrons, NICS(1)$_{zz}$ calculations[11] (see Supporting Information) reveal that only the peripheral benzenes are diatropic and that the inner rings are very weakly paratropic and/or atropic, similar to **1**.

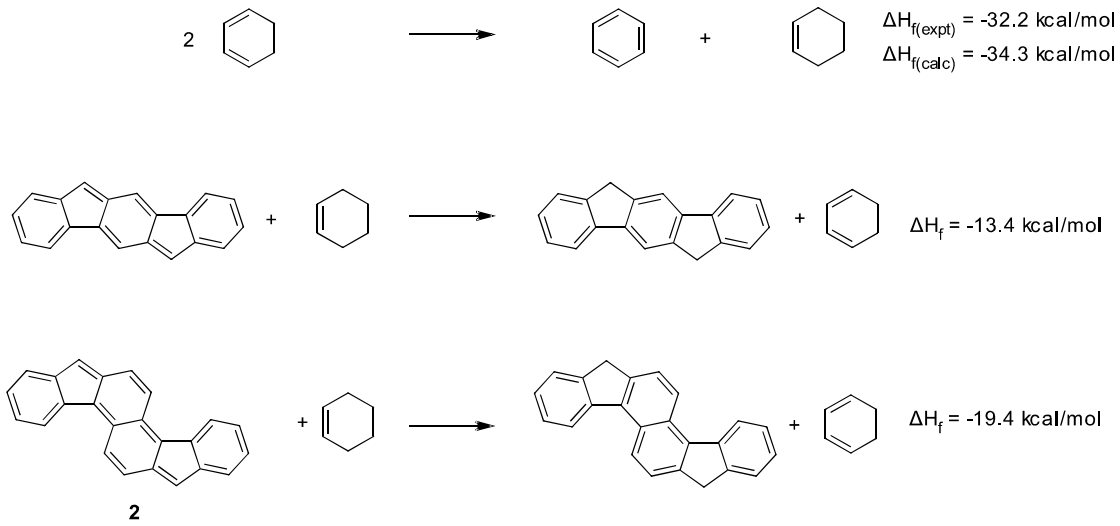


**Figure 1.** Calculated aromatic stabilization energies using electronic and zero point energies from B3LYP/6-311+G(d,p)//B3LYP/6-31G(d). Compound **2** is shown with IUPAC numbering scheme.

A second possibility we considered was that the fluorenofluorene might have an open-shell (biradical) configuration (e.g., **2'**, Figure 2). Recently a variety of extended polycyclic π-systems have been described that exhibit a singlet open-shell (OS) ground state (e.g., **3**) and thermally accessible triplet states (e.g., **4**, **5**).[12] We therefore considered an OS singlet and triplet state for **2** using symmetry broken UB3LYP; the OS singlet energy was corrected using the approximate spin projection method.[13] Using known 2,6-quinodimethylnaphthalene **6**[14] as a test case, the calculated triplet state was estimated at 15.4 kcal mol$^{-1}$ above the OS singlet, which is in reasonable agreement with the experimentally determined value of 12.6 ± 2.0 kcal mol$^{-1}$.[15] For **2** the closed shell and OS

singlet were calculated to be essentially the same energy. The square of the OS spin expectation value was miniscule ($<S^2> = 0.0001$), reinforcing that **2** should have a closed-shell ground state. The calculated triplet state for **2** is 16.1 kcal $mol^{-1}$ above the singlet.

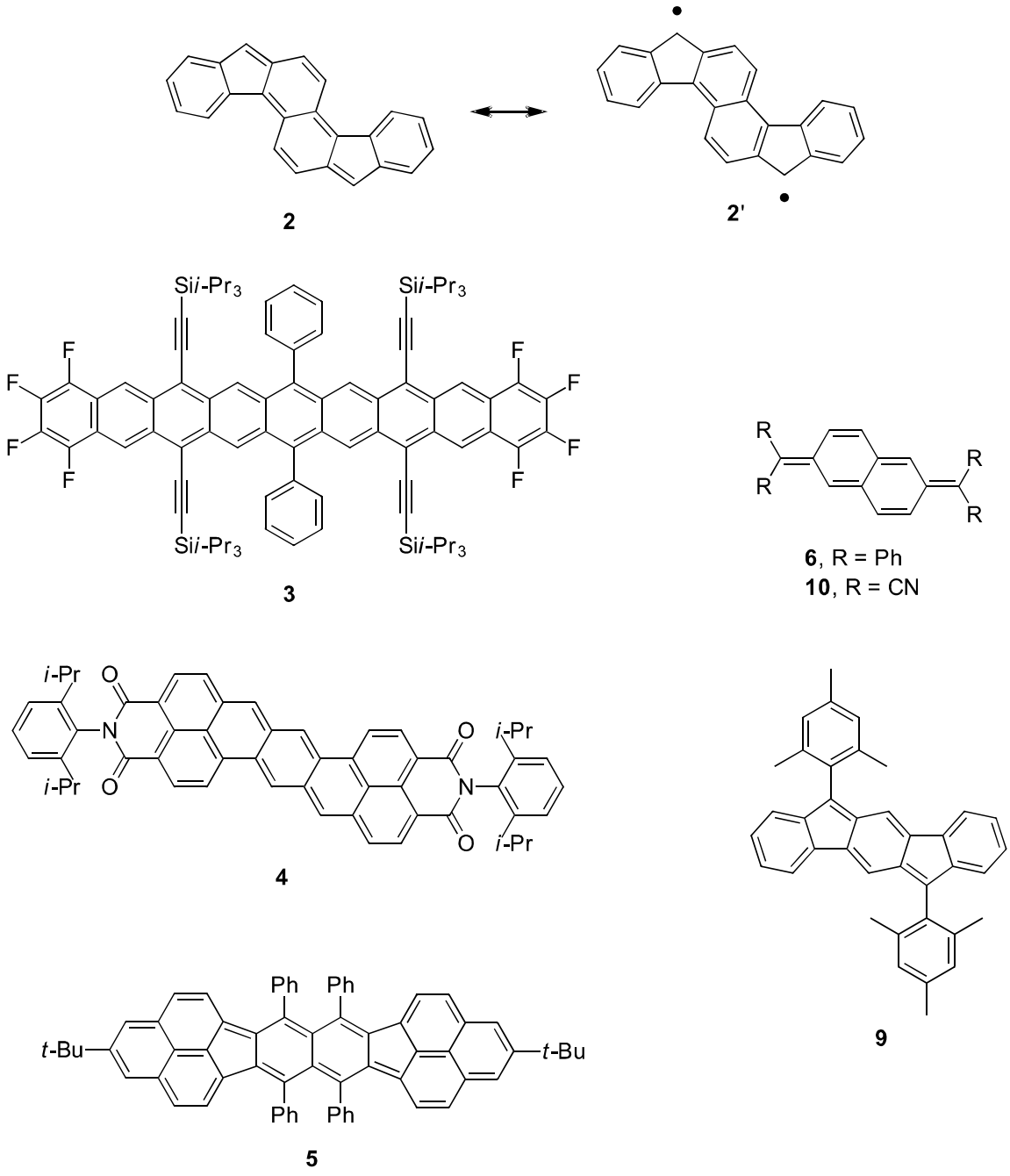


**Figure 2.** Closed-shell and open-shell forms of **2**, and recently reported molecules **3**–**5** that show significant biradical character.

Of the three possible fluorenofluorene variants that yield Kekulé hydrocarbons, we chose to experimentally investigate **7** since the requisite dione synthon **8** is a known molecule that can be prepared in seven steps from commercially available 2,6-dimethylnaphthalene.[16] We also felt that inclusion of mesityl groups would enhance the kinetic and thermodynamic stability of **7**. Gratifyingly, treatment of **7** with mesityllithium followed by reduction with $SnCl_2$ in toluene at room temperature yields fully conjugated **7** in 86% yield (Scheme 1). Unlike the IF derivatives, elevated temperatures for this reaction led to significant decomposition. Deep blue solutions of **7** exhibited no line broadening in the proton NMR spectrum (i.e., no triplet character) upon heating to 160 °C (see Supporting Information), and the EPR spectrum of the powder and solution sample showed no triplet signal. Structurally similar **6** exhibited no diradical character in the EPR spectrum below 180 °C.[15] Pure **7** is remarkably stable—the NMR spectrum showed no decomposition upon prolonged heating at 160 °C, and thermogravimetric analysis revealed less than 5% decomposition by ca. 350 °C. Another sample that was kept in $CDCl_3$ open to the atmosphere and exposed to ambient light exhibited by NMR only trace amounts of decomposition after 1 month.

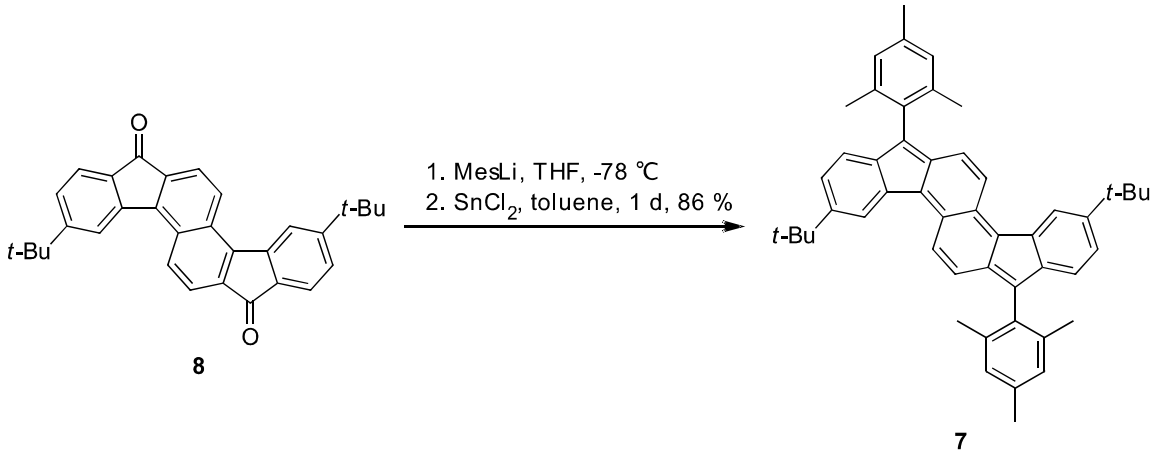


**Scheme 1**. Synthesis of 4,11-Di-*t*-butyl-1,8-dimesitylfluoreno-[4,3-*c*]fluorene **7**.

The lowest energy transition in the absorption spectrum of **7** (Figure 3) appears at 649 nm, compared to a $\lambda_{max}$ of 516 nm for dimesityl-IF **9**.[5c] These values correspond to optical energy gaps of 1.79 and 2.29 eV, respectively, which clearly show the effect of inclusion in the core of the second 6-membered ring and its two double bonds.

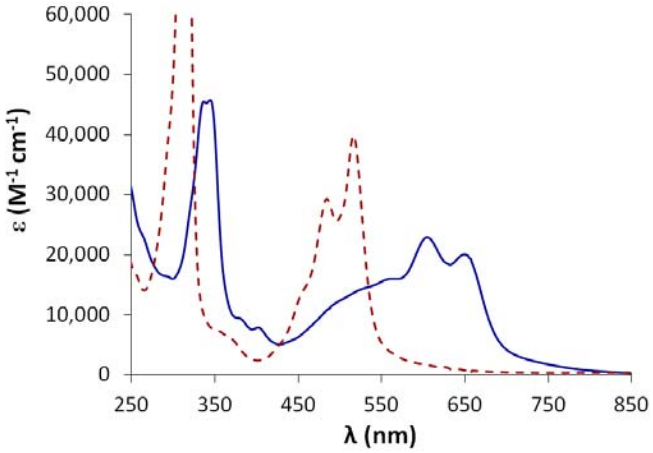


**Figure 3.** Electronic absorption spectra of **7** (solid blue) and **9** (dashed red) in $CH_2Cl_2$.

The cyclic voltammetry (CV) data for **7** exhibits redox amphoterism with two reversible reductions and two oxidations—the first oxidation reversible and the second quasi-reversible (Figure 4). The first reduction half wave potential is –0.87 V and the second –1.29 V, whereas the first oxidation half-wave potential is 0.82 V and the second 1.27 V.[17] The electron affinity of **7** is higher than that of **9**, which has a first reduction half-wave potential of –1.12 V.[5c] The LUMO energy of **7** was estimated at –3.77 eV from cyclic voltammetry,[18] an exceptionally low-lying LUMO for a polycyclic hydrocarbon that does not contain electron withdrawing groups. This corresponds to an electrochemical energy gap of 1.69 eV, which agrees well with the optically-determined value.

Compound **7** co-crystallized with benzene by slow evaporation, yielding single crystals suitable for x-ray diffraction. The molecular structure is shown in Figure 5, and relevant bond lengths are given in Table 1. The crystal structure of **7**•($C_6H_6$) establishes the closed shell ground state due to the discrete, alternating short (1.356–1.378 Å) and long (1.410–1.433 Å) bond lengths. The B3LYP/6-31G(d) minimized structure of **7** accurately replicates the bond length alternation in central rings and near homogeneity for

the outer 6-membered rings. To the best of our knowledge, this is the first structural elucidation of a neutral 2,6-naphthoquinone dimethide; the crystal structure of **5** revealed

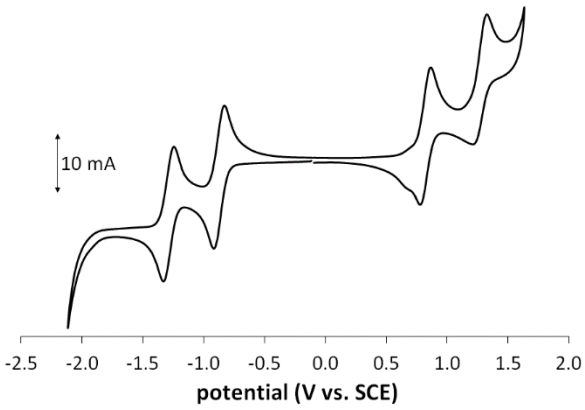


**Figure 4.** CV data for **7**. Data were recorded in a $CH_2Cl_2$ solution of 1 mM analyte and 0.1 M $Bu_4NOTf$ using a scan rate of 50 mV $s^{-1}$. The working electrode was a glassy carbon electrode with a Pt coil counter electrode and Ag wire pseudoreference. Values reported as the half-wave potential (vs. SCE) using the $Fc/Fc^+$ couple (0.46 V) as an internal standard; see reference 17.

a naphthalene-like core expected for an open-shell biradical.[12a] The X-ray data for the anion of structurally similar **10** with methyltriphenyl-phosphonium counter ion had a 2:1 stoichiometry and possessed longer bond lengths for the C(4)–C(5) double bond (Table 1) than neutral **7**•($C_6H_6$).[19] These differences are attributable to the negative charge distributed across the two independent molecules of **10**.

**Table 1.** Select bond lengths [Å].

| bond[a] | **7** (calc)[b] | **7**•($C_6H_6$) (x-ray) | **10**(a)[c] | **10**(b)[c] |
|---|---|---|---|---|
| C(1)–C(2) | 1.359 | 1.356(6) | 1.38 | 1.34 |
| C(1)–C(5a) | 1.446 | 1.433(6) | 1.40 | 1.45 |
| C(2)–C(3) | 1.429 | 1.410(6) | 1.46 | 1.47 |
| C(3)–C(4) | 1.455 | 1.433(6) | –[d] | –[d] |
| C(3)–C(6) | 1.386 | 1.378(6) | 1.42 | 1.38 |
| C(4)–C(5) | 1.387 | 1.377(6) | 1.50 | 1.43 |
| C(5)–C(5a) | 1.479 | 1.459(6) | 1.43 | 1.44 |

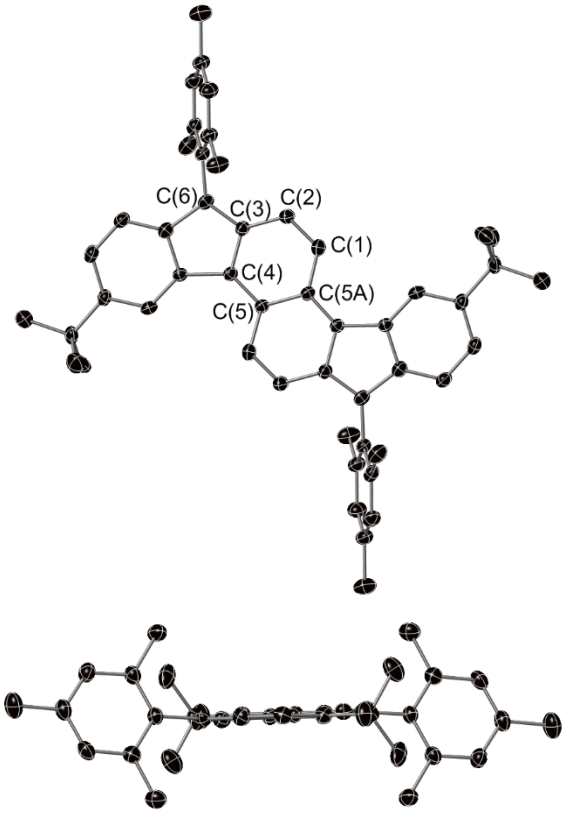


**Figure 5.** ORTEP showing top and side views of **7**•($C_6H_6$); solvent molecule and hydrogens omitted for clarity. Ellipsoids drawn at the 30% probability level.

Compound **7** is an intriguing addition to the molecular canon. In contrast to similar compounds that exhibit considerable diradical character, the lack of a radical stabilizing motif (e.g., phenalenyl unit in **5**) leads to a closed shell ground state for **7**.[12a,b] The redox amphoterism in the CV data suggests potential as an ambipolar electronic material, similar to IF **2**,[5c] and the unusual thermal and photochemical stability of **7** bode well for such applications. We are currently exploring use of the Sn-mediated dearomatization for the preparation of even larger, expanded π-conjugated polycyclic hydrocarbons.

APPENDIX A

EXPERIMENTAL DETAILS FOR CHAPTER II

**General Methods.** $^{1}H$ and $^{13}C$ NMR spectra were recorded in $CDCl_3$ using either a Varian Inova 300 ($^{1}H$: 299.93 MHz, $^{13}C$: 75.42 MHz) or 500 ($^{1}H$: 500.11 MHz, $^{13}C$: 125.75 MHz) spectrometer. Chemical shifts (δ) are expressed in ppm relative to the residual chloroform ($^{1}H$: 7.27 ppm, $^{13}C$: 77.23 ppm) reference. Coupling constants are expressed in hertz. IR spectra were recorded using a Nicolet Magna FTIR 550 spectrometer. UV-Vis spectra were recorded on an HP 8453 UV-Vis spectrometer. Fluorescence spectra and were recorded on a Horiba Jobin Yvon Fluoromax-4 spectrofluorimeter. High resolution mass spectra were recorded on a Waters Micromass MALDI Q-ToF Mass Spectrometer. THF was distilled over Na/benzophenone under $N_2$. Unless otherwise stated, all reagents were purchased and used as received. Compounds **9a** and **9b** were prepared according to reference [1].

**Indenofluorenyldione 10a**. Dione **9a** (0.150 g, 0.233 mmol), $Pd(PPh_3)Cl_2$ (0.009 g, 0.014 mmol), CuI (0.005 g, 0.028 mmol) in THF (30 mL) and DIPA (30 mL) was degassed with Ar for 50 min. TIPSA (0.21 mL, .932 mmol) was added to the mixture and the resulting solution was covered with Al foil and stirred overnight at 60 °C. Upon completion, the mixture was evaporated to dryness. The crude material was chromatographed over basic alumina (9:1 hexanes/$CH_2Cl_2$) to give **10a** (0.091 g, 61%) as a red crystalline solid. $^{1}H$ NMR ($CDCl_3$): δ 8.72 (d, $J$ = 7.3 Hz, 2H), 7.75 (d, $J$ = 7.0 Hz, 2H), 7.51 (dt, $J$ = 7.6, 1.2 Hz), 7.38 (dt, $J$ = 7.5, 0.7 Hz, 2H), 1.36-1.26 (m, 42H); $^{13}C$ NMR ($CDCl_3$): δ 190.06, 146.44, 142.06, 138.47, 134.44, 133.78, 129.60, 124.09, 123.49, 114.02, 106.78, 100.37, 18.65, 11.42; IR (NaCl): $\nu$ 2942, 2865, 1721, 1605, 1465, 1432, 1282, 1268, 1181, 928, 882, 764, 718, 680, 658 $cm^{-1}$; UV ($CHCl_3$) $\lambda_{max}$ (log ε): 312 (4.39), 327 (4.42), 343 (4.61), 519 (2.82) nm; Em. ($CHCl_3$) $\lambda_{max}$: 602 nm; HRMS (MALDI) for $C_{42}H_{51}O_2Si_2$ [M+1]: calcd 643.3428, found 643.3405.

**Indenofluorenyldione 10b**. Dione **9b** (0.146 g, 0.133 mmol), $Pd(PPh_3)_2Cl_2$ (5 mg, 0.005 mmol), and CuI (2 mg, 0.002 mmol) in THF (20 mL) and DIPA (20 mL) was degassed with Ar for 45 min. TIPSA (0.12 mL, 0.532 mmol) was added to the mixture and the resulting solution was covered with Al foil and stirred overnight at 60 °C. Upon completion, the mixture was evaporated to dryness and the crude product dissolved in

3:10 hexanes/$CH_2Cl_2$ and then passed through a pad of silica to remove insoluble material. The filtrate was evaporated to dryness and the crude product chromatographed on silica (1:9 hexanes/$CH_2Cl_2$) to give **10b** (0.088 g, 55%) as a red-orange solid. $^1$H NMR ($CDCl_3$): δ 8.24 (s, 2H), 7.43 (s, 2H), 2.56-2.52 (m, 8H), 1.57-1.53 (m, 8H), 1.37-1.23 (m, 98H), 0.91-0.85 (m, 12H); $^{13}$C NMR ($CDCl_3$): δ 190.34, 148.54, 146.37, 142.24, 139.91, 139.07, 132.11, 125.01, 124.56, 113.49, 150.60, 100.68, 34.22, 32.62, 32.17, 31.88, 31.01, 30.24, 29.66, 29.61, 29.55, 29.50, 29.31, 22.67, 18.78, 14.09, 11.46; IR (NaCl): *v* 2924, 2854, 1716, 1609, 1466, 1445, 1285, 1160, 1069, 997, 898, 882, 794, 678, 662, 619 cm$^{-1}$; UV ($CHCl_3$) $\lambda_{max}$ (log ε): 313 (4.47), 333 (4.33), 500 (3.08) nm; Em. ($CHCl_3$) $\lambda_{max}$: 565 nm; HRMS (MALDI) for $C_{82}H_{131}O_2Si_2$ [M+1]: calcd 1203.969, found 1203.972.

**Indenofluorene 8a**. TIPSA (0.104 mL, 0.466 mmol) in THF (5 mL) was degassed with Ar for 15 min and subsequently cooled to 0 °C. BuLi (0.300 mL, 0.466 mmol) was added and the mixture was stirred for 15 min at 0 °C. In a separate flask, dione **10a** (0.075 g, 0.117 mmol) in THF (10 mL) was degassed with Ar for 15 minutes, and then also cooled to 0 °C. The lithiate solution was cannulated into the flask containing **10a** and stirred for 2 h at 0 °C. Upon completion, the solution was diluted with ether (20 mL) and water (20 mL), and washed with brine (20 mL). The organic layer was dried ($MgSO_4$), filtered, and evaporated to dryness. The crude diol **11a** was then redissolved in toluene (15 mL) and anhydrous $SnCl_2$ (0.088 g, 0.466 mmol) was added. The resulting mixture was stirred overnight at 80 °C. Upon completion, the mixture was evaporated to dryness and chromatographed over neutral alumina (hexanes) to give **8a** (0.024 g, 21%) as a violet crystalline solid. $^1$H NMR ($CDCl_3$): δ 8.35 (d, $J$ = 7.8 Hz, 2H), 7.36 (d, $J$ = 7.3 Hz, 2H), 7.14 (t, $J$ = 7.3 Hz, 2H), 7.08 (t, $J$ = 7.6 Hz, 2H), 1.29-1.19 (m, 84H); $^{13}$C NMR ($CDCl_3$): δ 144.68, 141.78, 135.83, 135.55, 128.43, 127.82, 125.52, 123.99, 116.41, 114.61, 106.58, 104.03, 102.70, 18.95, 18.92, 12.32, 12.10; IR (NaCl): *v* 2943, 2889, 2865, 1521, 1462, 1378, 1366, 1334, 1301, 1150, 1110, 1074, 1016, 996, 953, 882, 869, 759, 754 cm$^{-1}$; UV ($CHCl_3$) $\lambda_{max}$ (log ε): 553 (3.69), 593 (3.91) nm; HRMS (MALDI) for $C_{64}H_{93}Si_4$ [M+1]: calcd 973.6354, found 973.6325.

**Indenofluorene 8b**. TIPSA (0.056 mL, 0.249 mmol) in THF (5 mL) was degassed with Ar for 15 min and subsequently cooled to 0 °C. BuLi (0.16 mL, 0.249

mmol) was added and the mixture was stirred for 15 min at 0 °C. In a separate flask, dione **10b** (0.075 g, 0.062 mmol) in THF (10 mL) was degassed with Ar for 15 min, and then also cooled to 0 °C. The lithiate solution was cannulated into the flask containing **10a** and the resulting mixture was stirred for 2 h at 0 °C. Upon completion, the solution was diluted with ether (20 mL) and water (20 mL), and washed with brine (20 mL). The organic layer was dried ($MgSO_4$) filtered, and evaporated to dryness. The crude diol **11b** was then redissolved in toluene (15 mL) and anhydrous $SnCl_2$ (0.045 g, 0.249 mmol) was added. The resulting mixture was stirred overnight at 80 °C. Upon completion, the mixture was evaporated to dryness and chromatographed over neutral alumina (hexanes) to give **8b** (0.052 g, 55%) as a blue crystalline solid. $^1$H NMR ($CDCl_3$): δ 7.96 (s, 2H), 7.15 (s, 2H), 2.56-2.52 (m, 8H), 1.57-1.53 (m, 8H), 1.37-1.20 (m, 148H), 0.91-0.85 (m, 12H); $^{13}$C NMR ($CDCl_3$): δ 143.29, 147.74, 141.58, 141.16, 135.90, 134.01, 125.31, 125.14, 123.24, 115.80, 113.55, 105.47, 14.82, 103.11, 34.08, 33.08, 32.15, 30.57, 29.90, 29.59, 22.93, 19.31, 19.22, 14.34, 12.65, 12.49; IR (NaCl): *v* 2924, 2863, 1524, 1463, 1689, 1338, 1166, 1189, 1075, 1017, 997, 918, 864 $cm^{-1}$; UV ($CHCl_3$) $\lambda_{max}$ (log ε): 570 (3.82), 613 (4.05) nm; HRMS (MALDI) for $C_{104}H_{173}Si_4$ [M+1]: calcd 1534.261, found 1534.258.

**Computational Methods**. All computations were calculated using the Gaussian 03[2] suite of programs at the B3LYP/6-31G+** level of theory. All stationary points were confirmed by harmonic frequency analysis and checked for stability for triplet and SCF convergence. The energies of the stationary points were determined, including zero point energies, at the same level of theory. NICS calculations were carried out using standard GIAO methods with Bq atoms (NICS probes) 1.0 Å above the geometric center of the ring.

Cartesian Coordinates of Desilylated **8a**
B3LYP/6-311+G** = -1074.19272033au
B3LYP/6-311+G** Zero Point Corrected Energy = -1073.906991 au
NIMAG = 0

| | | | |
|---|---|---|---|
| C | -5.51700900 | -0.71349300 | 0.00001800 |

| | | | |
|---|---|---|---|
| C | -4.87185000 | -1.95176200 | 0.00001900 |
| C | -3.47499200 | -2.04073000 | 0.00001400 |
| C | -2.72587400 | -0.86739100 | 0.00000800 |
| C | -3.38838200 | 0.38533300 | 0.00000800 |
| C | -4.77653700 | 0.47044700 | 0.00001300 |
| C | -1.28477100 | -0.59393500 | 0.00000300 |
| C | -1.11972200 | 0.85435100 | 0.00000200 |
| C | -2.38162600 | 1.44819500 | 0.00000100 |
| C | -0.19913900 | -1.44448100 | -0.00000500 |
| C | 1.11972200 | -0.85435100 | 0.00000000 |
| C | 1.28477100 | 0.59393500 | 0.00000100 |
| C | 0.19913900 | 1.44448100 | 0.00000300 |
| C | 2.38162500 | -1.44819500 | 0.00000400 |
| C | 3.38838200 | -0.38533300 | 0.00000400 |
| C | 2.72587400 | 0.86739100 | 0.00000100 |
| C | 4.77653700 | -0.47044700 | 0.00000600 |
| C | 5.51700900 | 0.71349300 | 0.00000600 |
| C | 4.87185000 | 1.95176200 | 0.00000300 |
| C | 3.47499200 | 2.04073000 | 0.00000000 |
| C | -2.74495100 | 2.80707000 | -0.00000200 |
| C | 0.35764700 | 2.85735700 | 0.00000300 |
| C | -0.35764700 | -2.85735700 | -0.00001200 |
| C | 2.74495100 | -2.80707000 | 0.00001200 |
| C | -3.17431100 | 3.93602300 | -0.00004700 |
| C | 0.49160300 | 4.05443500 | 0.00000300 |
| C | -0.49160300 | -4.05443500 | -0.00006900 |
| C | 3.17431100 | -3.93602300 | -0.00000200 |
| H | -6.60021600 | -0.67096600 | 0.00002200 |
| H | -5.46086900 | -2.86198100 | 0.00002400 |
| H | -2.99320800 | -3.00776500 | 0.00001500 |
| H | -5.26830900 | 1.43636600 | 0.00001200 |

| | | | |
|---|---|---|---|
| H | 5.26830900 | -1.43636600 | 0.00000900 |
| H | 6.60021600 | 0.67096500 | 0.00000800 |
| H | 5.46086900 | 2.86198100 | 0.00000200 |
| H | 2.99320800 | 3.00776500 | -0.00000200 |
| H | -3.51387500 | 4.94289600 | -0.00001800 |
| H | 0.59117300 | 5.11240900 | 0.00000200 |
| H | -0.59117400 | -5.11240900 | -0.00009800 |
| H | 3.51387600 | -4.94289500 | 0.00004900 |

APPENDIX B

EXPERIMENTAL DETAILS FOR CHAPTER III

**General methods.** $^{1}H$ and $^{13}C$ NMR spectra were recorded on a Bruker Avance III HD 600 with Prodigy BBO multinuclear Cryoprobe ($^{1}H$: 599.98 MHz, $^{13}C$: 150.88 MHz) or Varian Mercury 300 MHz ($^{1}H$: 300.09 MHz). Chemical shifts are reported in parts per million (ppm) relative to tetramethylsilane, which was referenced according to trace amounts of non-deuterated chloroform (7.26 ppm) or dimethylsulfoxide (2.5 ppm) for $^{1}H$ and $CDCl_3$ (77.23 ppm) and DMSO-d6 (39.51 ppm) for $^{13}C$. Absorption spectra were recorded on HP 8453 UV-Vis spectrometer. Glassware was dried in an oven at 100 °C and cooled under a stream of inert gas before use. Dry THF was distilled from potassium metal using benzophenone as an indicator under a nitrogen atmosphere. Sorbent Technologies silica G TLC plate w/UV254 aluminum backed, 200μm was used for TLC. Chromatography was performed using silica gel, tech grade, 60 Å, 230-400 mesh from Sigma-Aldrich. All commercial reagents were used as received unless otherwise noted. 5,11-Diiodoindeno[1,2-b]fluorene-6,12-dione[1] (**2**), (triisobutylsilyl)acetylene[2], and (triphenylsilyl)acetylene[3] were prepared according to literature procedures.

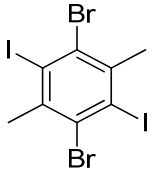


**2,5-Dibromo-3,6-diiodo-*p*-xylene (12)**. 2,5-Dibromo-*p*-xylene (10 g, 37.9 mmol), $K_2S_2O_8$ (33.8 g, 125 mmol) and $I_2$ (31.7 g, 125 mmol) in $CH_2Cl_2$ (380 mL) were cooled in an ice bath and then a mixture of TFA (151 mL) and $H_2SO_4$ (6.8 mL) was added slowly. The reaction flaks was covered with Al foil and stirred at 60 °C. After 1 d an aliquot from the reaction was analyzed and if not complete, additional $I_2$ (6 g) and $K_2S_2O_8$ (6 g) were added. When complete the reaction was quenched by slowly pouring into cold $H_2O$ (ca. 500 mL). The reaction was washed with $H_2O$ several times and then the organic layer was reduced to half volume in vacuo. The resultant colored solid was collected and washed with acetone to yield **12** (9.77 g, 18.9 mmol, 50%) as a white solid. $^{1}H$ NMR (300 MHz, $CDCl_3$) δ 3.03 (s, 6H); $^{13}C$ NMR (151 MHz, $CDCl_3$): δ 142.45, 131.02, 110.63, 37.61; HRMS (TOF MS ESI+) $[M]^+$ calcd for $C_8H_6Br_2I_2^+$ 513.6926; found 513.6906.

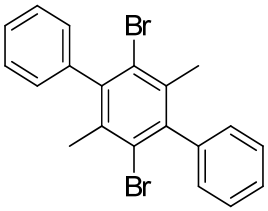


**2,5-Dibromo-3,6-dimethyl-*p*-terphenyl (14)**. A flask was charged with diiodide **13** (3.68 g, 7.14 mmol), phenylboronic acid (2.61 g, 21.4 mmol), $K_3PO_4$ (5.61 g, 29 mmol) and Pd(dppf)$Cl_2$•$CH_2Cl_2$ (0.11 g, 0.14 mmol). Another flask was filled with dioxane (100 mL) and $H_2O$ (27 mL). Both flasks were purged with $N_2$ or Ar for 45 min. The solvent was then transferred via cannula to the reaction flask and the mixture heated to 60 °C overnight. When complete, the cooled reaction was extracted with $Et_2O$ and washed with $H_2O$, 10% HCl solution, $H_2O$ and then dried over $MgSO_4$. The solvent was removed under reduced pressure and the white solid was used as collected (2.71 g, 6.52 mmol, 91%). Analytically pure white crystals were obtained by recrystallization from $Et_2O$. $^1$H NMR (600 MHz, $CDCl_3$) δ 7.47-7.52 (m, 4H), 7.40-7.44 (m, 2H), 7.20 (m, 4H), 2.20 (s, 6H); $^{13}$C NMR (151 MHz, $CDCl_3$): δ 143.34, 142.56, 135.73, 129.19, 128.71, 127.70, 126.80, 23.49; HRMS (TOF MS ESI+) $[M]^+$ calcd for $C_{20}H_{17}Br_2^+$ 414.9697; found 414.9704.

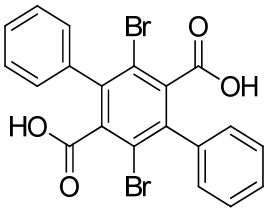


**2,5-Dibromo-3,6-diphenylterephthalic acid (15)**. *p*-Terphenyl **14** (2.51 g, 6 mmol), $KMnO_4$ (12 g, 76 mmol), pyridine (150 mL) and $H_2O$ (20 mL) were added to a flask equipped with a mechanical stirrer and condenser. The reaction was heated to reflux and four more portions of $KMnO_4$ (12 g each) were added every hour after reaching reflux. The mixture was refluxed overnight until the purple color of $KMnO_4$ was no longer visible. After cooling, the solid salts were collected by filtration and washed with of boiling 10% KOH solution. The combined solutions were then reduced to approximately half volume. After cooling to rt, the resulting solution was acidified carefully with conc. HCl and then cooled on ice. The precipitate was collected, washed with $H_2O$ (ca. 100

mL) and dried overnight at 70 °C to give **15** (2.38 g, 5.0 mmol, 83%) as a white solid. Analytically pure samples were obtained by recrystallization from EtOH. $^{1}$H NMR (600 MHz, DMSO-$d_6$) δ 13.62 (br s, 2H), 7.42-7.50 (m, 6H), 7.29-7.32 (m, 4H); $^{13}$C NMR (151 MHz, DMSO-$d_6$): δ 166.73, 139.82, 139.39, 137.38, 129.39, 128.57, 128.15, 118.81; HRMS (TOF MS ESI+) $[M]^+$ calcd for $C_{20}H_{12}Br_2O_4^+$ 473.9103; found 473.9093.

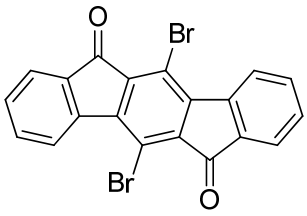


**5,11-Dibromoindeno[1,2-*b*]fluorene-6,12-dione (11)**. Terephthalic acid **15** (1.97 g, 4.13 mmol) was slowly added to stirred conc. $H_2SO_4$ (130 mL) which resulted in a rapid color changed to opaque dark brown. After stirring at rt for 16 h, the reaction mixture was poured slowly onto ice (ca. 400 g). The precipitate was collected and washed sequentially with $H_2O$, satd $NaHCO_3$ solution, $H_2O$, and then acetone. The solid was dried overnight at 70 °C to yield **11** (1.36 g, 3.08 mmol, 75%) as a bright orange solid. $^{1}$H NMR (600 MHz, $CDCl_3$) δ 8.67 (d, $J$ = 7.7 Hz, 2H), 7.77 (d, $J$ =7.2 Hz, 2H), 7.62 (dt, $J$ = 7.6, 1.3 Hz, 2H), 7.44 (t, $J$ = 7.5 Hz, 2H); $^{13}$C NMR (151 MHz, $CDCl_3$): δ 189.92, 147.02, 141.38, 137.30, 135.42, 134.22, 130.49, 124.95, 124.78, 115.14; HRMS (TOF MS ESI+) $[M]^+$ calcd for $C_{20}H_8Br_2O_2^+$ 437.8891; found 437.8871.

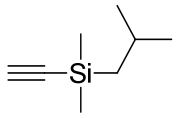


**Dimethyl(ethynyl)isobutylsilane**. A flask containing ethynylmagnesium bromide (50 mL, 0.5 M in THF, 25 mmol) was cooled in an ice bath and chloro(dimethyl)isobutylsilane (3.27 mL, 18.75 mmol) was injected slowly over 15 min. The mixture was warmed to rt and stirred for 2 h. The reaction mixture was quenched by slow addition of $H_2O$ and then extracted with $Et_2O$ and dried over $MgSO_4$. The organic layer was carefully concentrated and the crude silane (0.87 g) was used directly in the next step. $^{1}$H NMR (600 MHz, $CDCl_3$) δ 2.39 (s, 1H), 1.86 (n, $J$ = 6.7 Hz, 1H), 0.97 (d, $J$ = 6.6 Hz, 6H), 0.66 (d, $J$ = 7.0 Hz, 2H), 0.19 (s, 6H); $^{13}$C NMR (151 MHz, $CDCl_3$): δ

93.67, 90.19, 26.61, 26.26, 25.20, 0.73; HRMS (TOF MS ESI+) $[M]^+$ calcd for $C_7H_{13}Si^+$ 125.07866; found 125.07896.

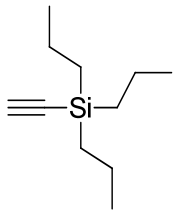

**Ethynyltripropylsilane.** The same procedure as above was used to prepare the desired silane, which was used directly in the next step. $^1$H NMR (600 MHz, $CDCl_3$) δ 2.36 (s, 1H), 1.42 (m, 6H), 0.99 (t, $J$ = 7.3 Hz, 9H), 0.63 (m, 6H); $^{13}$C NMR (151 MHz, $CDCl_3$): δ 94.24, 88.53, 18.39, 17.61, 16.02; HRMS (TOF MS ESI+) $[M]^+$ calcd for $C_{11}H_{22}Si^+$ 182.14908; found 182.15030.

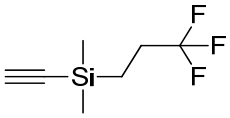

**Dimethyl(ethynyl)(3,3,3-trifluoropropyl)silane**. The same procedure as above was used to prepare the desired silane, which was used directly in the next step. $^1$H NMR (600 MHz, $CDCl_3$) δ 2.43 (s, 1H), 2.14 (m, 2H), 0.85 (m, 2H), 0.22 (s, 6H); $^{13}$C NMR (151 MHz, $CDCl_3$): δ 127.83 (q, $J$ = 276.3 Hz), 95.05, 87.59, 28.94 (q, $J$ = 30.31 Hz), 8.03 (d, $J$ = 2.2 Hz), 2.08; HRMS (TOF MS ESI+) $[M]^+$ calcd for $C_6H_8SiF_3^+$ 165.03474; found 165.03420.

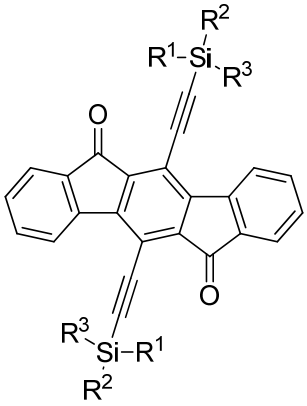

**Cross-coupling with 5,11-Diiodoindeno[1,2-*b*]fluorene-6,12-dione**. A mixture of dione **9** (0.100 g, 0.187 mmol), $Pd(PPh_3)_4$ (0.025 g, 0.022 mmol) and CuI (0.002 g, 0.011 mmol) in THF (30 mL) and *i*$Pr_2NH$ (30 mL) was degassed with Ar for 45 min. The appropriate ethynylsilane (0.748 mmol) was then added via syringe if it was a liquid. Alternatively, solid triphenylsilylacetylene was dissolved in THF (6 mL), degassed by Ar bubbling for 30 min and then transferred via cannula under inert atmosphere. The reaction mixture was then heated to 55-60 °C and monitored via NMR until complete, typically 24-48 h. After removal of the solvent, the residue was purified as indicated to give the desired product as an orange solid.

**8a** ($SiMe_3$). Chromatography on basic alumina (4:1 hexanes/$CH_2Cl_2$); 40% yield. $^1$H NMR (300 MHz, $CDCl_3$): δ 8.52 (d, *J* = 7.6 Hz, 2H), 7.71 (d, *J* = 7.3 Hz, 2H), 7.55 (td, *J* = 7.6, 1.2 Hz, 2H), 7.38 (td, *J* = 7.4, 0.9 Hz, 2H), 0.43 (s, 18H); $^{13}$C NMR (126 MHz, $CDCl_3$): δ 190.60, 146.65, 142.27, 138.55, 134.98, 134.09, 130.01, 124.28, 123.60, 114.21, 109.58, 99.01, –0.12; IR (KBr) *v* 1718 (CO) $cm^{-1}$; UV-Vis ($CHCl_3$) $\lambda_{max}$ 310, 330, 498, 524 nm; HRMS (ESI) for $C_{30}H_{27}O_2Si_2$ [$M^+$+H]: calcd 475.1550, found 475.1544.

**8b** ($SiEt_3$). Chromatography on basic alumina (4:1 hexanes/$CH_2Cl_2$); 8% yield. $^1$H NMR (600 MHz, $CDCl_3$) δ 8.62 (d, *J* = 7.6 Hz, 2H), 7.73 (d, *J* = 7.3 Hz, 2H), 7.53 (td, *J* = 7.6, 1.1 Hz, 2H), 7.38 (td, *J* = 7.5, 0.8 Hz, 2H), 1.19 (t, *J* = 7.9 Hz, 18H), 0.87 (q, *J* = 7.9 Hz, 12H); $^{13}$C NMR (151 MHz, $CDCl_3$) δ 190.50, 146.69, 142.34, 138.64, 134.82, 134.12, 129.93, 124.31, 123.66, 114.25, 107.87, 100.03, 7.74, 4.52; IR (KBr) *v* 1720 (CO) $cm^{-1}$; UV-Vis ($CHCl_3$) $\lambda_{max}$ 311, 332, 498, 522 nm; HRMS (ESI) for $C_{36}H_{39}O_2Si_2$ [$M^+$+H]: calcd 559.2489, found 559.2502.

**8c** ($SiMe_2$*t*-Bu). Chromatography on neutral alumina (9:1 hexanes/$CH_2Cl_2$ increasing polarity to 3:2 hexanes/$CH_2Cl_2$); 17% yield. $^1$H NMR (600 MHz,$CDCl_3$) δ 8.59 (d, *J* = 7.6 Hz, 2H), 7.73 (d, *J* = 7.0 Hz, 2H), 7.53 (td, *J* = 7.6, 1.2 Hz, 2H), 7.38 (td, *J* = 7.5, 0.8 Hz, 2H), 1.14 (s, 9H), 0.38 (s, 6H); $^{13}$C NMR (151 MHz, $CDCl_3$) δ 190.49, 146.70, 142.32, 138.63, 134.87, 134.11, 129.95, 124.34, 123.64, 114.20, 108.38, 99.73, 26.43, 17.09, –4.52; IR (KBr) *v* 1720 (CO) $cm^{-1}$; UV-Vis ($CHCl_3$) $\lambda_{max}$ 312, 331, 498, 526 nm; HRMS (ESI) for $C_{36}H_{38}O_2Si_2$ [$M^+$+H]: calcd 559.2489, found 559.2479.

**8d** (Si*i*-Pr$_3$). Chromatography on basic alumina (9:1 hexanes/$CH_2Cl_2$); 61% yield. $^1$H NMR (500 MHz, $CDCl_3$) δ 8.72 (d, *J* = 7.3 Hz, 2H), 7.75 (d, *J* = 7.0 Hz, 2H), 7.51 (dt, *J* = 7.6, 1.2 Hz), 7.38 (dt, *J* = 7.5, 0.7 Hz, 2H), 1.36-1.26 (m, 42H); $^{13}$C NMR (125 MHz, $CDCl_3$) δ 190.06, 146.44, 142.06, 138.47, 134.44, 133.78, 129.60, 124.09, 123.49, 114.02, 106.78, 100.37, 18.65, 11.42; IR (NaCl) *v* 1721 (CO) cm$^{-1}$; UV-Vis ($CHCl_3$) $\lambda_{max}$ 313, 333, 500, 525 nm; HRMS (ESI) for $C_{42}H_{51}O_2Si_2$ [$M^+$+H]: calcd 643.3428, found 643.3405.

**8e** (Si*i*-Bu$_3$). Chromatography on basic alumina (hexanes increasing polarity to 5:1 hexanes/$CH_2Cl_2$); 7% yield.$^1$H NMR (300 MHz, $CDCl_3$) δ 8.63 (d, *J* = 7.6 Hz, 2H), 7.73 (d, *J* = 6.8 Hz, 2H), 7.52 (td, *J* = 7.6, 1.3 Hz, 2H), 7.38 (td, *J* = 7.5, 0.9 Hz, 2H), 2.05 (m, 6H), 1.07 (d, *J* = 6.6 Hz, 36H), 0.91 (d, *J* = 7.0 Hz, 12H); $^{13}$C NMR (151 MHz, $CDCl_3$) δ 190.20, 146.58, 142.34, 138.65, 134.61, 134.10, 129.87, 124.28, 123.72, 114.33, 109.38, 100.52, 26.67, 25.34, 25.14; IR (KBr) *v* 1721 (CO) cm$^{-1}$; UV-Vis ($CHCl_3$) $\lambda_{max}$ 314, 333, 498, 524 nm; HRMS (ESI) for $C_{48}H_{63}O_2Si_2$ [$M^+$+H]: calcd 727.4367, found 727.4424.

**8f** ($SiPh_3$). Chromatography on neutralized alumina (20:1 hexanes/$CH_2Cl_2$ increasing polarity to 3:1 hexanes/$CH_2Cl_2$); 15% yield. $^1$H NMR (600 MHz, $CDCl_3$) δ 8.24 (d, *J* = 7.6 Hz, 2H), 7.92–7.84 (m, 12H), 7.71 (d, *J* = 7.3 Hz, 2H), 7.54–7.44 (m, 18H), 7.29 (t, *J* = 7.4 Hz, 2H), 7.07 (t, *J* = 7.6 Hz, 2H); $^{13}$C NMR (151 MHz, $CDCl_3$) δ 190.21, 147.20, 141.97, 138.83, 136.10, 135.05, 134.00, 132.79, 130.44, 129.99, 128.42, 124.39, 123.92, 113.95, 104.41, 102.82; IR (KBr) *v* 1720 (CO) cm$^{-1}$; UV-Vis ($CHCl_3$) $\lambda_{max}$ 312, 333, 496, 520 nm; HRMS (ESI) for $C_{60}H_{39}O_2Si_2$ [$M^+$+H]: calcd 847.2489, found 847.2490.

**Cross-coupling with 5,11-Dibromoindeno[1,2-*b*]fluorene-6,12-dione**. A pressure reaction vessel charged with dione **11** (0.73 g, 1.6 mmol), CuI (0.02 g, 0.08 mmol), $Pd(PPh_3)_2Cl_2$ (0.120 g, 0.17 mmol) in $Et_3N$ (15 mL) and THF (10 mL) was degassed with by evacuating and backfilling the reaction vessel with Ar (3x). The appropriate ethynylsilane (8.3 mmol) was added and the sealed flask was stirred at 100 °C for 36 h. After cooling to rt, the solvent was removed in vacuo and the residue was purified by column chromatography on silica (see below for eluent conditions) to give the product as an orange solid. Analytical samples were obtained using a recycling HPLC with polystyrene beads eluting with $CHCl_3$.

**8b** ($SiEt_3$). 4:1 hexanes/$CH_2Cl_2$; 27% yield. Characterization data are listed above.

**8d** (Si*i*-$Pr_3$). 9:1 hexanes/$CH_2Cl_2$; 38% yield. Characterization data are listed above.

**8g** ($SiPr_3$). 4:1 hexanes/$CH_2Cl_2$; 72% yield. $^1$H NMR (600 MHz, $CDCl_3$) δ 8.59 (d, *J* = 7.6 Hz, 2H), 7.72 (d, *J* = 7.3 Hz, 2H), 7.51 (td, *J* = 7.5, 1.3 Hz, 2H), 7.39 (t, *J* = 7.4 Hz, 2H), 1.61 (m, 12H), 1.07 (t, *J* = 7.3 Hz, 18H), 0.86 (m, 12H); $^{13}$C NMR (151 MHz, $CDCl_3$): δ 190.42, 146.63, 142.34, 138.60, 134.71, 134.11, 129.91, 124.31, 123.66, 114.24, 108.45, 99.98, 18.58, 17.80, 16.09; UV/Vis ($CHCl_3$) $\lambda_{max}$ :312, 332, 524 nm ; HRMS (TOF MS ESI+) for $C_{42}H_{51}O_2Si_2^+$ [$M^+$+H]: calcd 643.3428; found 643.3397.

**8h** ($SiMe_2(CH_2)_2CF_3$). 4:1 hexanes/$CH_2Cl_2$ increasing polarity to 7:3 hexanes/$CH_2Cl_2$; 20% yield. $^1$H NMR (600 MHz, $CDCl_3$) δ 8.45 (d, *J* = 7.6 Hz, 2H), 7.72 (d, *J* = 7.7 Hz, 2H), 7.54 (dt, *J* = 7.6, 1.2 Hz, 2H), 7.40 (dt, *J* = 7.5, 0.8 Hz , 2H), 2.39 (m, 4H), 1.08 (m, 4H), 0.45 (s, 12H); $^{13}$C NMR (151 MHz, $CDCl_3$): δ 190.28, 146.65, 142.08, 138.75, 135.06, 134.06, 130.25, 124.51, 123.39, 113.87, 106.74, 100.35, 29.0 (q, *J* = 30.1 Hz), 8.16 (q, *J* = 2.2 Hz), -2.06, -3.63; UV/Vis ($CHCl_3$) $\lambda_{max}$ 308, 330, 516 nm; HRMS (TOF MS ESI+) for $C_{34}H_{29}O_2F_6Si_2^+$ [$M^+$+H]: calcd 639.1610; found 639.1606.

**8i** ($SiMe_2$*i*-Bu). 4:1 hexanes/$CH_2Cl_2$; 35% yield. $^1$H NMR (600 MHz, $CDCl_3$) δ 8.54 (d, *J* = 7.7 Hz, 2H), 7.71 (d, *J* = 7.2 Hz, 2H), 7.53 (dt, *J* = 7.6, 1.3 HZ, 2H), 7.37 (dt, *J* = 7.4, 1.0 Hz, 2H), 2.03 (n, *J* = 6.7 Hz 2H), 1.08 (d, *J* = 6.6 Hz, 12H), 0.88 (d, *J* = 6.6 Hz, 4H), 0.43 (s, 12H); $^{13}$C NMR (151 MHz, $CDCl_3$): δ 190.51, 146.61, 142.29, 138.57, 134.86, 134.08, 129.96, 124.28, 123.62, 114.23, 109.54, 99.43, 26.64, 26.43, 25.36, 0.76; UV/Vis ($CHCl_3$) $\lambda_{max}$ 311, 331, 523 nm; HRMS (TOF MS ESI+) for $C_{36}H_{39}O_2Si_2^+$ [$M^+$+H]: calcd 559.2489; found 559.2502.

**8j** ($SiMe_2Ph$). 4:1 hexanes/$CH_2Cl_2$; 24% yield. $^1$H NMR (600 MHz, $CDCl_3$) δ 8.37 (m, 2H), 7.82 (m, 4H), 7.70 (m, 2H), 7.45 (m, 6H), 7.34 (m, 4H), 0.68 (s, 12H); $^{13}$C NMR (151 MHz, $CDCl_3$): δ 190.50, 146.82, 138.64, 136.06, 135.03, 134.20, 134.02, 130.01, 129.98, 128.34, 124.30, 123.73, 114.09, 107.53, 100.34, 10.7; UV/Vis ($CHCl_3$) $\lambda_{max}$ :310, 331, 521 nm; HRMS (TOF MS ESI+) [$M]^+$ for $C_{40}H_{31}O_2Si_2^+$: calcd 599.1863; found 599.1870.

APPENDIX C

EXPERIMENTAL DETAILS FOR CHAPTER IV

**General Experimental Details**

NMR spectra were collected on a Bruker Avance III HD 600 with Prodigy BBO multinuclear Cryoprobe ($^{1}$H: 599.98 MHz, $^{13}$C: 150.88 MHz). Chemical shifts are reported in parts per million (ppm) relative to tetramethylsilane, which was referenced according to trace amounts of non-deuterated THF (1.73 & 3.58 ppm) for $^{1}$H NMR and THF-$d_8$ (67.57 & 25.37 ppm) for $^{13}$C NMR. Absorbance spectra were collected on a Perkin Elmer Lambda-1050 UV/Vis/NIR spectrophotometer. EPR spectra was collected on a Bruker EMX-080. THF was dried over Na/K alloy for NMR and EPR experiments. For absorbance spectra THF was distilled from a potassium/benzophenone still. Indenofluorenes **6a** and **6b** were synthesized as previously reported.

**Preparation of Anion Radical 6a$^{\bullet -}$**

An apparatus (Figure S1) was constructed from borosilicate glass and dried in a 100 °C oven. The apparatus was then cooled to room temperature under nitrogen and approximately 0.05 mg of **6a** was collected on a melting point capillary that was open on both ends and deposited at point A. Potassium metal was added at point B and then opening C was sealed with an oxygen/natural gas torch. Vacuum was pulled (approx. $10^{-6}$ torr) and potassium metal was sublimed with a Bunsen burner, resulting in a metal mirror inside D. The apparatus was then sealed at point E. Dry THF (approx. 1 mL) from a NaK still was directly distilled through the vacuum system to A and the apparatus was sealed at point F. Controlled exposure to the potassium mirror resulted in the changing of the solution color from purple to a light yellow, from which the EPR spectrum in Figure 5 was obtained.

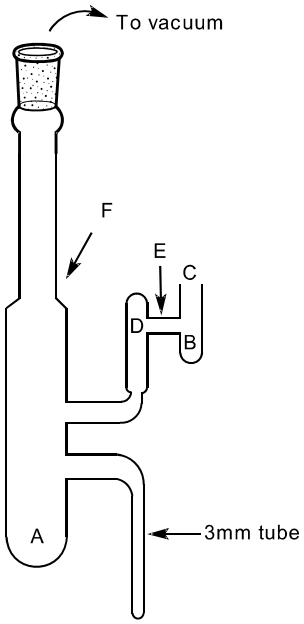


**Figure S1**. Apparatus used for generation of anion radical.

**Preparation of Dianion 6a$^{2-}$ for NMR Studies**

A dry J-Young NMR tube was charged with **6a** (3 mg, 0.01 mmol) and 18-crown-6 ether (3 mg, 0.02 mmol). A glass pedestal was then added followed by a freshly cut piece of potassium metal. THF-$d_8$ (approx. 0.7 mL) was distilled from a NaK still directly through the vacuum line into the NMR tube, which was then sealed from the vacuum line. NMR spectra of the neutral species was collected, then the solution was shaken on the potassium metal and the reduction was monitored via EPR. When the EPR signal became very weak, the NMR spectra of the dianion were collected. $^1$H NMR (600 MHz, THF-$d_8$) δ 8.34 (s, 2H), 7.94 (d, $J$ = 7.5 Hz, 2H), 7.49 (d, $J$ = 7.8 Hz, 2H), 6.93 (t, $J$ = 7.3 Hz, 2H), 6.53 (t, $J$ = 7.1 Hz, 2H); $^{13}$C NMR (600 MHz, THF-$d_8$) δ 143.99, 133.66, 124.97, 124.83, 121.89, 119.65, 119.16, 116.81, 110.58, 105.55, 89.09, 75.25

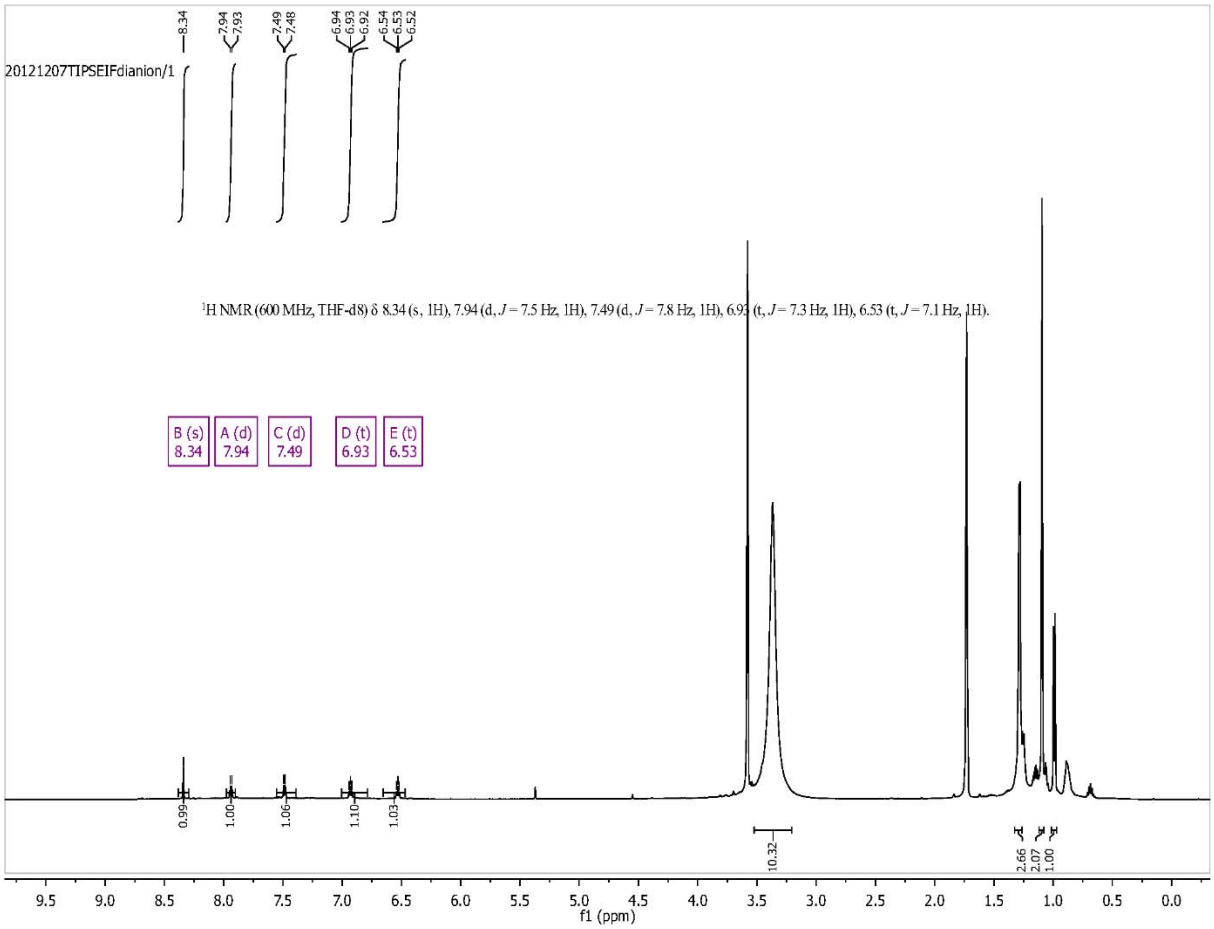


**Figure S2**. $^{1}$H NMR spectrum of dianion **6a**$^{2-}$.

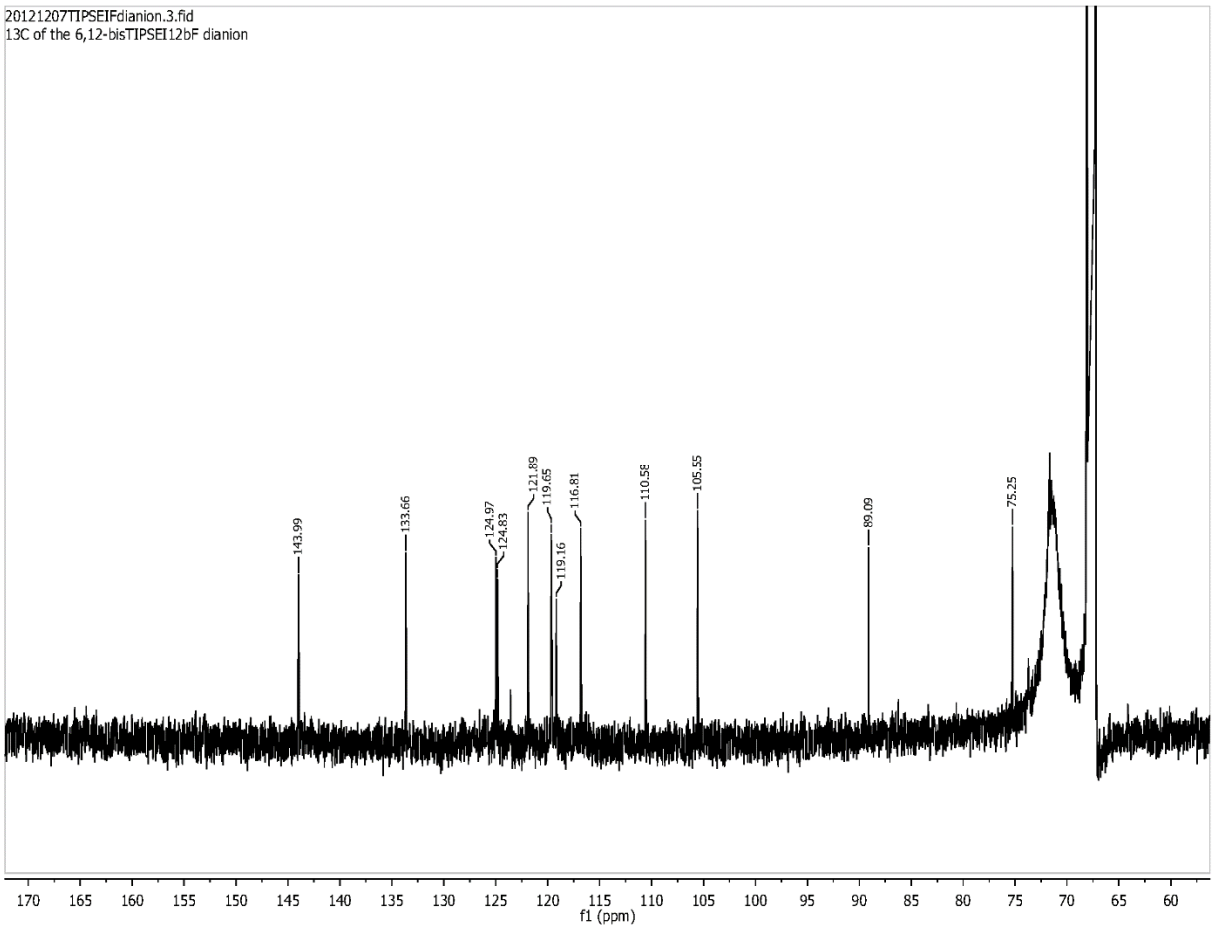


**Figure S3**. $^{13}$C NMR spectrum of dianion **6a**$^{2-}$.

**Preparation of Single Crystals of Dianion 6b$^{2-}$**

THF (2 mL) was added to a closed system containing **6b** (3 mg, 0.0035 mmol) and Rb metal (excess, approx. 6 equiv.). The initial color of the reaction solution was green. The mixture was stirred for 24 h at room temperature and then filtered. The filtrate was layered with 18-crown-6 (2 equiv.) in hexanes (2 mL) and kept at 10 °C. Some small amount of a fine light-yellow precipitate was observed after 72 h. This precipitate was filtered off leaving a green solution that was re-layered with hexanes (1.5 mL) and kept at 10 °C. Green crystals (blocks) were observed in 96 h in modest yield (approx. 20%).

**X-Ray Diffraction Data for 6a**

X-ray diffraction data for **6a** were collected at 173 K on a Bruker Apex diffractometer using MoKα-radiation (λ=0.71073 Å). Absorption corrections were applied by SADABS. The structure was determined by direct methods and refined on $F^2$ by a full matrix least-squares procedure. All non-H atoms were refined with anisotropic thermal parameters. All H atoms were refined in calculated positions in a rigid group model. All calculations were performed by the Bruker SHELXTL 6.10 package.

**Table S1.** Crystallographic Data for **6a**.

| | |
|---|---|
| Empirical formula | $C_{42}H_{52}Si_2$ |
| $M_r$ | 613.02 |
| Crystal system | Monoclinic |
| Space group | *P2(1)/c* |
| $a$ (Å) | 11.393(3) |
| $b$ (Å) | 16.693(4) |
| $c$ (Å) | 11.163(2) |
| $\alpha$ (º) | 90.00 |
| $\beta$ (º) | 119.083(4) |
| $\gamma$ (º) | 90.00 |
| $V$ (Å$^3$) | 1855.4(7) |
| $Z$ | 2 |
| $\rho_{calcd}$ [g·cm$^{-3}$] | 1.097 |
| $\mu$ [mm$^{-1}$] | 0.122 |
| reflections collected | 17344 |
| 2θ range for data collection | 2.72−50.00 |
| independent reflections | 3245 |
| data/restraints/parameters | 3245/0/199 |
| $R_1$,[a] $wR_2$[b] [$I>2\sigma(I)$] | 0.0824, 0.1955 |
| $R_1$,[a] $wR_2$[b] (all data) | 0.0970, 0.2037 |
| quality of fit[c] | 1.098 |
| peak/hole [e Å$^{-3}$] | 0.498/–0.305 |

[a] $R_1 = \Sigma||F_o|-|F_c||/\Sigma|F_o|$.

[b] $wR_2 = [\Sigma[w(F_o^2-F_c^2)^2]/\Sigma[w(F_o^2)^2]]^{½}$.

[c] Quality-of-fit = $[\Sigma[w(F_o^2-F_c^2)^2]/(N_{obs}-N_{params})]^{½}$, based on all data.

**X-Ray Diffraction Data for $6b^{2-}$**

X-ray diffraction data for $\mathbf{6b^{2-}}$ were collected on a Bruker SMART APEX CCD-based X-ray diffractometer with graphite-monochromated Mo-K$\alpha$ radiation ($\lambda$ = 0.71073 Å) at $T$ = 100(2) K. Data were corrected for absorption effects using the empirical method SADABS. The structures were solved by direct methods and refined using the Bruker SHELXTL (Version 6.14) software package. All non-H atoms were refined with anisotropic thermal parameters. Hydrogen atoms were included at idealized positions using the riding model.

**Table S2.** Crystallographic Data for $\mathbf{6b^{2-}}$.

| | |
|---|---|
| Empirical formula | $C_{92}H_{140}O_{14}Rb_2Si_2$ |
| $M_r$ | 1697.16 |
| Crystal system | Triclinic |
| Space group | *P -1* |
| $a$ (Å) | 15.372(5) |
| $b$ (Å) | 15.458(5) |
| $c$ (Å) | 20.271(6) |
| $\alpha$ (º) | 84.859(4) |
| $\beta$ (º) | 78.483(4) |
| $\gamma$ (º) | 75.506(4) |
| $V$ (Å$^3$) | 4566(2) |
| $Z$ | 2 |
| $\rho_{calcd}$ [g·cm$^{-3}$] | 1.235 |
| $\mu$ [mm$^{-1}$] | 1.157 |
| reflections collected | 39077 |
| 2θ range for data collection | 2.72−50.00 |
| independent reflections | 15977 |
| data/restraints/parameters | 15977/0/991 |
| $R_1$,[a] $wR_2$[b] [$I$>2σ($I$)] | 0.0801, 0.1379 |
| $R_1$,[a] $wR_2$[b] (all data) | 0.1989, 0.1704 |
| quality of fit[c] | 0.853 |
| peak/hole [e Å$^{-3}$] | 0.487/–0.465 |

[a] $R_1 = \Sigma||F_o|-|F_c||/\Sigma|F_o|$.

[b] $wR_2 = [\Sigma[w(F_o^2-F_c^2)^2]/\Sigma[w(F_o^2)^2]]^{½}$.

[c] Quality-of-fit = $[\Sigma[w(F_o^2-F_c^2)^2]/(N_{obs}-N_{params})]^{½}$, based on all data.

**Preparation of Samples for Electronic Absorption Spectra Measurements**

In an inert dry glovebox **6a** (approx. 0.2 mg) and 18-crown-6 ether (approx. 1 mg) was added to a quartz cuvette with a screw cap and a glass pedestal was added followed by dry THF (approx. 1 mL). A freshly cut piece of potassium metal was then added and the cuvette was sealed shut. Spectra were collected periodically during the course of the reduction.

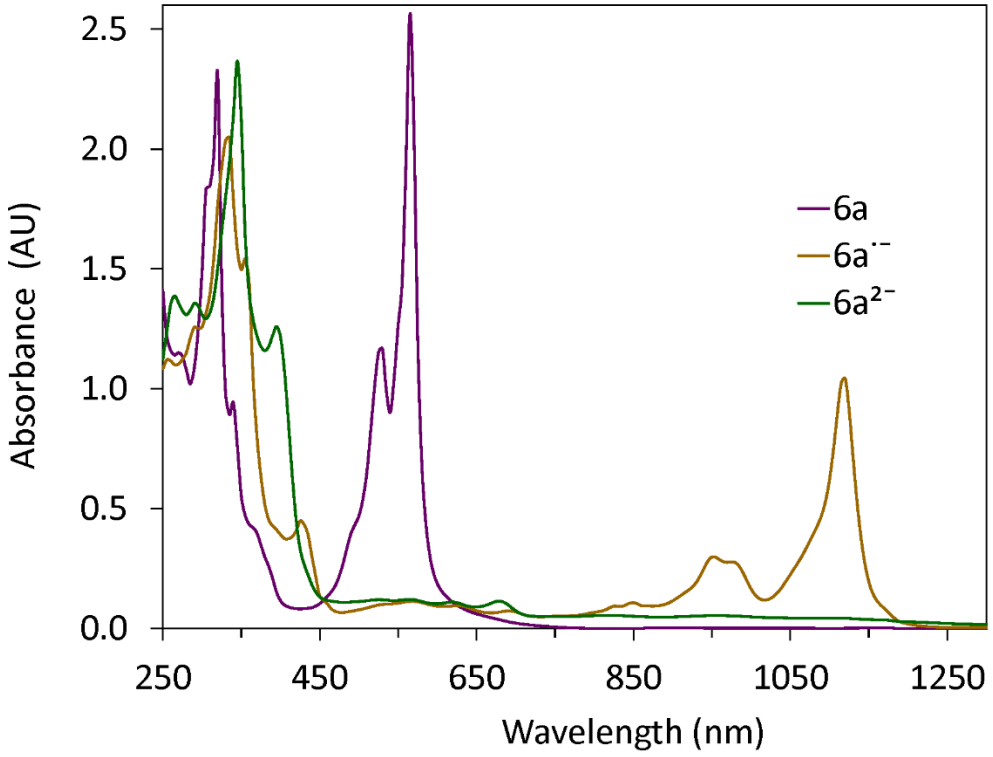


**Figure S4**. Electronic absorption spectra of **6a**, **6a**$^{\bullet-}$ and **6a**$^{2-}$ in nm (see paper for x-axis in eV).

**Computational Details**

Geometries were minimized with the methods mentioned in text and verified as minima by frequency analysis. The coordinates as well as energies for the geometry minimizations are located in their respective files.

Neutral **6c**

RB3LYP/6-31++G(d,p)

Geometry: neutral.xyz

Zero-point correction= 0.474600 (Hartree/Particle)

Thermal correction to Energy= 0.508372

Thermal correction to Enthalpy= 0.509317

Thermal correction to Gibbs Free Energy= 0.406121

Sum of electronic and zero-point Energies= –1738.663164

Sum of electronic and thermal Energies= –1738.629392

Sum of electronic and thermal Enthalpies= –1738.628447

Sum of electronic and thermal Free Energies= –1738.731643

Anion Radical **6c**$^{\bullet-}$

UB3LYP/6-31++G(d,p)

Geometry: anion.xyz

Zero-point correction= 0.471775 (Hartree/Particle)

Thermal correction to Energy= 0.505663

Thermal correction to Enthalpy= 0.506607

Thermal correction to Gibbs Free Energy= 0.401441

Sum of electronic and zero-point Energies= –1738.751531

Sum of electronic and thermal Energies= –1738.717643

Sum of electronic and thermal Enthalpies= –1738.716699

Sum of electronic and thermal Free Energies= –1738.821864

Dianion **6a**$^{2-}$

RB3LYP/6-31++G(d,p)

Geometry: dianion.xyz

Zero-point correction= 0.469054 (Hartree/Particle)

Thermal correction to Energy= 0.503068

Thermal correction to Enthalpy= 0.504012

Thermal correction to Gibbs Free Energy= 0.400173

Sum of electronic and zero-point Energies= –1738.723116

Sum of electronic and thermal Energies= –1738.689102

Sum of electronic and thermal Enthalpies= –1738.688158

Sum of electronic and thermal Free Energies= –1738.791998

# APPENDIX D

# EXPERIMENTAL DETAILS FOR CHAPTER V

## Experimental Details

All molecules were synthesized as previously reported.[1–3]

Femtosecond transient absorption (fsTA) measurements were made using a regeneratively amplified Ti:sapphire laser system operating at 832 nm and a 1 kHz repetition rate as described previously.[4–6] The output of the amplifier was frequency-doubled to 416 nm using a 200 μm thick lithium triborate crystal to produce 120 fs excitation pulses. The frequency-doubled output of the amplifier was used to pump a two-stage optical parametric amplifier to generate 495 nm, 130 fs laser pulses. A small portion of the fundamental was focused onto a sapphire disk to generate the white-light probe spanning 440–800 nm. Spectral and kinetic data were collected with a CCD array detector and a 7 ns pump–probe delay track. Solution samples had an absorbance of 0.3-0.7 in dry toluene at the excitation wavelength and were irradiated in 2 mm quartz cuvettes with 1 μJ/pulse focused to a 0.2 mm diameter spot. The total instrument response function (IRF) was 180 fs. Transient spectra were averaged for 5 s. Kinetic traces corresponding to the ground state bleach and excited state absorption for each spectrum were fit using a Levenberg-Marquardt nonlinear leastsquares fit to a sum of exponentials convoluted with a Gaussian instrument response function.

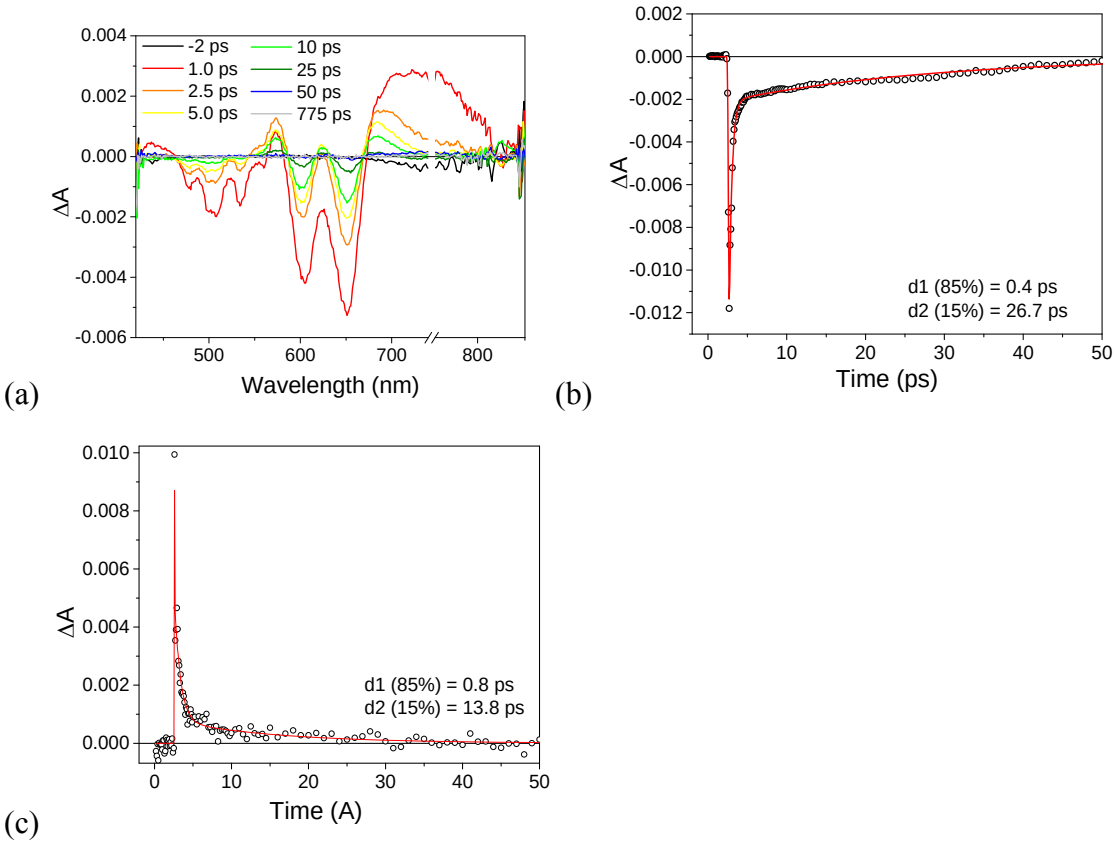


Figure S1. (a) fsTA of **1a** in toluene at indicated times following 120 fs, 495 nm laser pulses; (b) kinetic fit of additional ground state bleach feature at 602 nm; kinetic fit of excited state absorption feature at 711 nm.

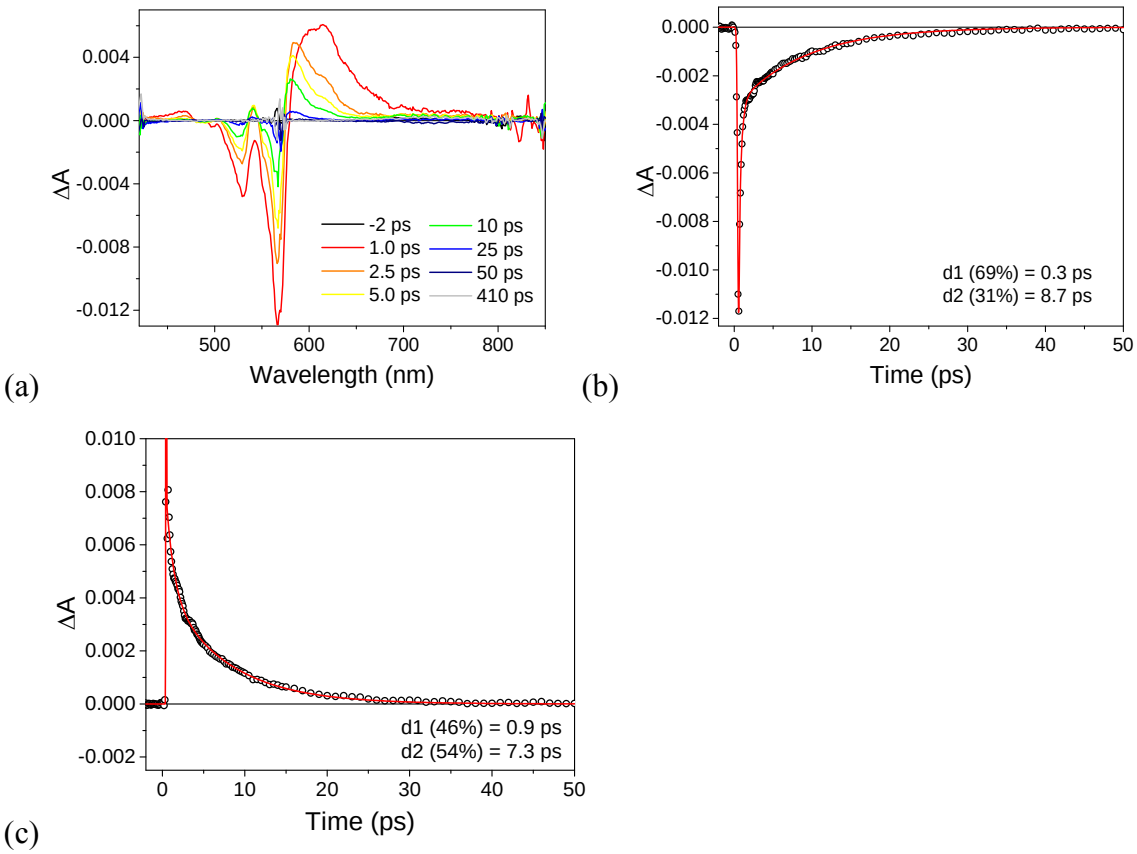


Figure S2. (a) fsTA of **2a** in toluene at indicated times following 120 fs, 495 nm laser pulses; (b) kinetic fit of additional ground state bleach feature at 529 nm; (c) kinetic fit of excited state absorption feature at 600 nm.

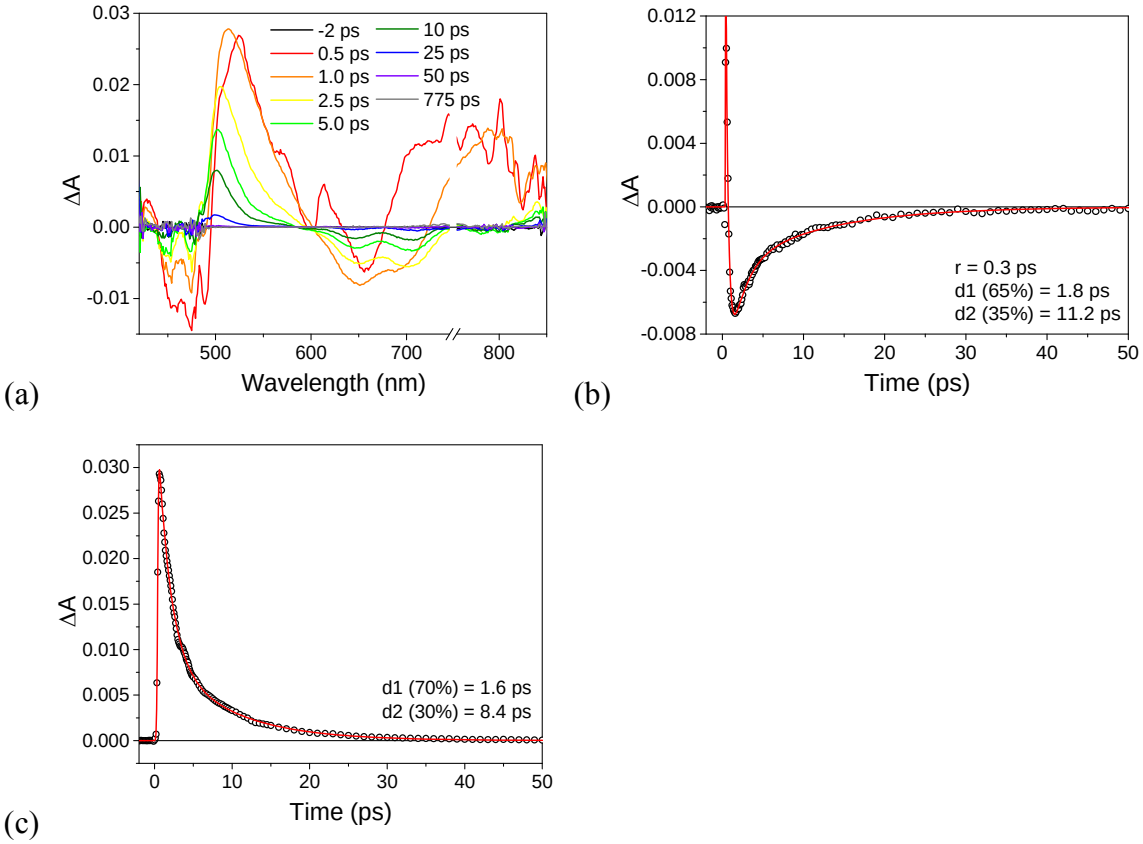


Figure S3. (a) fsTA of **3a** in toluene at indicated times following 120 fs, 495 nm laser pulses; (b) kinetic fit of additional ground state bleach at 700 nm; (c)kinetic fit of excited state absorption at 522 nm. Note that overlap with the excited state at 700 nm introduces an additional rise component to the fit.

**Computational Details**

For all structures the ground states were minimized using FORS(4,4)/cc-pVDZ. The $S_1$ state and the conical intersection geometries were minimized using state averaged FORS(4,4) averaging over the $S_0$ and $S_1$ states with equal weights for each. The $S_0$ and $S_1$ geometries were verified as stationary points by frequency analysis. No symmetry was enforced when searching for the conical intersections and the geometries were considered minimized when a maximum gradient of less than 0.0004 Hatree/bohr was located, as set by OPTTOL in GAMESS. The programs Macmolplt,[7] Chemcraft,[8] and CYLview[9] were used to generate and view structures.

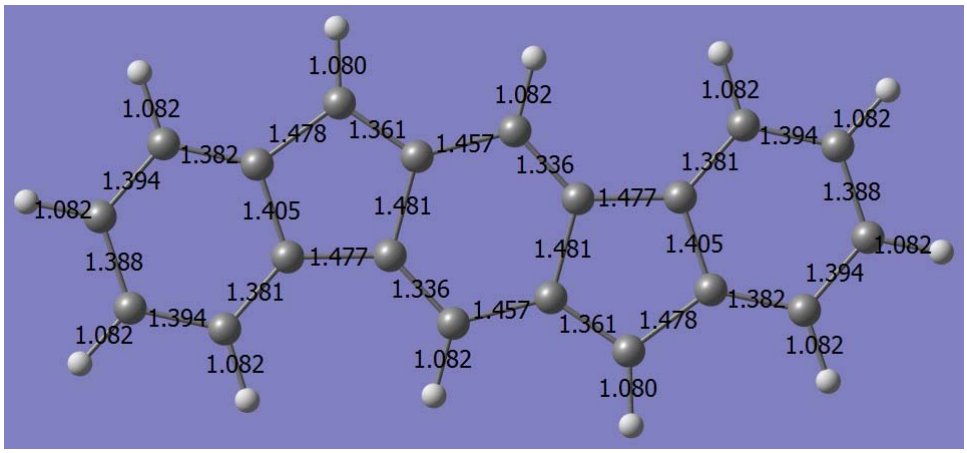


$S_0$

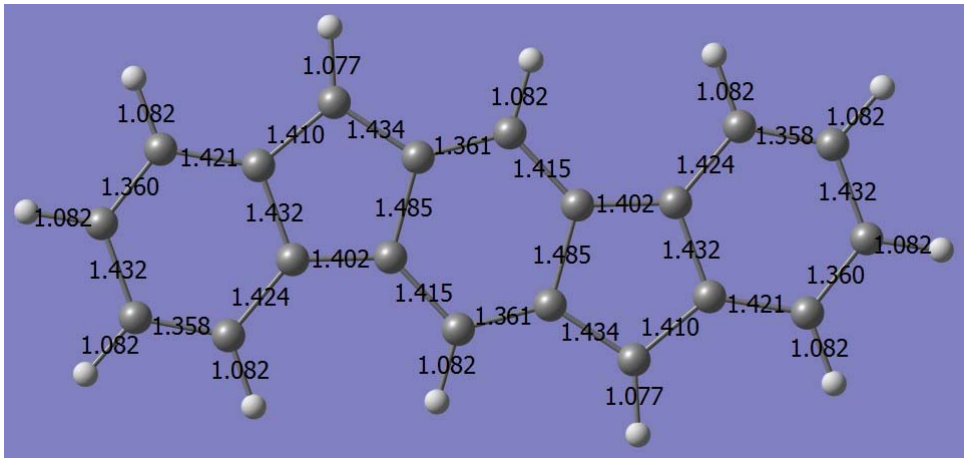


$S_1$

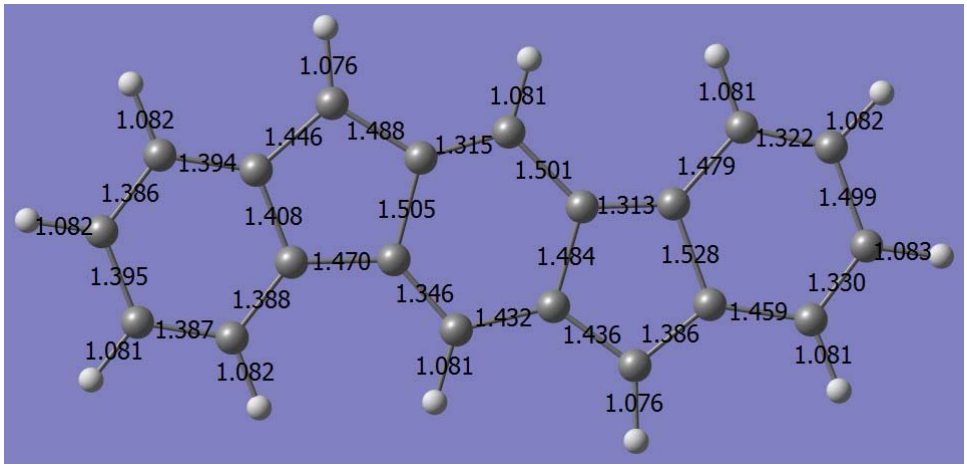


$S_0/S_1$ conical intersection

Figure S4. Indeno[1,2-*b*]fluorene. FORS(4,4)/cc-pVDZ optimized geometries.

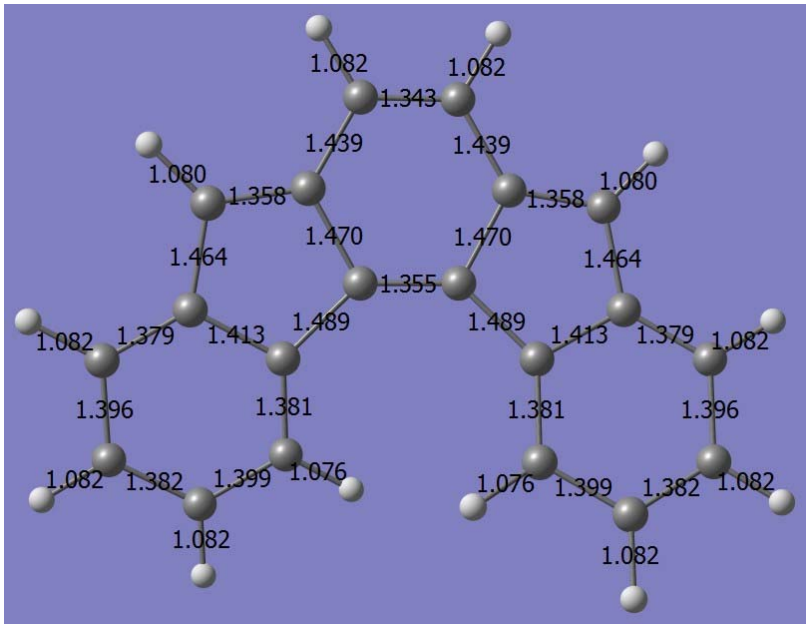
1.082
1.082
1.343
1.439
1.439
1.080
1.358
1.358
1.080
1.470
1.470
1.464
1.464
1.355
1.082
1.379
1.413
1.489
1.489
1.413
1.379
1.082
1.396
1.381
1.381
1.396
1.082
1.382
1.399
1.076
1.076
1.399
1.382
1.082
1.082
1.082

$S_0$

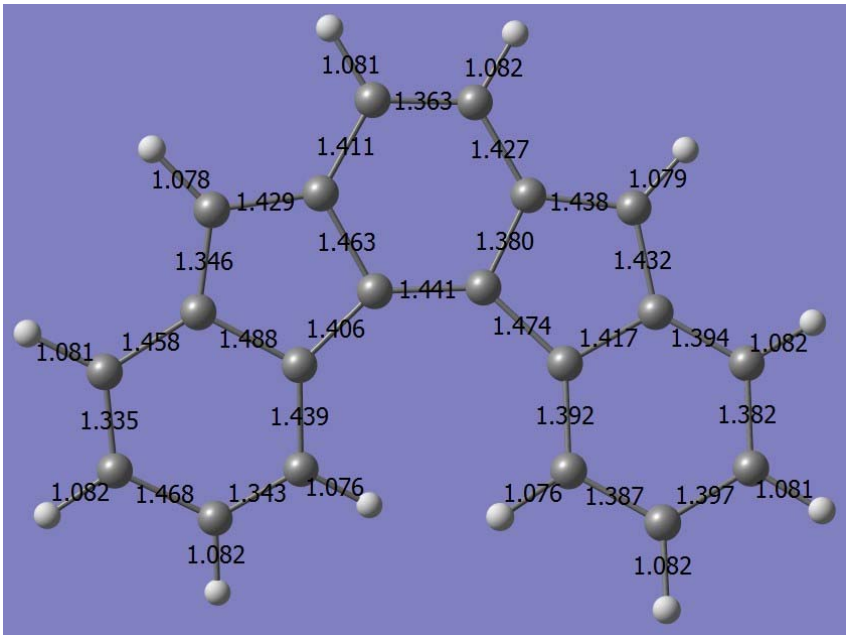
1.081
1.082
1.363
1.411
1.427
1.078
1.429
1.438
1.079
1.463
1.380
1.346
1.432
1.441
1.081
1.458
1.488
1.406
1.474
1.417
1.394
1.082
1.335
1.439
1.392
1.382
1.082
1.468
1.343
1.076
1.076
1.387
1.397
1.081
1.082
1.082

$S_1$

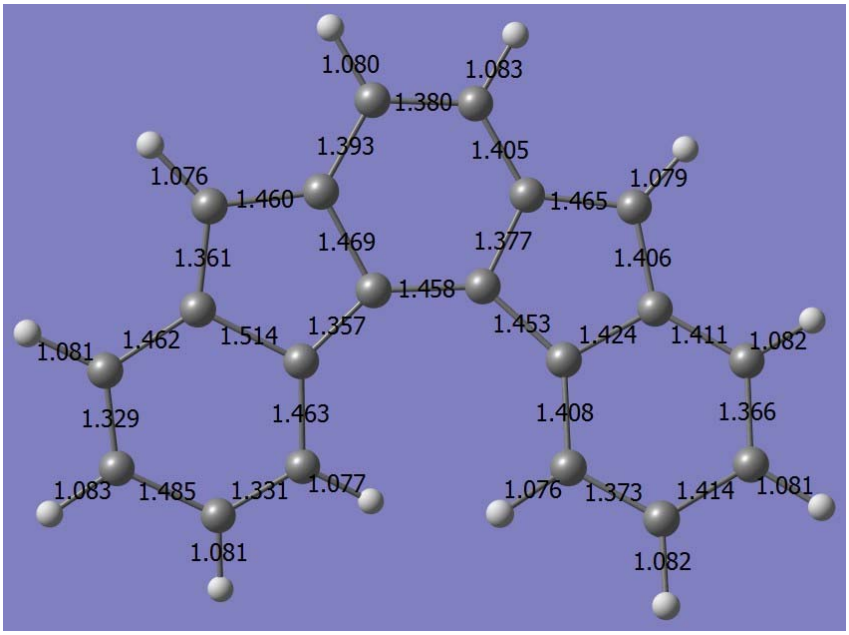


$S_0/S_1$ conical intersection

Figure S5. Indeno[2,1-*c*]fluorene. FORS(4,4)/cc-pVDZ optimized geometries.

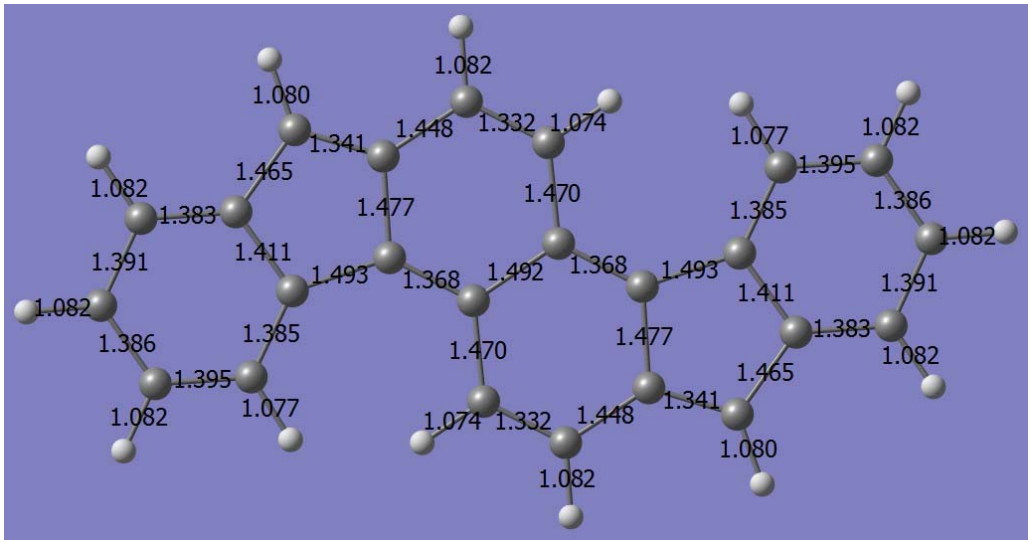


$S_0$

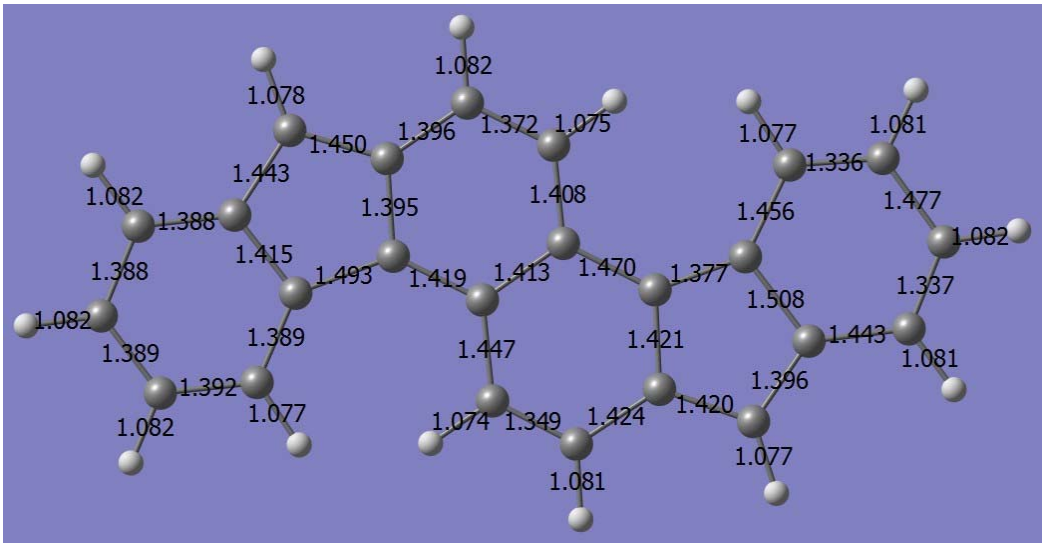


$S_1$

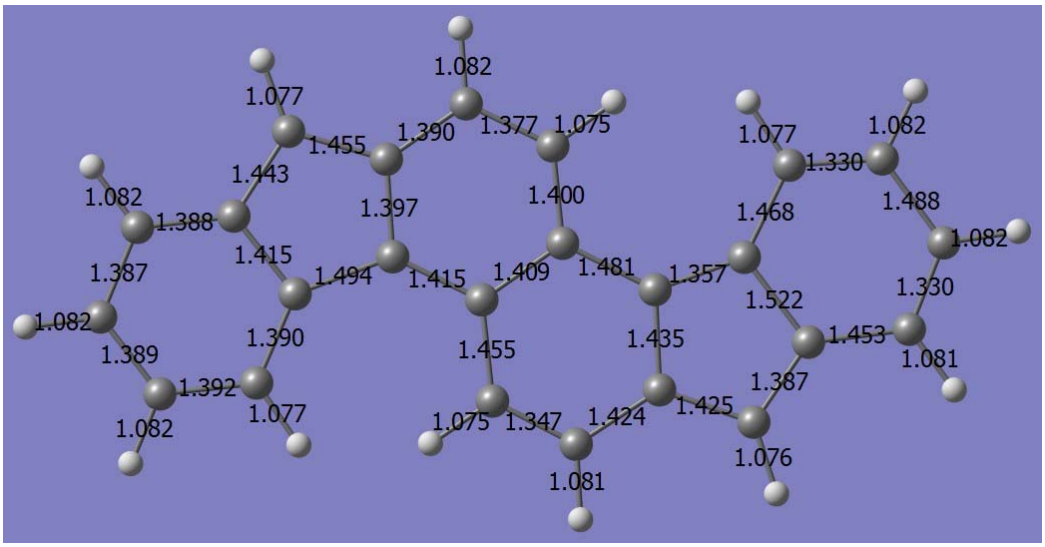


$S_0/S_1$ conical intersection

Figure S6. Fluoreno[4,3-*c*]fluorene. FORS(6,6)/cc-pVDZ optimized geometries.

TD-CAM-B3LYP/6311+G(2df,2p) transition information:

Fluoreno[4,3-*c*]fluorene

| state | | energy (Ha) | excitation (eV) | transition dipole (A.U.) | | | oscillator strength |
|---|---|---|---|---|---|---|---|
| | | | | X | Y | Z | |
| 0 | AG | -922.7172465987 | 0.000 | | | | |
| 1 | AG | -922.6300501647 | 2.373 | 0.000 | 0.000 | 0.000 | 0.000 |
| 2 | BU | -922.6246063191 | 2.521 | 3.281 | 0.362 | 0.000 | 0.673 |
| 3 | BU | -922.5979042752 | 3.247 | -1.836 | -0.511 | 0.000 | 0.289 |
| 4 | AG | -922.5770143613 | 3.816 | 0.000 | 0.000 | 0.000 | 0.000 |
| 5 | AG | -922.5692845461 | 4.026 | 0.000 | 0.000 | 0.000 | 0.000 |
| 6 | BU | -922.5499057503 | 4.554 | 2.600 | 0.456 | 0.000 | 0.777 |
| 7 | AG | -922.5482172615 | 4.600 | 0.000 | 0.000 | 0.000 | 0.000 |
| 8 | BU | -922.5438595116 | 4.718 | -2.375 | 0.397 | 0.000 | 0.670 |
| 9 | AG | -922.5376246755 | 4.888 | 0.000 | 0.000 | 0.000 | 0.000 |
| 10 | BU | -922.5341866871 | 4.981 | 0.622 | 0.004 | 0.000 | 0.047 |

STATE # 1 ENERGY = 2.372736 EV

OSCILLATOR STRENGTH = 0.000000

LAMBDA DIAGNOSTIC = 0.742 (RYDBERG/CHARGE TRANSFER CHARACTER)

SYMMETRY OF STATE = AG

| OCC | VIR | EXCITATION AMPLITUDE | DE-EXCITATION AMPLITUDE |
|---|---|---|---|
| I | A | X(I->A) | Y(A->I) |
| --- | --- | -------- | -------- |
| 64 | 80 | -0.038906 | 0.002023 |
| 74 | 80 | -0.051874 | 0.003154 |
| 76 | 80 | 0.050213 | -0.003302 |
| 78 | 80 | 0.989407 | -0.031855 |
| 77 | 83 | 0.090794 | -0.003803 |
| 79 | 83 | -0.030316 | 0.021267 |
| 78 | 92 | 0.032471 | 0.002135 |

Indeno[1,2-*b*]fluorene

| state | | energy (Ha) | excitation (eV) | transition dipole (A.U.) | | | oscillator strength |
|---|---|---|---|---|---|---|---|
| | | | | X | Y | Z | |
| 0 | AG | -769.1374924636 | 0.000 | | | | |
| 1 | AG | -769.0393524245 | 2.671 | 0.000 | 0.000 | 0.000 | 0.000 |
| 2 | BU | -769.0291006288 | 2.949 | 2.733 | -0.418 | 0.000 | 0.552 |
| 3 | AG | -768.9881286127 | 4.064 | 0.000 | 0.000 | 0.000 | 0.000 |
| 4 | BU | -768.9782350703 | 4.334 | -0.664 | 0.525 | 0.000 | 0.076 |
| 5 | AG | -768.9739567137 | 4.450 | 0.000 | 0.000 | 0.000 | 0.000 |
| 6 | BU | -768.9616530570 | 4.785 | -3.711 | 0.385 | 0.000 | 1.631 |
| 7 | BU | -768.9487403284 | 5.136 | -0.603 | -0.614 | 0.000 | 0.093 |
| 8 | AG | -768.9395379413 | 5.387 | 0.000 | 0.000 | 0.000 | 0.000 |
| 9 | AG | -768.9377947567 | 5.434 | 0.000 | 0.000 | 0.000 | 0.000 |
| 10 | BU | -768.9338148091 | 5.542 | -0.401 | -0.124 | 0.000 | 0.024 |

STATE # 1 ENERGY = 2.670526 EV

OSCILLATOR STRENGTH = 0.000000

LAMBDA DIAGNOSTIC = 0.715 (RYDBERG/CHARGE TRANSFER CHARACTER)

SYMMETRY OF STATE = AG

| | | EXCITATION | DE-EXCITATION |
|---|---|---|---|
| OCC | VIR | AMPLITUDE | AMPLITUDE |
| I | A | X(I->A) | Y(A->I) |
| --- | --- | -------- | -------- |
| 60 | 67 | 0.083763 | -0.007613 |
| 61 | 67 | -0.068841 | 0.003706 |
| 65 | 67 | -0.988404 | 0.029800 |
| 63 | 68 | 0.059942 | -0.002438 |
| 63 | 70 | -0.065840 | 0.004354 |
| 65 | 71 | 0.033948 | 0.003204 |

Indeno[2,1-*c*]fluorene

| state | | energy (Ha) | excitation (eV) | transition dipole (A.U.) | | | oscillator strength |
|---|---|---|---|---|---|---|---|
| | | | | X | Y | Z | |
| 0 | A | -769.1312124153 | 0.000 | | | | |
| 1 | B | -769.0479036414 | 2.267 | 1.255 | -0.010 | 0.000 | 0.087 |
| 2 | B | -769.0099572896 | 3.300 | 1.897 | 0.022 | 0.000 | 0.291 |
| 3 | A | -769.0078983174 | 3.356 | 0.000 | 0.000 | -0.527 | 0.023 |
| 4 | B | -768.9747223642 | 4.258 | -2.349 | 0.023 | 0.000 | 0.575 |
| 5 | A | -768.9697201217 | 4.394 | 0.000 | 0.000 | -0.207 | 0.005 |
| 6 | B | -768.9497559751 | 4.938 | -1.317 | 0.027 | 0.000 | 0.210 |
| 7 | B | -768.9413145873 | 5.167 | -1.124 | -0.103 | 0.000 | 0.161 |
| 8 | A | -768.9398471706 | 5.207 | 0.000 | 0.000 | 0.940 | 0.113 |
| 9 | B | -768.9364086186 | 5.301 | 0.132 | -0.069 | 0.000 | 0.003 |
| 10 | A | -768.9359113293 | 5.314 | 0.000 | 0.000 | 0.798 | 0.083 |

STATE # 1 ENERGY = 2.266947 EV

OSCILLATOR STRENGTH = 0.087459

LAMBDA DIAGNOSTIC = 0.790 (RYDBERG/CHARGE TRANSFER CHARACTER)

SYMMETRY OF STATE = B

| | | EXCITATION | DE-EXCITATION |
|---|---|---|---|
| OCC | VIR | AMPLITUDE | AMPLITUDE |
| I | A | X(I->A) | Y(A->I) |
| --- | --- | -------- | -------- |
| 54 | 67 | -0.050004 | 0.003985 |
| 65 | 67 | -0.350402 | -0.003183 |
| 66 | 67 | -0.927036 | 0.071352 |
| 65 | 68 | 0.046917 | 0.028975 |
| 66 | 68 | 0.082134 | 0.006393 |
| 64 | 70 | 0.070647 | -0.000838 |
| 65 | 75 | 0.030272 | 0.013402 |
| 66 | 75 | 0.040487 | -0.005161 |

Coordinates for Compounds as described by xyz file format

Fluoreno[4,3-*c*]fluorene

$S_0$

38

C24H14

| | | | |
|---|---|---|---|
| C | -0.618543670 | 0.416647858 | 0.000000000 |
| C | 0.618543670 | -0.416647858 | 0.000000000 |
| C | 0.469131050 | -1.878752895 | 0.000000000 |
| C | -0.469131050 | 1.878752895 | 0.000000000 |
| H | 1.359173569 | -2.480611398 | 0.000000000 |

| | | | |
|---|---|---|---|
| H | -1.359173569 | 2.480611398 | 0.000000000 |
| C | -1.835708330 | -0.206871414 | 0.000000000 |
| C | 1.835708330 | 0.206871414 | 0.000000000 |
| C | -1.930423140 | -1.680334712 | 0.000000000 |
| C | 1.930423140 | 1.680334712 | 0.000000000 |
| C | -0.721226922 | -2.476947466 | 0.000000000 |
| C | 0.721226922 | 2.476947466 | 0.000000000 |
| H | -0.800519165 | -3.555671742 | 0.000000000 |
| H | 0.800519165 | 3.555671742 | 0.000000000 |
| C | -3.215992608 | -2.063256122 | 0.000000000 |
| C | 3.215992608 | 2.063256122 | 0.000000000 |
| C | -3.248261077 | 0.276238366 | 0.000000000 |
| C | 3.248261077 | -0.276238366 | 0.000000000 |
| C | -4.068439721 | -0.871643351 | 0.000000000 |
| C | 4.068439721 | 0.871643351 | 0.000000000 |
| C | -3.844746030 | 1.526241601 | 0.000000000 |
| C | 3.844746030 | -1.526241601 | 0.000000000 |
| C | -5.448141331 | -0.773952384 | 0.000000000 |
| C | 5.448141331 | 0.773952384 | 0.000000000 |
| C | -5.236284059 | 1.624582265 | 0.000000000 |
| C | 5.236284059 | -1.624582265 | 0.000000000 |
| H | -3.271787744 | 2.438452491 | 0.000000000 |
| H | 3.271787744 | -2.438452491 | 0.000000000 |
| C | -6.031307921 | 0.489430467 | 0.000000000 |
| C | 6.031307921 | -0.489430467 | 0.000000000 |
| H | -6.063506456 | -1.663922545 | 0.000000000 |
| H | 6.063506456 | 1.663922545 | 0.000000000 |
| H | -5.696276114 | 2.603558423 | 0.000000000 |
| H | 5.696276114 | -2.603558423 | 0.000000000 |
| H | -7.108872816 | 0.586384378 | 0.000000000 |
| H | 7.108872816 | -0.586384378 | 0.000000000 |

| | | | |
|---|---|---|---|
| H | -3.579626900 | -3.080263962 | 0.000000000 |
| H | 3.579626900 | 3.080263962 | 0.000000000 |

$S_1$

38

C24H14

| | | | |
|---|---|---|---|
| C | -0.579511257 | 0.347567848 | 0.000000000 |
| C | 0.588224412 | -0.447967316 | 0.000000000 |
| C | 0.462357021 | -1.849998999 | 0.000000000 |
| C | -0.446984386 | 1.788736130 | 0.000000000 |
| H | 1.342184693 | -2.467183483 | 0.000000000 |
| H | -1.338753647 | 2.388110558 | 0.000000000 |
| C | -1.846922332 | -0.289886268 | 0.000000000 |
| C | 1.893305158 | 0.228342186 | 0.000000000 |
| C | -1.921038931 | -1.683045402 | 0.000000000 |
| C | 1.944184610 | 1.648234972 | 0.000000000 |
| C | -0.764237632 | -2.464071180 | 0.000000000 |
| C | 0.746197159 | 2.417444537 | 0.000000000 |
| H | -0.832516898 | -3.543823864 | 0.000000000 |
| H | 0.799781034 | 3.497257854 | 0.000000000 |
| C | -3.309623974 | -2.099339369 | 0.000000000 |
| C | 3.283061334 | 2.122105122 | 0.000000000 |
| C | -3.248539329 | 0.223513306 | 0.000000000 |
| C | 3.191699053 | -0.230805247 | 0.000000000 |
| C | -4.110295236 | -0.898665068 | 0.000000000 |
| C | 4.088463213 | 0.981849064 | 0.000000000 |
| C | -3.814450579 | 1.492101042 | 0.000000000 |
| C | 3.840702904 | -1.533997216 | 0.000000000 |
| C | -5.490660564 | -0.756094858 | 0.000000000 |
| C | 5.522734872 | 0.821186940 | 0.000000000 |

| | | | |
|---|---|---|---|
| C | -5.200000067 | 1.630312568 | 0.000000000 |
| C | 5.174726993 | -1.614496367 | 0.000000000 |
| H | -3.219988404 | 2.389874796 | 0.000000000 |
| H | 3.262254474 | -2.442055085 | 0.000000000 |
| C | -6.034785824 | 0.520397569 | 0.000000000 |
| C | 6.034531739 | -0.413926450 | 0.000000000 |
| H | -6.130857594 | -1.628372237 | 0.000000000 |
| H | 6.158044592 | 1.696191850 | 0.000000000 |
| H | -5.629283286 | 2.623297444 | 0.000000000 |
| H | 5.658507418 | -2.581612034 | 0.000000000 |
| H | -7.108433238 | 0.652327854 | 0.000000000 |
| H | 7.106739593 | -0.560008376 | 0.000000000 |
| H | -3.673434700 | -3.113972178 | 0.000000000 |
| H | 3.602617608 | 3.150469360 | 0.000000000 |

$S_0/S_1$ Conical Intersection

38

C24H14

| | | | |
|---|---|---|---|
| C | -0.578968431 | 0.337701845 | -0.000444611 |
| C | 0.583654659 | -0.458129292 | -0.000311791 |
| C | 0.459849179 | -1.852704223 | 0.000260358 |
| C | -0.441963341 | 1.786268008 | -0.000232810 |
| H | 1.339613301 | -2.470051619 | 0.000704505 |
| H | -1.334880562 | 2.384440692 | -0.000144486 |
| C | -1.846169292 | -0.293020458 | -0.000352586 |
| C | 1.900404873 | 0.218808743 | -0.000160761 |
| C | -1.921692035 | -1.688201476 | -0.000415165 |
| C | 1.948689659 | 1.652762928 | 0.000531997 |
| C | -0.771484065 | -2.468035777 | 0.000127270 |
| C | 0.747783304 | 2.418108397 | 0.000116497 |

| | | | |
|---|---|---|---|
| H | -0.837999714 | -3.547618753 | 0.000546998 |
| H | 0.799305095 | 3.497731918 | 0.000112790 |
| C | -3.316413692 | -2.102664825 | -0.000843121 |
| C | 3.290864889 | 2.130620695 | 0.001183520 |
| C | -3.248382992 | 0.221351241 | -0.000139751 |
| C | 3.180933372 | -0.228866487 | -0.000030236 |
| C | -4.111993745 | -0.899279535 | -0.000270835 |
| C | 4.086486909 | 0.994848725 | 0.000652058 |
| C | -3.812803193 | 1.491129485 | -0.000012903 |
| C | 3.841377007 | -1.539603351 | -0.000554449 |
| C | -5.492345788 | -0.753925989 | 0.000144809 |
| C | 5.530004633 | 0.826138256 | 0.000563377 |
| C | -5.197789563 | 1.631952434 | 0.000097701 |
| C | 5.169205190 | -1.614589507 | -0.000167589 |
| H | -3.217235487 | 2.388333633 | -0.000127908 |
| H | 3.262896595 | -2.447570043 | -0.000620618 |
| C | -6.034279790 | 0.523041767 | 0.000399906 |
| C | 6.035113481 | -0.404705433 | 0.000037852 |
| H | -6.133520517 | -1.625452193 | 0.000267208 |
| H | 6.164486956 | 1.701455649 | 0.000631596 |
| H | -5.625777236 | 2.625488570 | -0.000115043 |
| H | 5.658678801 | -2.579063430 | 0.000054358 |
| H | -7.107741314 | 0.656479525 | 0.000545832 |
| H | 7.106654561 | -0.556035617 | -0.000247339 |
| H | -3.680378402 | -3.116822384 | 0.000033890 |
| H | 3.605816695 | 3.159677882 | -0.001820522 |

Indeno[1,2-*b*]fluorene

$S_0$

32

C20H12

| | | | |
|---|---|---|---|
| C | -1.353730935 | -0.413138327 | 0.000000000 |
| C | 1.353730935 | 0.413138327 | 0.000000000 |
| C | 0.967462500 | -1.016176754 | 0.000000000 |
| C | -0.967462500 | 1.016176754 | 0.000000000 |
| C | -0.441283174 | -1.388754278 | 0.000000000 |
| C | 0.441283174 | 1.388754278 | 0.000000000 |
| H | -0.716091980 | -2.435379279 | 0.000000000 |
| H | 0.716091980 | 2.435379279 | 0.000000000 |
| C | 2.830768263 | 0.436538333 | 0.000000000 |
| C | -2.830768263 | -0.436538333 | 0.000000000 |
| C | -3.273975893 | 0.897078051 | 0.000000000 |
| C | 3.273975893 | -0.897078051 | 0.000000000 |
| C | -2.091289527 | 1.783439424 | 0.000000000 |
| C | 2.091289527 | -1.783439424 | 0.000000000 |
| H | 2.131079878 | -2.862608909 | 0.000000000 |
| H | -2.131079878 | 2.862608909 | 0.000000000 |
| C | 3.737902835 | 1.478098723 | 0.000000000 |
| C | -3.737902835 | -1.478098723 | 0.000000000 |
| H | 3.407163699 | 2.508283959 | 0.000000000 |
| H | -3.407163699 | -2.508283959 | 0.000000000 |
| C | 5.100270755 | 1.181241968 | 0.000000000 |
| C | -5.100270755 | -1.181241968 | 0.000000000 |
| H | 5.823355859 | 1.985856652 | 0.000000000 |
| H | -5.823355859 | -1.985856652 | 0.000000000 |
| C | 4.624756439 | -1.190107173 | 0.000000000 |
| C | -4.624756439 | 1.190107173 | 0.000000000 |
| H | 4.972456153 | -2.214825489 | 0.000000000 |
| H | -4.972456153 | 2.214825489 | 0.000000000 |
| C | 5.537365567 | -0.136034907 | 0.000000000 |
| C | -5.537365567 | 0.136034907 | 0.000000000 |

| | | | |
|---|---|---|---|
| H | 6.598552713 | -0.347189848 | 0.000000000 |
| H | -6.598552713 | 0.347189848 | 0.000000000 |

$S_1$

32

C20H12

| | | | |
|---|---|---|---|
| C | 1.338145252 | 0.376538520 | 0.000000000 |
| C | -1.338145747 | -0.376538328 | 0.000000000 |
| C | -0.947528598 | 1.056146152 | 0.000000000 |
| C | 0.947528299 | -1.056146221 | 0.000000000 |
| C | 0.367934694 | 1.407062035 | 0.000000000 |
| C | -0.367934408 | -1.407062468 | 0.000000000 |
| H | 0.670579006 | 2.445934572 | 0.000000000 |
| H | -0.670578598 | -2.445935041 | 0.000000000 |
| C | -2.740004677 | -0.411584133 | 0.000000000 |
| C | 2.740004923 | 0.411584103 | 0.000000000 |
| C | 3.229918860 | -0.933903623 | 0.000000000 |
| C | -3.229918743 | 0.933903807 | 0.000000000 |
| C | 2.148751935 | -1.839214268 | 0.000000000 |
| C | -2.148752010 | 1.839214538 | 0.000000000 |
| H | -2.209818627 | 2.914935651 | 0.000000000 |
| H | 2.209818755 | -2.914935360 | 0.000000000 |
| C | -3.656227852 | -1.501785029 | 0.000000000 |
| C | 3.656227647 | 1.501784835 | 0.000000000 |
| H | -3.293323780 | -2.520727984 | 0.000000000 |
| H | 3.293323755 | 2.520727829 | 0.000000000 |
| C | -4.989715310 | -1.244423370 | 0.000000000 |
| C | 4.989715462 | 1.244423174 | 0.000000000 |
| H | -5.701547264 | -2.058668195 | 0.000000000 |
| H | 5.701547256 | 2.058668138 | 0.000000000 |

| | | | |
|---|---|---|---|
| C | -4.631974728 | 1.166920549 | 0.000000000 |
| C | 4.631974550 | -1.166920408 | 0.000000000 |
| H | -5.014496205 | 2.178592628 | 0.000000000 |
| H | 5.014496028 | -2.178592491 | 0.000000000 |
| C | -5.477839431 | 0.101457419 | 0.000000000 |
| C | 5.477839513 | -0.101457135 | 0.000000000 |
| H | -6.547700467 | 0.264587951 | 0.000000000 |
| H | 6.547700509 | -0.264587848 | 0.000000000 |

$S_0/S_1$ Conical Intersection

32

C20H12

| | | | |
|---|---|---|---|
| C | -1.301168758 | -0.347684281 | 0.017628541 |
| C | 1.403485228 | 0.391681046 | 0.005551811 |
| C | 0.981308627 | -1.030725438 | 0.026689744 |
| C | -0.904799148 | 1.104265890 | 0.017728641 |
| C | -0.413013627 | -1.358515031 | 0.024813688 |
| C | 0.358375506 | 1.469309482 | 0.003871714 |
| H | -0.727322577 | -2.392784040 | 0.030415422 |
| H | 0.660250878 | 2.507594342 | -0.000129437 |
| C | 2.716097110 | 0.424605883 | -0.001233331 |
| C | -2.771058164 | -0.375453338 | 0.012937260 |
| C | -3.263423066 | 0.943300119 | 0.029145752 |
| C | 3.223226219 | -1.017032096 | 0.024136548 |
| C | -2.168672157 | 1.888517325 | 0.037188596 |
| C | 2.139098602 | -1.880953486 | 0.038490901 |
| H | 2.149172581 | -2.956480844 | 0.066935895 |
| H | -2.246558437 | 2.961871078 | 0.052354539 |
| C | 3.710787904 | 1.519304062 | -0.032042390 |
| C | -3.639491537 | -1.458298809 | -0.009121539 |

| | | | |
|---|---|---|---|
| H | 3.370264458 | 2.545350444 | -0.056575648 |
| H | -3.259834805 | -2.471046293 | -0.020291660 |
| C | 4.999642101 | 1.223952229 | -0.035574181 |
| C | -5.006707397 | -1.227189404 | -0.020310065 |
| H | 5.749142504 | 2.003038823 | -0.066532162 |
| H | -5.696012308 | -2.059827589 | -0.047079587 |
| C | 4.664284368 | -1.244514309 | 0.033645377 |
| C | -4.639364887 | 1.167585496 | 0.033317524 |
| H | 5.046576721 | -2.255497640 | 0.065209902 |
| H | -5.032893560 | 2.174690552 | 0.057549384 |
| C | 5.480784434 | -0.195183814 | 0.001685113 |
| C | -5.496689308 | 0.078729731 | 0.004045568 |
| H | 6.552358278 | -0.350275008 | 0.003725053 |
| H | -6.566355786 | 0.243644918 | -0.001526974 |

Indeno[2,1-*c*]fluorene

$S_0$

32

C20H12

| | | | |
|---|---|---|---|
| C | -0.669759286 | 0.050060528 | -3.102939205 |
| C | 0.669759286 | -0.050060528 | -3.102939205 |
| C | -1.380722142 | 0.077685827 | -1.852060465 |
| C | 1.380722142 | -0.077685827 | -1.852060465 |
| C | -0.677511251 | 0.000062987 | -0.563940500 |
| C | 0.677511251 | -0.000062987 | -0.563940500 |
| C | -2.717722412 | 0.175256972 | -1.637869994 |
| C | 2.717722412 | -0.175256972 | -1.637869994 |
| C | -2.978619495 | 0.106822564 | -0.198534845 |
| C | 2.978619495 | -0.106822564 | -0.198534845 |
| H | -1.231492494 | 0.094464202 | -4.026089253 |
| H | 1.231492494 | -0.094464202 | -4.026089253 |

| | | | |
|---|---|---|---|
| H | -3.478246587 | 0.267076800 | -2.398988682 |
| H | 3.478246587 | -0.267076800 | -2.398988682 |
| C | -1.743963464 | -0.033276463 | 0.474389650 |
| C | 1.743963464 | 0.033276463 | 0.474389650 |
| C | -4.175134536 | 0.108754354 | 0.487202818 |
| C | 4.175134536 | -0.108754354 | 0.487202818 |
| C | -1.743052725 | -0.241080109 | 1.839743686 |
| C | 1.743052725 | 0.241080109 | 1.839743686 |
| C | -2.956616690 | -0.244606737 | 2.536002332 |
| C | 2.956616690 | 0.244606737 | 2.536002332 |
| H | -0.834839744 | -0.433967480 | 2.382764829 |
| H | 0.834839744 | 0.433967480 | 2.382764829 |
| C | -4.155432601 | -0.058054679 | 1.873289487 |
| C | 4.155432601 | 0.058054679 | 1.873289487 |
| H | -5.113830709 | 0.221626708 | -0.038873933 |
| H | 5.113830709 | -0.221626708 | -0.038873933 |
| H | -5.084347874 | -0.060893851 | 2.427937969 |
| H | 5.084347874 | 0.060893851 | 2.427937969 |
| H | -2.951519961 | -0.403537206 | 3.605896104 |
| H | 2.951519961 | 0.403537206 | 3.605896104 |

$S_1$

32

C20H12

| | | | |
|---|---|---|---|
| C | -0.652337352 | 0.064071970 | -3.033816659 |
| C | 0.704582415 | -0.067616915 | -3.049369753 |
| C | -1.355700782 | 0.101548161 | -1.792287815 |
| C | 1.399021065 | -0.112281707 | -1.821976645 |
| C | -0.730327306 | 0.020590599 | -0.564275625 |
| C | 0.710012261 | -0.024214793 | -0.533993067 |

| | | | |
|---|---|---|---|
| C | -2.780836923 | 0.175498215 | -1.615875789 |
| C | 2.810801914 | -0.189843073 | -1.612662374 |
| C | -3.037266229 | 0.100627769 | -0.208791739 |
| C | 3.025939578 | -0.108257230 | -0.286075386 |
| H | -1.209407962 | 0.121022869 | -3.959978449 |
| H | 1.251085737 | -0.118874616 | -3.980371179 |
| H | -3.517706884 | 0.258821092 | -2.399692157 |
| H | 3.551360299 | -0.274430977 | -2.392028719 |
| C | -1.792430779 | -0.024296852 | 0.456586035 |
| C | 1.729275399 | 0.023782627 | 0.432744005 |
| C | -4.243048285 | 0.092499537 | 0.489845155 |
| C | 4.264573206 | -0.110705781 | 0.482597569 |
| C | -1.791773676 | -0.218271030 | 1.835238837 |
| C | 1.760663967 | 0.246448367 | 1.854521751 |
| C | -2.997388712 | -0.231486371 | 2.521550661 |
| C | 2.935744593 | 0.258783026 | 2.505283548 |
| H | -0.879741297 | -0.388765972 | 2.380307559 |
| H | 0.851647363 | 0.440006972 | 2.397624015 |
| C | -4.217414042 | -0.064380018 | 1.862784439 |
| C | 4.210431616 | 0.055988529 | 1.806110337 |
| H | -5.182324265 | 0.197180107 | -0.037269396 |
| H | 5.205932202 | -0.240567807 | -0.033510482 |
| H | -5.139789762 | -0.075345303 | 2.427189127 |
| H | 5.119391042 | 0.060699421 | 2.393540064 |
| H | -2.990818810 | -0.382473686 | 3.593074009 |
| H | 2.961610408 | 0.437972872 | 3.571578124 |

$S_0/S_1$ Conical Intersection

32

C20H12

| | | | |
|---|---|---|---|
| C | -0.664206019 | 0.082220049 | -3.005729377 |
| C | 0.707164668 | -0.066465706 | -3.034802451 |
| C | -1.348454809 | 0.134529590 | -1.779431880 |
| C | 1.400048124 | -0.115059196 | -1.827281466 |
| C | -0.724553315 | 0.045318482 | -0.555094345 |
| C | 0.731702565 | -0.013813926 | -0.523229490 |
| C | -2.802003656 | 0.194995550 | -1.604924510 |
| C | 2.845602034 | -0.211188806 | -1.646517536 |
| C | -3.038599610 | 0.104919231 | -0.221680677 |
| C | 3.045905069 | -0.106434367 | -0.304187113 |
| H | -1.222677260 | 0.136818168 | -3.931877100 |
| H | 1.239627389 | -0.128751173 | -3.972845287 |
| H | -3.536120146 | 0.279725404 | -2.391014449 |
| H | 3.576252228 | -0.296546068 | -2.432147395 |
| C | -1.782887969 | -0.017340677 | 0.438871605 |
| C | 1.717735973 | 0.039997897 | 0.408242954 |
| C | -4.253924351 | 0.084768033 | 0.494323528 |
| C | 4.278086786 | -0.116369092 | 0.483288856 |
| C | -1.786909351 | -0.230044239 | 1.830894753 |
| C | 1.755429684 | 0.264880118 | 1.853320051 |
| C | -2.982211022 | -0.256656106 | 2.506180063 |
| C | 2.916603247 | 0.264027417 | 2.504577169 |
| H | -0.873560571 | -0.405123917 | 2.372073628 |
| H | 0.845317876 | 0.473087173 | 2.390026144 |
| C | -4.222957117 | -0.082889845 | 1.850123601 |
| C | 4.206369751 | 0.045679760 | 1.800782020 |
| H | -5.193226033 | 0.193558710 | -0.032166636 |
| H | 5.224580727 | -0.255154206 | -0.021108269 |
| H | -5.138926027 | -0.103173356 | 2.424117683 |
| H | 5.109843996 | 0.038642409 | 2.397455734 |
| H | -2.977002920 | -0.424458701 | 3.575555193 |

| | | | |
|---|---|---|---|
| H | 2.947950059 | 0.446301389 | 3.570065000 |

APPENDIX E

EXPERIMENTAL DETAILS FOR CHAPTER VI

**General methods.** $^{1}H$ and $^{13}C$ NMR spectra were recorded on a Varian Inova 600 MHz ($^{1}H$: 599.98 MHz, $^{13}C$: 150.88 MHz and Varian Mercury 300 MHz ($^{1}H$: 300.09 MHz). Chemical shifts are reported in parts per million (ppm) relative to tetramethylsilane, which was referenced according to trace amounts of non-deuterated chloroform (7.26 ppm) or 1,2-dichlorobenzene (7.19 ppm) for $^{1}H$ and $CDCl_3$ (77.23 ppm) for $^{13}C$. Absorption spectra were recorded on HP 8453 UV-Vis spectrometer. Thermogravimetric analyses (TGA) was performed on a TA Instruments Q500 heating at 10 °C per minute. Glassware was dried in an oven at 100 °C and cooled under a stream of inert gas before use. Dry THF was distilled from potassium metal using benzophenone as an indicator under a nitrogen atmosphere. Sorbent Technologies silica G TLC platw w/UV254 aluminum backed, 200μm was used for TLC. Chromatography was performed using silica gel, tech grade, 60 Å, 230-400 mesh from Sigma-Aldrich. All commercial reagents were used as received unless otherwise noted.

**4,11-Di-*tert*-butyl-1,8-dimesitylfluoreno[4,3-*c*]fluorene** (**7**). Mesityllithium was prepared by purging THF (20 mL) with Ar gas and then adding 2-bromomesitylene (0.08 mL, 0.57 mmol) via syringe. The solution was cooled to –78 °C and then *n*-butyllithium in hexanes (1.6 M, 0.35 mL, 0.56 mmol) was added dropwise. The reaction was stirred at –78 °C for 1.5 h and then cannulated to a flask that was charged with 4,11-di-*tert*-butylfluoreno[4,3-*c*]fluorene-1,8-dione (**8**)[S1] (50 mg, 0.11 mmol) in dry, Ar-degassed THF (10 mL). The opaque orange solution was then stirred for 2 h at –78 °C during which time the solution changed to clear green. The reaction was quenched with cold 10% HCl solution, extracted with diethyl ether, washed with $H_2O$, dried over $MgSO_4$. The solvent was removed and the yellow oil was put under vacuum ($10^{-4}$ torr) for several hours to remove volatile impurities.

The crude diol was placed in a 20 mL scintillation vial along with $SnCl_2$ (64 mg, 0.34 mmol) and toluene (15 mL), which was evacuated and backfilled with Ar gas three times. The reaction was monitored via silica TLC (1:4 ethyl acetate:hexanes) until no starting material was present (~22 h). The solvent was removed under vacuum ($10^{-4}$ torr) and the resulting blue solid was run through a silica plug (1:4 dichloromethane:hexanes)

collecting the deep blue colored product. This was left under vacuum ($10^{-4}$ torr) overnight to remove remaining volatiles, yielding pure **7** (61 mg, 86%). $^{1}$H NMR (600 MHz, $CDCl_3$) δ 7.92 (s, 2H), 7.60 (d, $J$ = 9.4 Hz, 2H), 7.08 (dd, $J$ = 7.9, 1.2 Hz, 2H), 7.00 (s, 4H), 6.76 (d, $J$ = 7.3 Hz, 2H), 6.75 (d, $J$ = 8.9 Hz, 2H), 2.38 (s, 6H), 2.16 (s, 12H), 1.37 (s, 18H); $^{13}$C NMR (151 MHz, $CDCl_3$): δ 150.21, 143.71, 141.35, 138.00, 137.56, 137.32, 134.24, 132.91, 130.47, 128.33, 125.56, 124.74, 122.63, 122.06, 121.75, 35.22, 31.62, 21.39, 20.53; UV-Vis ($CHCl_3$) $\lambda_{max}$ (ε) 337 (45,490), 344 (45,740), 604 (22,890), 649 (20,070) nm; HRMS (TOF MS ESI+) [M]+$H^+$ calcd for $C_{50}H_{51}^+$ 651.3991; found 651.3979.

**X-Ray Crystallography**. Diffraction intensities for **7·($C_6H_6$)** were collected at 173(2) K on a Bruker Apex CCD diffractometer using MoKα radiation λ= 0.71073 Å. Space group was determined based on systematic absences. Absorption corrections were applied by SADABS.[S2] Structure was solved by direct methods and Fourier techniques and refined on $F^2$ using full matrix least-squares procedures. All non-H atoms were refined with anisotropic thermal parameters. All H atoms were refined in calculated positions in a rigid group model. It was found that crystal structure of **4·($C_6H_6$)** includes a solvent $C_6H_6$ molecule. The main molecule and the solvent molecule are located in the crystal structure on inversion centers. X-ray diffraction from crystals of **4·($C_6H_6$)** is very weak especially at high angles. The X-ray diffraction data were collected up to $2\theta$=56°, but only reflections with $2\theta \leq 50°$ were used in the final refinement due to poor statistics for reflections at high angles. All calculations were performed by the Bruker SHELXTL (v. 6.10) package.[S3]

*Crystallographic Data for* **7·($C_6H_6$)**: $C_{56}H_{56}$, M = 729.01, 0.16 x 0.08 x 0.02 mm, T = 173 K, monoclinic, space group $C2/c$, $a$ = 26.50(3) Å, $b$ = 14.575(18) Å, $c$ = 11.213(14) Å, β = 99.66(3)°, $V$ = 4269(9) Å3, $Z$ = 4, Z'=0.5, $D_c$ = 1.134 Mg m$^{-3}$, $\mu$ = 0.064 mm$^{-1}$, $F$(000) = 1568, $2\theta_{max}$ = 50.00°, 12304 reflections, 3118 independent reflections [$R_{int}$ = 0.1224], R1 = 0.0813, wR2 = 0.1667 and GOF = 1.023, max/min residual electron density +0.229/–0.252 eÅ$^{-3}$.

**Computational Details**

All calculations were done using the Gaussian 09 suite of program and visualized using GaussView5.[S4]

**Table S1**. Energies, in hartrees, used for isodesmic calculations. Energies are the sum of the electronic energy ($E_{el}$) and zero point energy ($E_{ZPE}$). Calculated using B3LYP/6-311+G(d,p)//B3LYP/6-31G(d).

| compound | $E_{el}$ | $E_{ZPE}$ | Scaled $E_{ZPE}$[a] | $H_f = E_{el}$+ Scaled $E_{ZPE}$ |
|---|---|---|---|---|
| benzene | -232.311197453 | 0.099937 | 0.098708 | -232.212489678 |
| cyclohexadiene | -233.483876926 | 0.121813 | 0.120315 | -233.363562226 |
| cyclohexene | -234.713157759 | 0.145644 | 0.143853 | -234.569305180 |
| **1** | -769.528138815 | 0.250096 | 0.247020 | -769.281118996 |
| **1-2H** | -770.778235305 | 0.273417 | 0.270054 | -770.508181334 |
| **2** | -923.186607879 | 0.296421 | 0.292775 | -922.893832857 |
| **2-2H** | -924.446591674 | 0.320082 | 0.316145 | -924.130446683 |

[a] Reference S5.

For determining energies of the states UB3LYP/6-31G(d) minimized structures were used. The open shell (OS) singlet and triplet energies were computed using broken symmetry DFT (BS-UB3LYP/6-311+G(d,p)) . Closed shell (CS) energies were calculated using RB3LYP/6-311+G(d,p). OS energies were corrected using the approximate spin projection (AP) method as defined in Equation 1 and 2.[S6]

Eq 1. $$J = \frac{E_{OS} - E_T}{<S^2>_T - <S^2>_{OS}}$$

Eq 2. $$E_{AP-OS} = E_{OS} + J \cdot < S^2 >_{OS}$$

Where J is an effective exchange integral, $E_{OS}$ is the OS singlet energy, $E_T$ is the OS triplet energy, $<S^2>_{OS}$ is the spin expectation value squared for the OS singlet, $<S^2>_T$ is the spin expectation value squared for the triplet, $E_{AP\text{-}OS}$ is the approximate spin projection (AP) energy for the open shell singlet.

**Table S2**. Computed energies of states, in hartrees, with UB3LYP/6-31G(d) minimized structures.

| | **2**[a] | **6**[a] |
|---|---|---|
| $E_{CS}$ | -923.186555211 | -1387.80504434 |
| $E_{OS}$ | -923.186556522 | -1387.80518296 |
| $\langle S^2 \rangle_{OS}$ | 0.0001 | 0.0079 |
| $E_T$ | -923.160897661 | -1387.78079952 |
| $\langle S^2 \rangle_T$ | 2.0003 | 2.0006 |
| J | -0.012828148 | -0.012236383 |
| $E_{AP\text{-}OS}$ | -923.186557805 | -1387.80527963 |
| $E_{CS}–E_{AP\text{-}OS}$ | 0.000002594 (0.001) | 0.00023529 (0.15) |
| $E_T–E_{AP\text{-}OS}$ | 0.025660144 (16.10) | 0.02448011 (15.36) |

[a] energies in brackets are in kcal $mol^{-1}$

**Figure S1**. NICS(1)zz values of **1** and **2**. Calculated using GIAO B3LYP/6-311++G(d,p)//B3LYP/6-31G(d).

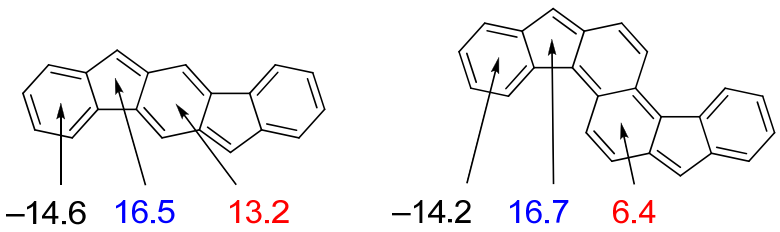


Details for **2**

UB3LYP/6-31G(d)

Electronic energy ($E_{el}$) = –922.973904288

Zero point energy ($E_{ZPE}$) = 0.299004

$E_{el} + E_{ZPE}$ = –922.674901

Imaginary Frequencies = 0

Coordinates

| Symbol | X | Y | Z |
|---|---|---|---|
| H | -2.442769 | -1.396540 | -0.187761 |

| | | | |
|---|---|---|---|
| H | 2.442769 | 1.396540 | -0.187761 |
| H | 3.556820 | -0.777355 | -0.189748 |
| H | -3.556820 | 0.777355 | -0.189748 |
| H | 2.403236 | 3.258013 | 0.202560 |
| H | -1.708499 | 6.084671 | 0.009834 |
| H | 2.572539 | 5.697454 | 0.266607 |
| H | 0.551014 | 7.126004 | 0.168674 |
| H | -2.403236 | -3.258013 | 0.202560 |
| H | 1.708499 | -6.084671 | 0.009834 |
| H | -2.572539 | -5.697454 | 0.266607 |
| H | -0.551014 | -7.126004 | 0.168674 |
| H | -3.119498 | 3.584321 | -0.109881 |
| H | 3.119498 | -3.584321 | -0.109881 |
| C | 1.696264 | -1.911258 | -0.079898 |
| C | 0.238821 | -1.840094 | -0.037827 |
| C | -0.409968 | -0.616885 | -0.077381 |
| C | -1.850981 | -0.494445 | -0.125969 |
| C | 0.409968 | 0.616885 | -0.077381 |
| C | 1.850981 | 0.494445 | -0.125969 |
| C | 2.472997 | -0.712196 | -0.137125 |
| C | -0.238821 | 1.840094 | -0.037827 |
| C | -1.696264 | 1.911258 | -0.079898 |
| C | -2.472997 | 0.712196 | -0.137125 |
| C | -2.095470 | 3.227973 | -0.074501 |
| C | 0.238821 | 3.239648 | 0.025833 |
| C | -0.923273 | 4.074116 | -0.008198 |
| C | 1.491573 | 3.839749 | 0.135300 |
| C | -0.816982 | 5.463117 | 0.038948 |
| C | 1.590831 | 5.239390 | 0.183267 |
| C | 0.452185 | 6.044608 | 0.130838 |
| C | 2.095470 | -3.227973 | -0.074501 |
| C | -0.238821 | -3.239648 | 0.025833 |
| C | 0.923273 | -4.074116 | -0.008198 |
| C | -1.491573 | -3.839749 | 0.135300 |
| C | 0.816982 | -5.463117 | 0.038948 |
| C | -1.590831 | -5.239390 | 0.183267 |
| C | -0.452185 | -6.044608 | 0.130838 |

Details for **6**

UB3LYP/6-31G(d)

$E_{el}$ = –1387.47147778

$E_{ZPE}$ = 0.504971

$E_{el} + E_{ZPE}$ = –1386.966507

Imaginary Frequencies = 0

Coordinates

| Symbol | X | Y | Z |
|---|---|---|---|
| H | -2.027572 | 1.870307 | -0.016176 |
| H | 2.660216 | 2.426713 | -0.022844 |
| H | 0.255185 | 2.781342 | -0.050081 |
| H | 2.027545 | -1.870318 | -0.016168 |
| H | -0.255210 | -2.781354 | -0.050055 |
| H | -2.660242 | -2.426724 | -0.022814 |
| H | 6.300820 | 0.697776 | -1.223582 |
| H | 3.794359 | 1.762880 | 2.101999 |
| H | 7.897730 | 2.471350 | -0.590229 |
| H | 5.389019 | 3.537895 | 2.738058 |
| H | 7.451880 | 3.907880 | 1.394146 |
| H | 5.975011 | -1.267619 | 1.265516 |
| H | 3.357175 | -1.575160 | -2.129404 |
| H | 7.005923 | -3.430802 | 0.669461 |
| H | 4.388563 | -3.737865 | -2.731161 |
| H | 6.217933 | -4.684161 | -1.332355 |
| H | -6.300837 | -0.697800 | -1.223602 |
| H | -3.794382 | -1.762892 | 2.101989 |
| H | -7.897746 | -2.471372 | -0.590247 |
| H | -5.389035 | -3.537914 | 2.738043 |
| H | -7.451898 | -3.907900 | 1.394131 |
| H | -5.975020 | 1.267670 | 1.265513 |
| H | -3.357138 | 1.575138 | -2.129378 |
| H | -7.005868 | 3.430879 | 0.669444 |
| H | -4.388462 | 3.737872 | -2.731148 |
| H | -6.217824 | 4.684215 | -1.332365 |
| C | 1.995578 | 1.570631 | -0.002995 |
| C | 0.653838 | 1.769382 | -0.026855 |
| C | -0.281564 | 0.670343 | -0.047526 |
| C | 0.281539 | -0.670355 | -0.047524 |
| C | 1.644057 | -0.855905 | -0.050761 |
| C | 2.582961 | 0.237615 | -0.021090 |
| C | -1.644082 | 0.855895 | -0.050758 |
| C | -0.653863 | -1.769394 | -0.026841 |
| C | -1.995603 | -1.570642 | -0.002980 |

| | | | |
|---|---|---|---|
| C | -2.582985 | -0.237627 | -0.021084 |
| C | -3.966656 | -0.036337 | -0.008620 |
| C | 3.966631 | 0.036331 | -0.008623 |
| C | 4.910711 | 1.111622 | 0.374017 |
| C | 6.097738 | 1.321401 | -0.358147 |
| C | 4.681245 | 1.930888 | 1.498503 |
| C | 6.997472 | 2.321829 | 0.000276 |
| C | 5.586101 | 2.927032 | 1.860795 |
| C | 6.746359 | 3.131260 | 1.111330 |
| C | 4.569207 | -1.267787 | -0.371527 |
| C | 5.623743 | -1.809183 | 0.392338 |
| C | 4.142430 | -1.989989 | -1.504678 |
| C | 6.204330 | -3.029027 | 0.055004 |
| C | 4.730000 | -3.206694 | -1.846376 |
| C | 5.760272 | -3.735237 | -1.065897 |
| C | -4.910735 | -1.111631 | 0.374009 |
| C | -6.097757 | -1.321419 | -0.358161 |
| C | -4.681267 | -1.930900 | 1.498493 |
| C | -6.997490 | -2.321847 | 0.000262 |
| C | -5.586119 | -2.927049 | 1.860782 |
| C | -6.746378 | -3.131277 | 1.111317 |
| C | -4.569207 | 1.267793 | -0.371522 |
| C | -5.623732 | 1.809221 | 0.392335 |
| C | -4.142395 | 1.989986 | -1.504666 |
| C | -6.204281 | 3.029080 | 0.054994 |
| C | -4.729925 | 3.206708 | -1.846369 |
| C | -5.760193 | 3.735278 | -1.065902 |

Details for **7**

B3LYP/6-31G(d)

$E_{el}$ = –1935.50062137

$E_{ZPE}$ = 0.852874

$E_{el} + E_{ZPE}$ = –1934.647748

Imaginary Frequencies = 0

B3LYP/6-311+G(d,p)//B3LYP/6-31G(d)

$E_{el}$ = –1935.62118729

Coordinates

| Symbol | X | Y | Z |
|---|---|---|---|
| C | 2.455973 | 0.709459 | 0.128367 |
| C | 1.766292 | -0.571189 | 0.077023 |
| C | 0.381953 | -0.633931 | 0.131964 |
| C | -0.347227 | -1.880637 | 0.202158 |
| C | -0.381074 | 0.633037 | 0.131467 |
| C | 0.348107 | 1.879792 | 0.200796 |
| C | 1.706410 | 1.923091 | 0.214818 |
| C | -1.765409 | 0.570250 | 0.076362 |
| C | -2.455107 | -0.710375 | 0.128327 |
| C | -1.705537 | -1.923937 | 0.215944 |
| C | -3.828231 | -0.520729 | 0.119291 |
| C | -2.821545 | 1.600941 | -0.013437 |
| C | -4.071818 | 0.913110 | 0.030038 |
| C | -2.816695 | 2.982416 | -0.171334 |
| C | -5.266242 | 1.620500 | -0.053656 |
| C | -4.022324 | 3.716968 | -0.253904 |
| C | -5.232463 | 3.014076 | -0.185786 |
| C | 3.829095 | 0.519831 | 0.119706 |
| C | 2.822457 | -1.601887 | -0.012367 |
| C | 4.072730 | -0.914021 | 0.030780 |
| C | 2.817566 | -2.983383 | -0.170020 |
| C | 5.267145 | -1.621410 | -0.053137 |
| C | 4.023192 | -3.717932 | -0.252772 |
| C | 5.233333 | -3.015009 | -0.185084 |
| C | -4.878280 | -1.567527 | 0.171803 |
| C | -5.584308 | -1.801438 | 1.373239 |
| C | -6.573902 | -2.788692 | 1.400187 |
| C | -6.892040 | -3.549091 | 0.271706 |
| C | -6.181009 | -3.303870 | -0.906105 |
| C | -5.181468 | -2.328704 | -0.979540 |
| C | 4.878354 | 1.567493 | 0.171229 |
| C | 5.184379 | 2.323585 | -0.982291 |
| C | 6.187523 | 3.295705 | -0.911744 |
| C | 6.895107 | 3.546208 | 0.266618 |
| C | 6.579791 | 2.784719 | 1.395572 |
| C | 5.587051 | 1.800994 | 1.371549 |
| C | 5.270673 | 1.020748 | 2.628126 |
| C | 4.463040 | 2.084561 | -2.290628 |
| C | 7.952561 | 4.623991 | 0.326376 |
| C | -5.263336 | -1.023926 | 2.630347 |
| C | -4.455178 | -2.096717 | -2.286411 |
| C | -7.990166 | -4.586057 | 0.316079 |

| | | | |
|---|---|---|---|
| C | -3.958116 | 5.246255 | -0.426250 |
| C | 3.959003 | -5.247242 | -0.424900 |
| C | 5.357447 | -5.890714 | -0.489318 |
| C | 3.200617 | -5.872641 | 0.770655 |
| C | 3.214334 | -5.588982 | -1.738244 |
| C | -3.199329 | 5.871801 | 0.768977 |
| C | -5.356541 | 5.889813 | -0.490320 |
| C | -3.213856 | 5.587765 | -1.739890 |
| H | 0.213250 | -2.800720 | 0.292620 |
| H | -0.212366 | 2.799968 | 0.290268 |
| H | 2.232973 | 2.870438 | 0.294764 |
| H | -2.232061 | -2.871229 | 0.296826 |
| H | -1.881899 | 3.522247 | -0.257791 |
| H | -6.218262 | 1.096390 | -0.027772 |
| H | -6.174432 | 3.546825 | -0.247336 |
| H | 1.882740 | -3.523209 | -0.256220 |
| H | 6.219186 | -1.097308 | -0.027733 |
| H | 6.175291 | -3.547745 | -0.246863 |
| H | -7.106901 | -2.970743 | 2.331649 |
| H | -6.412137 | -3.884828 | -1.797198 |
| H | 6.425717 | 3.868194 | -1.806360 |
| H | 7.119488 | 2.961561 | 2.324221 |
| H | 4.216599 | 1.128077 | 2.910109 |
| H | 5.452824 | -0.052300 | 2.498002 |
| H | 5.882333 | 1.367339 | 3.466852 |
| H | 4.486852 | 1.026615 | -2.575688 |
| H | 3.406214 | 2.370254 | -2.231680 |
| H | 4.921417 | 2.664309 | -3.097902 |
| H | 7.528714 | 5.580041 | 0.662467 |
| H | 8.753509 | 4.362298 | 1.026428 |
| H | 8.404503 | 4.797354 | -0.656083 |
| H | -4.208830 | -1.133338 | 2.909923 |
| H | -5.444042 | 0.049585 | 2.502014 |
| H | -5.873836 | -1.370535 | 3.469912 |
| H | -4.477745 | -1.040112 | -2.576506 |
| H | -3.398632 | -2.382377 | -2.222686 |
| H | -4.911157 | -2.680015 | -3.092479 |
| H | -8.957279 | -4.154975 | 0.023687 |
| H | -7.786570 | -5.416381 | -0.368845 |
| H | -8.111083 | -4.999227 | 1.323202 |
| H | 5.939368 | -5.518286 | -1.339944 |
| H | 5.933219 | -5.709240 | 0.425401 |
| H | 5.258715 | -6.975763 | -0.606969 |

| | | | |
|---|---|---|---|
| H | 3.711866 | -5.655308 | 1.715376 |
| H | 2.177007 | -5.492134 | 0.850653 |
| H | 3.142435 | -6.962281 | 0.657508 |
| H | 2.191029 | -5.199079 | -1.742990 |
| H | 3.735844 | -5.166675 | -2.604649 |
| H | 3.156463 | -6.676302 | -1.871794 |
| H | -2.175704 | 5.491281 | 0.848721 |
| H | -3.141155 | 6.961426 | 0.655647 |
| H | -3.710290 | 5.654633 | 1.713891 |
| H | -5.938789 | 5.517227 | -1.340652 |
| H | -5.932000 | 5.708607 | 0.424646 |
| H | -5.257777 | 6.974829 | -0.608266 |
| H | -2.190617 | 5.197693 | -1.744955 |
| H | -3.735732 | 5.165448 | -2.606069 |
| H | -3.155865 | 6.675064 | -1.873574 |

Details for benzene

B3LYP/6-31G(d)

Imaginary Frequencies = 0

B3LYP/6-311+G(d,p)//B3LYP/6-31G(d)

$E_{el}$ = –232.311197453

$E_{ZPE}$ = 0.099937

$E_{el} + E_{ZPE}$ = –232.211260

Coordinates

| Symbol | X | Y | Z |
|---|---|---|---|
| H | 0.000000 | 2.483721 | -0.000105 |
| H | 0.000000 | 1.241951 | 2.150892 |
| H | 0.000000 | 1.241751 | -2.150854 |
| H | 0.000000 | -1.241751 | -2.150854 |
| H | 0.000000 | -2.483721 | -0.000105 |
| H | 0.000000 | -1.241951 | 2.150892 |
| C | 0.000000 | 1.396705 | 0.000013 |
| C | 0.000000 | 0.698542 | 1.209454 |
| C | 0.000000 | 0.698263 | -1.209456 |
| C | 0.000000 | -0.698263 | -1.209456 |
| C | 0.000000 | -1.396705 | 0.000013 |
| C | 0.000000 | -0.698542 | 1.209454 |

Details for cyclohexadiene

B3LYP/6-31G(d)

Imaginary Frequencies = 0

B3LYP/6-311+G(d,p)//B3LYP/6-31G(d)

$E_{el}$ = –233.483876926

$E_{ZPE}$ = 0.121813

$E_{el} + E_{ZPE}$ = –233.362064

Coordinates

| Symbol | X | Y | Z |
|---|---|---|---|
| H | -0.011912 | 2.513027 | 0.115951 |
| H | 0.175371 | 1.244734 | 2.210999 |
| H | -0.175371 | -1.244734 | 2.210999 |
| H | 0.011912 | -2.513027 | 0.115951 |
| H | -1.385674 | 0.656746 | -1.361714 |
| H | 0.109454 | 1.284709 | -2.036938 |
| H | 1.385674 | -0.656746 | -1.361714 |
| H | -0.109454 | -1.284709 | -2.036938 |
| C | -0.047042 | 1.425702 | 0.113711 |
| C | 0.047042 | 0.732087 | 1.260242 |
| C | -0.047042 | -0.732087 | 1.260242 |
| C | 0.047042 | -1.425702 | 0.113711 |
| C | -0.295977 | 0.710829 | -1.195336 |
| C | 0.295977 | -0.710829 | -1.195336 |

Details for cyclohexene

B3LYP/6-31G(d)

Imaginary Frequencies = 0

B3LYP/6-311+G(d,p)//B3LYP/6-31G(d)

$E_{el}$ = –234.713157759

$E_{ZPE}$ = 0.145644

$E_{el} + E_{ZPE}$ = –234.567514

Coordinates

| Symbol | X | Y | Z |
|---|---|---|---|

| | | | |
|---|---|---|---|
| H | -1.199394 | 2.254574 | 0.112845 |
| H | 1.199405 | 2.254568 | -0.112846 |
| H | 1.889518 | -0.090048 | -1.131858 |
| H | 2.386338 | 0.163868 | 0.527143 |
| H | -1.889517 | -0.090039 | 1.131860 |
| H | -2.386339 | 0.163880 | -0.527141 |
| H | 1.244705 | -2.105940 | 0.054216 |
| H | 0.592944 | -1.192295 | 1.412663 |
| H | -1.244716 | -2.105934 | -0.054216 |
| H | -0.592951 | -1.192292 | -1.412664 |
| C | -0.666053 | 1.305944 | 0.057201 |
| C | 0.666059 | 1.305941 | -0.057201 |
| C | 1.498904 | 0.047944 | -0.110708 |
| C | -1.498903 | 0.047952 | 0.110709 |
| C | 0.698282 | -1.192254 | 0.318685 |
| C | -0.698288 | -1.192250 | -0.318686 |

Details for **1**

B3LYP/6-31G(d)

Imaginary Frequencies = 0

B3LYP/6-311+G(d,p)//B3LYP/6-31G(d)

$E_{el}$ = –769.528138815

$E_{ZPE}$ = 0.250096

$E_{el} + E_{ZPE}$ = –769.278043

Coordinates

| Symbol | X | Y | Z |
|---|---|---|---|
| H | 2.149307 | 1.350092 | 0.000000 |
| H | -2.149307 | -1.350092 | 0.000000 |
| H | 3.356704 | -1.254867 | 0.000000 |
| H | -3.356704 | 1.254867 | 0.000000 |
| H | 3.543692 | -4.165180 | 0.000000 |
| H | -1.460312 | -3.975631 | 0.000000 |
| H | -3.543692 | 4.165180 | 0.000000 |
| H | 1.460312 | 3.975631 | 0.000000 |
| H | 2.195141 | -6.255316 | 0.000000 |
| H | -0.276223 | -6.158012 | 0.000000 |

| | | | |
|---|---|---|---|
| H | -2.195141 | 6.255316 | 0.000000 |
| H | 0.276223 | 6.158012 | 0.000000 |
| C | 0.005735 | 1.415081 | 0.000000 |
| C | 1.216097 | 0.790831 | 0.000000 |
| C | 1.246561 | -0.645346 | 0.000000 |
| C | -1.246561 | 0.645346 | 0.000000 |
| C | -1.216097 | -0.790831 | 0.000000 |
| C | -0.005735 | -1.415081 | 0.000000 |
| C | 2.305546 | -1.524198 | 0.000000 |
| C | -2.305546 | 1.524198 | 0.000000 |
| C | -0.373356 | 2.832393 | 0.000000 |
| C | 0.373356 | -2.832393 | 0.000000 |
| C | 1.798516 | -2.886414 | 0.000000 |
| C | 2.457577 | -4.116652 | 0.000000 |
| C | -0.373356 | -4.004090 | 0.000000 |
| C | -1.798516 | 2.886414 | 0.000000 |
| C | -2.457577 | 4.116652 | 0.000000 |
| C | 0.373356 | 4.004090 | 0.000000 |
| C | 1.695769 | -5.290219 | 0.000000 |
| C | 0.297658 | -5.235312 | 0.000000 |
| C | -1.695769 | 5.290219 | 0.000000 |
| C | -0.297658 | 5.235312 | 0.000000 |

Details for **1-2H**

B3LYP/6-31G(d)

Imaginary Frequencies = 0

B3LYP/6-311+G(d,p)//B3LYP/6-31G(d)

$E_{el}$ = –770.778235305

$E_{ZPE}$ = 0.273417

$E_{el} + E_{ZPE}$ = –770.504818

Coordinates

| Symbol | X | Y | Z |
|---|---|---|---|
| H | 2.172667 | 1.262068 | 0.000000 |
| H | -2.172667 | -1.262068 | 0.000000 |
| H | 3.025101 | -1.513718 | 0.879536 |
| H | -3.025101 | 1.513718 | -0.879536 |
| H | 3.325398 | -4.410067 | 0.000000 |
| H | -1.635707 | -3.813290 | 0.000000 |

| | | | |
|---|---|---|---|
| H | -3.325398 | 4.410067 | 0.000000 |
| H | 1.635707 | 3.813290 | 0.000000 |
| H | 1.816719 | -6.385710 | 0.000000 |
| H | -0.641692 | -6.087505 | 0.000000 |
| H | -1.816719 | 6.385710 | 0.000000 |
| H | 0.641692 | 6.087505 | 0.000000 |
| H | 3.025101 | -1.513718 | -0.879536 |
| H | -3.025101 | 1.513718 | 0.879536 |
| C | 0.006386 | 1.388930 | 0.000000 |
| C | 1.232976 | 0.713921 | 0.000000 |
| C | 1.214835 | -0.675493 | 0.000000 |
| C | -1.214835 | 0.675493 | 0.000000 |
| C | -1.232976 | -0.713921 | 0.000000 |
| C | -0.006386 | -1.388930 | 0.000000 |
| C | 2.379589 | -1.646638 | 0.000000 |
| C | -2.379589 | 1.646638 | 0.000000 |
| C | -0.291938 | 2.826001 | 0.000000 |
| C | 0.291938 | -2.826001 | 0.000000 |
| C | 1.692595 | -2.997815 | 0.000000 |
| C | 2.246422 | -4.272588 | 0.000000 |
| C | -0.555606 | -3.936805 | 0.000000 |
| C | -1.692595 | 2.997815 | 0.000000 |
| C | -2.246422 | 4.272588 | 0.000000 |
| C | 0.555606 | 3.936805 | 0.000000 |
| C | 1.395414 | -5.383975 | 0.000000 |
| C | 0.006386 | -5.214964 | 0.000000 |
| C | -1.395414 | 5.383975 | 0.000000 |
| C | -0.006386 | 5.214964 | 0.000000 |

Details for **2**

B3LYP/6-31G(d)

Imaginary Frequencies = 0

B3LYP/6-311+G(d,p)//B3LYP/6-31G(d)

$E_{el}$ = –923.186607879

$E_{ZPE}$ = 0.296421

$E_{el} + E_{ZPE}$ = –922.890187

Coordinates

| Symbol | X | Y | Z |
|---|---|---|---|

| | | | |
|---|---|---|---|
| H | -1.383956 | -2.449794 | -0.190850 |
| H | 1.383957 | 2.449798 | -0.190804 |
| H | -0.795901 | 3.552684 | -0.192891 |
| H | 0.795901 | -3.552681 | -0.192919 |
| H | 3.243968 | 2.419957 | 0.205307 |
| H | 6.093507 | -1.675988 | 0.010547 |
| H | 5.682725 | 2.602680 | 0.270994 |
| H | 7.122310 | 0.589072 | 0.172011 |
| H | -3.243964 | -2.419954 | 0.205341 |
| H | -6.093508 | 1.675984 | 0.010527 |
| H | -5.682721 | -2.602681 | 0.271020 |
| H | -7.122309 | -0.589076 | 0.172010 |
| H | 3.600594 | -3.100534 | -0.111443 |
| H | -3.600599 | 3.100536 | -0.111444 |
| C | -1.920027 | 1.686262 | -0.081359 |
| C | -1.841163 | 0.229301 | -0.038688 |
| C | -0.614684 | -0.413172 | -0.078840 |
| C | -0.484831 | -1.853521 | -0.128198 |
| C | 0.614684 | 0.413174 | -0.078835 |
| C | 0.484831 | 1.853523 | -0.128175 |
| C | -0.725048 | 2.469257 | -0.139502 |
| C | 1.841162 | -0.229300 | -0.038687 |
| C | 1.920026 | -1.686260 | -0.081359 |
| C | 0.725048 | -2.469255 | -0.139519 |
| C | 3.238838 | -2.078462 | -0.075637 |
| C | 3.237980 | 0.255765 | 0.026158 |
| C | 4.078677 | -0.901770 | -0.008196 |
| C | 3.831009 | 1.511723 | 0.137325 |
| C | 5.467057 | -0.787916 | 0.039952 |
| C | 5.230051 | 1.618587 | 0.186346 |
| C | 6.041494 | 0.484371 | 0.133350 |
| C | -3.238840 | 2.078464 | -0.075651 |
| C | -3.237980 | -0.255765 | 0.026158 |
| C | -4.078678 | 0.901768 | -0.008205 |
| C | -3.831007 | -1.511722 | 0.137340 |
| C | -5.467058 | 0.787913 | 0.039941 |
| C | -5.230049 | -1.618588 | 0.186361 |
| C | -6.041493 | -0.484374 | 0.133350 |

Details for **2-2H**

B3LYP/6-31G(d)

Imaginary Frequencies = 0

B3LYP/6-311+G(d,p)//B3LYP/6-31G(d)

$E_{el}$ = –924.446591674

$E_{ZPE}$ = 0.320082

$E_{el} + E_{ZPE}$ = –924.126510

Coordinates

| Symbol | X | Y | Z |
|---|---|---|---|
| H | 1.361557 | -2.430587 | 0.198081 |
| H | -1.361557 | 2.430592 | 0.198028 |
| H | 0.828632 | 3.517094 | 0.238671 |
| H | -0.828631 | -3.517089 | 0.238752 |
| H | -3.169966 | 2.411989 | -0.284529 |
| H | -6.177007 | -1.550453 | 0.012229 |
| H | -5.595204 | 2.697187 | -0.365610 |
| H | -7.118296 | 0.745701 | -0.212930 |
| H | 3.169964 | -2.411994 | -0.284502 |
| H | 6.177007 | 1.550453 | 0.012170 |
| H | 5.595202 | -2.697194 | -0.365587 |
| H | 7.118295 | -0.745705 | -0.212949 |
| H | -3.586137 | -2.700233 | 1.039831 |
| H | 3.586141 | 2.700253 | 1.039761 |
| H | -3.565975 | -2.817454 | -0.715435 |
| H | 3.565973 | 2.817440 | -0.715507 |
| C | 1.925155 | 1.653958 | 0.113493 |
| C | 1.867073 | 0.261692 | 0.048074 |
| C | 0.599110 | -0.405285 | 0.074433 |
| C | 0.472495 | -1.819418 | 0.135339 |
| C | -0.599110 | 0.405287 | 0.074426 |
| C | -0.472494 | 1.819421 | 0.135300 |
| C | 0.760161 | 2.433951 | 0.171148 |
| C | -1.867073 | -0.261691 | 0.048088 |
| C | -1.925155 | -1.653956 | 0.113536 |
| C | -0.760160 | -2.433947 | 0.171205 |
| C | -3.353250 | -2.139249 | 0.123211 |
| C | -3.256067 | 0.250711 | -0.035723 |
| C | -4.138086 | -0.855016 | 0.022494 |
| C | -3.797510 | 1.534898 | -0.187635 |
| C | -5.515461 | -0.688399 | -0.035855 |
| C | -5.183555 | 1.698172 | -0.248047 |
| C | -6.042519 | 0.600023 | -0.165931 |

| | | | |
|---|---|---|---|
| C | 3.353251 | 2.139252 | 0.123153 |
| C | 3.256067 | -0.250711 | -0.035734 |
| C | 4.138086 | 0.855016 | 0.022458 |
| C | 3.797509 | -1.534901 | -0.187626 |
| C | 5.515461 | 0.688398 | -0.035894 |
| C | 5.183554 | -1.698177 | -0.248041 |
| C | 6.042518 | -0.600026 | -0.165948 |

Variable Temperature $^{1}$H NMR Spectrum of **7**

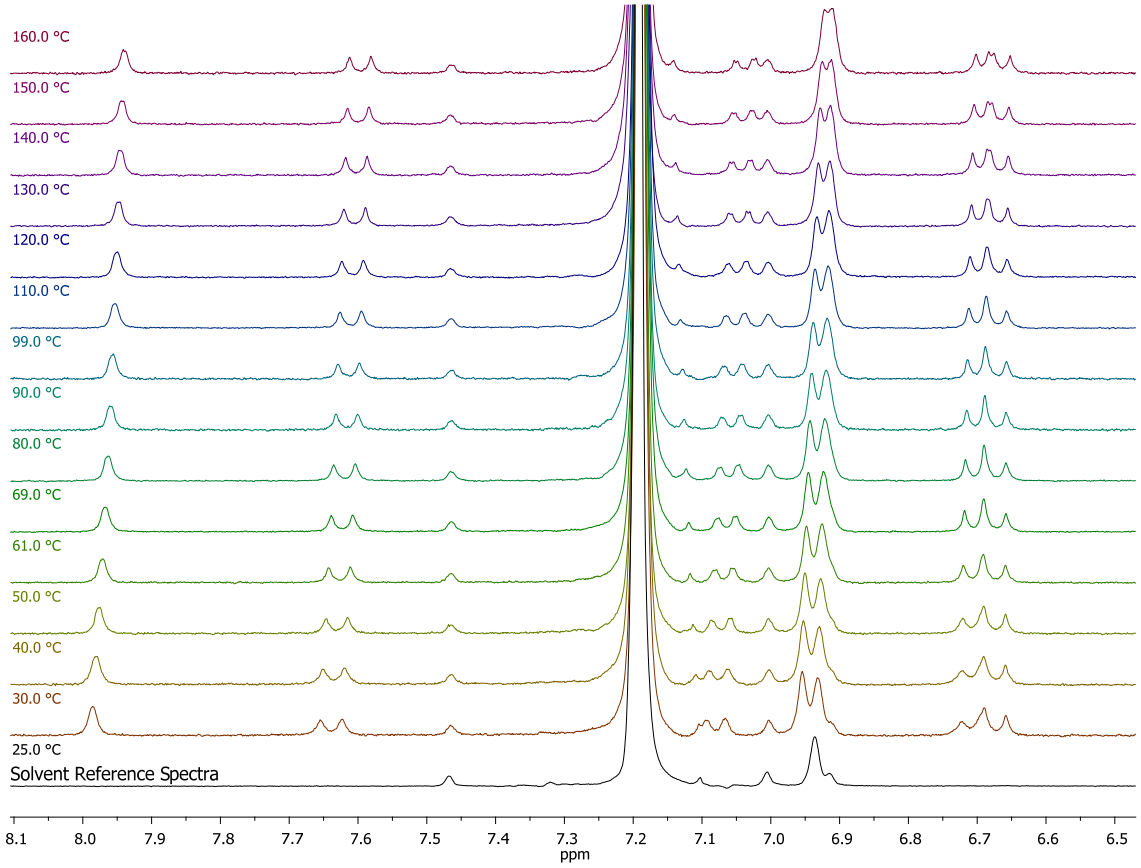


TGA of **7**.

Sample: 20120308MesfluFlu
Size: 10.5320 mg
Method: Isothermal for
Comment: Ramp 10 deg/min

TGA

File: C:...\TGA\20120308MesFluFluTGA.001
Operator: Brad
Run Date: 08-Mar-2012 11:31
Instrument: TGA Q500 V6.7 Build 203

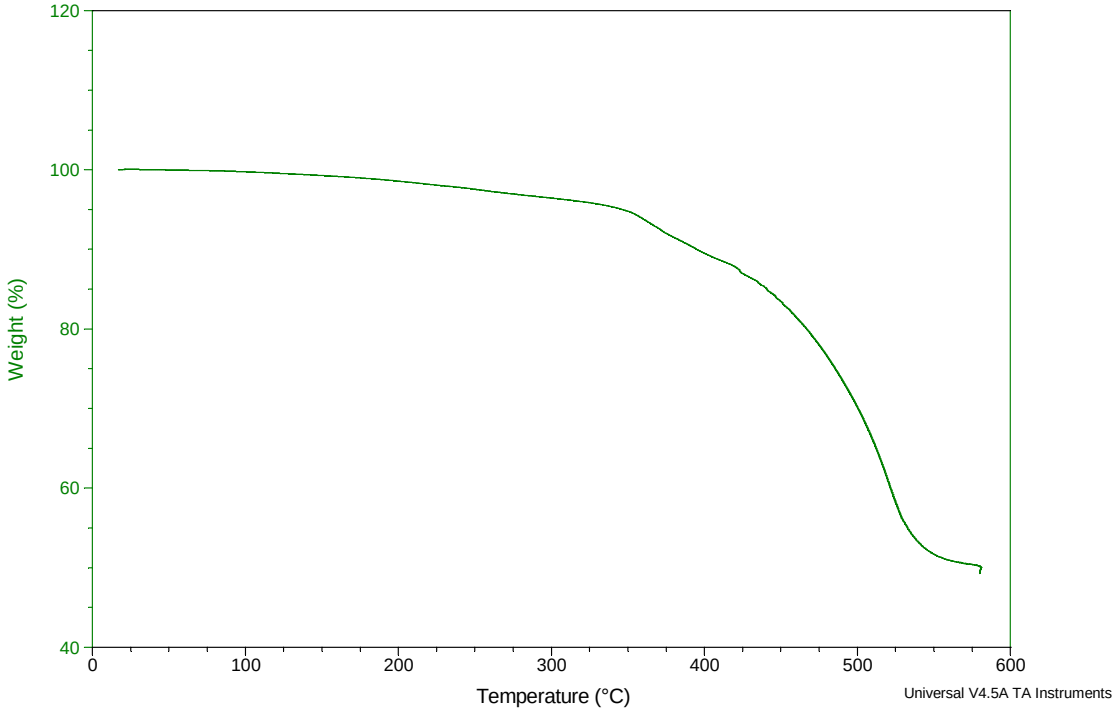

REFERENCES CITED

Chapter I


(1) Zhou, Q.; Carroll, P. J.; Swager, T. M. *J. Org. Chem.* **1994**, *59*, 1294–1301.

(2) Anthony, J. E. *Angew. Chem. Int. Ed.* **2008**, *47*, 452–483.

(3) Spitler, E. L.; Johnson, C. A., II; Haley, M. M. *Chem. Rev.* **2006**, *106*, 5344–5386.

(4) Anthony, J. E.; Brooks, J. S.; Eaton, D. L.; Parkin, S. R. *J. Am. Chem. Soc.* **2001**, *123*, 9482–9483.

(5) Chase, D. T.; Rose, B. D.; McClintock, S. P.; Zakharov, L. N.; Haley, M. M. *Angew. Chem. Int. Ed.* **2011**, *50*, 1127–1130.

(6) Chase, D. T.; Fix, A. G.; Rose, B. D.; Weber, C. D.; Nobusue, S.; Stockwell, C. E.; Zakharov, L. N.; Lonergan, M. C.; Haley, M. M. *Angew. Chem. Int. Ed.* **2011**, *50*, 11103–11106.

(7) Chase, D. T.; Fix, A. G.; Kang, S. J.; Rose, B. D.; Weber, C. D.; Zhong, Y.; Zakharov, L. N.; Lonergan, M. C.; Nuckolls, C.; Haley, M. M. *J. Am. Chem. Soc.* **2012**, *134*, 10349–10352.

(8) Rose, B. D.; Chase, D. T.; Weber, C. D.; Zakharov, L. N.; Lonergan, M. C.; Haley, M. M. *Org. Lett.* **2011**, *13*, 2106–2109.

(9) Shimizu, A.; Tobe, Y. *Angew. Chem. Int. Ed.* **2011**, *50*, 6906–6910.

(10) Shimizu, A.; Kishi, R.; Nakano, M.; Shiomi, D.; Sato, K.; Takui, T.; Hisaki, I.; Miyata, M.; Tobe, Y. *Angew. Chem., Int. Ed.* **2013**, *52*, 6076–6079.

(11) Nishida, J.; Tsukaguchi, S.; Yamashita, Y. *Chem. Eur. J.* **2012**, *18*, 8964–8970.

(12) Fix, A. G.; Deal, P. E.; Vonnegut, C. L.; Rose, B. D.; Zakharov, L. N.; Haley, M. M. *Org. Lett.* **2013**, *15*, 1362–1365.

(13) Rose, B. D.; Vonnegut, C. L.; Zakharov, L. N.; Haley, M. M. *Org. Lett.* **2012**, *14*, 2426–2429.

(14) Young, B. S.; Chase, D. T.; Marshall, J. L.; Vonnegut, C. L.; Zakharov, L. N.; Haley, M. M. *Chem. Sci.* **2014**, *5*, 1008–1014.

(15) Kendrick, M. J.; Neunzert, A.; Payne, M. M.; Purushothaman, B.; Rose, B. D.; Anthony, J. E.; Haley, M. M.; Ostroverkhova, O. *J. Phys. Chem. C* **2012**, *116*, 18108–18116.

## Chapter II


[1] a) A. T. Balaban, M. Banciu, V. Ciorba, *Annulenes, Benzo-, Hetero-, Homo-Derivatives and their Valence Isomers*, CRC Press, Boca Raton, **1987**; b) H. Hopf, *Classics in Hydrocarbon Chemistry*, Wiley-VCH, Weinheim, **2000**; c) J. E. Anthony, *Chem. Rev.* **2006**, *106*, 5028–5048; d) J. E. Anthony, *Angew. Chem.* **2008**, *120*, 460–492; *Angew. Chem. Int. Ed.* **2008**, *47*, 452–483.

[2] a) *Functional Organic Materials* (Eds.: T. J. J. Müller, U. H. F. Bunz), Wiley-VCH, Weinheim, **2007**; b) *Organic Light Emitting Devices: Synthesis, Properties and Applications* (Eds.: K. Mullen, U. Scherf), Wiley-VCH, Weinheim, **2006**; c) *Carbon-Rich Compounds* (Eds.: M. M. Haley, R. R. Tykwinski), Wiley-VCH, Weinheim, **2006**.

[3] a) J. E. Anthony, J. S. Brooks, D. L. Eaton, S. R. Parkin, *J. Am. Chem. Soc.* **2001**, *123*, 9482–9483; b) J. E. Anthony, D. L. Eaton, S. R Parkin, *Org. Lett.* **2002**, *4*, 15–18.

[4] a) A. Vollmer, H. Weiss, S. Rentenberger, I. Salzmann, J. P. Rabe, N. Koch, *Surf. Sci.* **2006**, *600*, 4004–4007; b) A. R. Reddy, M. Bendikov, *Chem. Commun.* **2006**, 1179–1181; c) I. Kaur, W. Jia, R. P. Kopreski, S. Selvarasah, M. R. Dokmeci, C. Pramanik, N. E. McGruer, G. P. Miller, *J. Am. Chem. Soc.* **2008**, *130*, 16274–16286.

[5] a) Q. Miao, T.-Q. Nguyen, T. Someya, G. B. Blanchet, C. Nuckolls, *J. Am. Chem. Soc.* **2003**, *125*, 10284–10287; b) S. Miao, S. M. Brombosz, P. v. R. Schleyer, J. I. Wu, S. Barlow, S. R. Marder, K. I. Hardcastle, U. H. F. Bunz, *J. Am. Chem. Soc.* **2008**, *130*, 7339–7344; c) Q. Tang, J. Liu, H. S. Chan, Q. Miao, *Chem. Eur. J.* **2009**, *15*, 3965–3969; d) U. H. F. Bunz, *Chem. Eur. J.* **2009**, *15*, 6780–6789.

[6] a) M. Saito, M. Nakamura, T. Tajima, T. *Chem. Eur. J.* **2008**, *14*, 6062–6068; b) T. Kawase, A. Konishi, Y. Hirao, K. Matsumoto, H. Kurata, T. Kubo, *Chem. Eur. J.* **2009**, *15*, 2653–2661; c) U. L. Zerubba, T. D. Tilley, *J. Am. Chem. Soc.* **2009**, *131*, 2796–2797; d) H. Zhang, T. Karasawa, H. Yamada, A. Wakamiya, S. Yamaguchi, S. *Org. Lett.* **2009**, *11*, 3076–3079; e) M. Saito, *Symmetry* **2010**, *2*, 950–969; f) U. L. Zerubba, T. D. Tilley, *J. Am. Chem. Soc.* **2010**, *132*, 11012–11014; g) T. Kawase, T. Fujiwara, C. Kitamura, A. Konishi, Y. Hirao, K. Matsumoto, H. Kurata, T. Kubo, S. Shinamura, H. Mori, E. Miyazaki, K. Takimiya, *Angew. Chem.* **2010**, *122*, 7894–7898; *Angew. Chem. Int. Ed.* **2010**, *49*, 7728–7732.

[7] K. Hafner, B. Stowasser, H. P. Krimmer, S. Fischer, M. C. Boehm, H. J. Lindner, *Angew. Chem.* **1986**, *98*, 646–648; *Angew. Chem. Int. Ed.* **1986**, *25*, 630–632.

[8] W. S. Trahanovsky, S. P. Lorimor, *J. Org. Chem.* **2006**, *71*, 1784–1794, and references therein.

[9] a) H. Usta, A. Facchetti, T. J. Marks, *Org. Lett.* **2008**, *10*, 1385–1388; b) H. Usta, A. Facchetti, T. J. Marks, *J. Am. Chem. Soc.* **2008**, *130*, 8580–8581; c) H. Usta, C. Risko, Z. Wang, H. Huang, M. K. Deliomergolu, A. Zhukhovitskiy, A. Facchetti, T. J. Marks, *J. Am. Chem. Soc.* **2009**, *131*, 5586–5608.

[10] a) C. Poriel, J.-J. Liang, J. Rault-Berthelot, F. Barrière, N. Cocherel, A. M. Z. Slawin, D. Horhant, M. Virboul, G. Alcaraz, N. Audebrand, L. Vignau, N. Huby, G. Wantz, L. Hirsch, *Chem. Eur. J.* **2007**, *13*, 10055–10069; b) C.-P. Chen, S.-H. Chan, T.-C. Chao, C. Ting, B.-T. Ko, *J. Am. Chem. Soc.* **2008**, *130*, 12828–12833; c) N. Cocherel, C. Poriel, J. Rault-Berthelot, F. Barrière, N. Audebrand, A. M. Z. Slawin, L. Vignau, L. *Chem. Eur. J.* **2008**, *14*, 11328–11342; d) W. Zhang, J. Smith, R. Hamilton, M. Heeney, J. Kirkpatrick, K. Song, S. E. Watkins, T. Anthopoulos, I. McCulloch, *J. Am. Chem. Soc.* **2009**, *131*, 10814–10815; e) W. Zhang, J. Smith, S. E. Watkins, R. Gysel, M. McGehee, A. Salleo, J. Kirkpatrick, S. Ashraf, T. Anthopoulos, M. Heeney, I. McCulloch, *J. Am. Chem. Soc.* **2010**, *132*, 11437–11439.

[11] Q. Zhou, P. J. Carroll, T. M. Swager, *J. Org. Chem.* **1994**, *59*, 1294–1301.

[12] H. Reisch, U. Wiesler, U. Scherf, N. Tuytuylkov, *Macromolecules* **1996**, *29*, 8204–8210.

[13] A. Shimizu, M. Uruichi, K. Yakushi, H. Matsuzaki, H. Okamoto, M. Nakano, Y. Hirao, K. Matsumoto, H. Kurata, T. Kubo, *Angew. Chem.* **2009**, *121*, 5590–5594; *Angew. Chem. Int. Ed.* **2009**, *48*, 5482–5486.

[14] a) L. K. Montgomery, J. C. Huffman, E. A. Jurczak, M. P. Grendze, *J. Am. Chem. Soc.* **1986**, *108*, 6004–6011. b) For a closely related acene-like derivative, see: J.-i. Nishida, Y. Fujiwara, Y. Yamashita, *Org. Lett.* **2009**, *11*, 1813–1816.

[15] M. J. Frisch, G. W. Trucks, H. B. Schlegel, G. E. Scuseria, M. A. Robb, J. R. Cheeseman, J. A. Montgomery, Jr., T. Vreven, K. N. Kudin, J. C. Burant, J. M. Millam, S. S. Iyengar, J. Tomasi, V. Barone, B. Mennucci, M. Cossi, G. Scalmani, N. Rega, G. A. Petersson, H. Nakatsuji, M. Hada, M. Ehara, K. Toyota, R. Fukuda, J. Hasegawa, M. Ishida, T. Nakajima, Y. Honda, O. Kitao, H. Nakai, M. Klene, X. Li, J. E. Knox, H. P. Hratchian, J. B. Cross, C. Adamo, J. Jaramillo, R. Gomperts, R. E. Stratmann, O. Yazyev, A. J. Austin, R. Cammi, C. Pomelli, J. W. Ochterski, P. Y. Ayala, K. Morokuma, G. A. Voth, P. Salvador, J. J. Dannenberg, V. G. Zakrzewski, S. Dapprich, A. D. Daniels, M. C. Strain, O. Farkas, D. K. Malick, A. D. Rabuck, K. Raghavachari, J. B. Foresman, J. V. Ortiz, Q. Cui, A. G. Baboul, S. Clifford, J. Cioslowski, B. B. Stefanov, G. Liu, A. Liashenko, P. Piskorz, I. Komaromi, R. L. Martin, D. J. Fox, T. Keith, M. A. Al-Laham, C. Y. Peng, A. Nanayakkara, M. Challacombe, P. M. W. Gill, B. Johnson, W. Chen, M. W. Wong, C. Gonzalez, and J. A. Pople, *Gaussian 03*, Revision B.04, Gaussian, Inc., Pittsburgh PA, 2003.

[16] M. Kataoka, A. Toyota, *J. Chem. Research (S)* **1998**, *5*, 278–279.

[17] a) D. Cremer, H. Günther, *Liebigs. Ann. Chem.* **1972**, *763*, 87–108; b) H. Günther, A. Shyoukh, D. Cremer, K. H. Frisch, *Liebigs. Ann. Chem.* **1978**, 150–164.

[18] a) R. H. Mitchell, *Chem. Rev.* **2001**, *101*, 1301–1315; b) R. H. Mitchell, R. Zhang, W. Fan, D. J. Berg, *J. Am. Chem. Soc.* **2005**, *127*, 16251–16254

Chapter III

(1) (a) Balaban, A. T.; Banciu, M.; Ciorba, V. *Annulenes, Benzo-, Hetero-, Homo-Derivatives and their Valence Isomers*; CRC Press: Boca Raton, Fla., 1987. (b) Hopf, H. *Classics in Hydrocarbon Chemistry : Syntheses, Concepts, Perspectives*; Wiley-VCH: Weinheim; New York, 2000. (c) Harvey, R. G. *Polycyclic Aromatic Hydrocarbons*; Wiley-VCH, 1997.

(2) (a) Zaumseil, J.; Sirringhaus, H. *Chem. Rev.* **2007**, *107*, 1296–1323. (b) Di, C.; Zhang, F.; Zhu, D. *Adv. Mater.* **2013**, *25*, 313–330.

(3) Schlenker, C. W.; Thompson, M. E. *Top. Curr. Chem.* **2012**, *312*, 175–212.

(4) Xiao, L.; Chen, Z.; Qu, B.; Luo, J.; Kong, S.; Gong, Q.; Kido, J. *Adv. Mater.* **2011**, *23*, 926–952.

(5) *Introduction to Organic Electronic and Optoelectronic Materials and Devices*; Sun, S.-S.; Dalton, L. R., Eds.; CRC Press, 2008.

(6) Fix, A. G.; Chase, D. T.; Haley, M. M. *Top. Curr. Chem.* **2012**, DOI: 10.1007/128_2012_376.

(7) (a) Chase, D. T.; Fix, A. G.; Rose, B. D.; Weber, C. D.; Nobusue, S.; Stockwell, C. E.; Zakharov, L. N.; Lonergan, M. C.; Haley, M. M. *Angew. Chem. Int. Ed.* **2011**, *50*, 11103–11106. (b) Chase, D. T.; Fix, A. G.; Kang, S. J.; Rose, B. D.; Weber, C. D.; Zhong, Y.; Zakharov, L. N.; Lonergan, M. C.; Nuckolls, C.; Haley, M. M. *J. Am. Chem. Soc.* **2012**, *134*, 10349–10352.

(8) Rose, B. D., Sumner, N. J.; Filatov, A. S.; Peters, S. J.; Zakharov, L. N.; Petrukhina, M. A.; Haley, M. M., *J. Am. Chem. Soc.* **2014**, *136*, accepted.

(9) Nishida, J.; Tsukaguchi, S.; Yamashita, Y. *Chem. – Eur. J.* **2012**, *18*, 8964–8970.

(10) Miyata, Y.; Minari, T.; Nemoto, T.; Isoda, S.; Komatsu, K. *Org. Biomol. Chem.* **2007**, *5*, 2592–2598.

(11) Nakagawa, T.; Kumaki, D.; Nishida, J.; Tokito, S.; Yamashita, Y. *Chem. Mater.* **2008**, *20*, 2615–2617.

(12) Usta, H.; Risko, C.; Wang, Z.; Huang, H.; Deliomeroglu, M. K.; Zhukhovitskiy, A.; Facchetti, A.; Marks, T. J. *J. Am. Chem. Soc.* **2009**, *131*, 5586–5608.

(13) Anthony, J. E. *Angew. Chem. Int. Ed.* **2008**, *47*, 452–483.

(14) (a) Anthony, J. E.; Brooks, J. S.; Eaton, D. L.; Parkin, S. R. *J. Am. Chem. Soc.* **2001**, *123*, 9482–9483. (b) Coropceanu, V.; Li, Y.; Yi, Y.; Zhu, L.; Bredas, J.-L. *MRS Bull.* **2013**, *38*, 57–71.

(15) Rose, B. D.; Chase, D. T.; Weber, C. D.; Zakharov, L. N.; Lonergan, M. C.; Haley, M. M. *Org. Lett.* **2011**, *13*, 2106–2109.

(16) Zhou, Q.; Carroll, P. J.; Swager, T. M. *J. Org. Chem.* **1994**, *59*, 1294–1301.

(17) Rahman, M. A.; Shito, F.; Kitamura, T. *Synthesis* **2010**, 27–29.

(18) Reiss, H.; Heller, A. *J. Phys. Chem.* **1985**, *89*, 4207–4213.

(19) Frisch, M. J.; Trucks, G. W.; Schlegel, H. B.; Scuseria, G. E.; Robb, M. A.; Cheeseman, J. R.; Scalmani, G.; Barone, V.; Mennucci, B.; Petersson, G. A.; Nakatsuji, H.; Caricato, M.; Li, X.; Hratchian, H. P.; Izmaylov, A. F.; Bloino, J.; Zheng, G.; Sonnenberg, J. L.; Hada, M.; Ehara, M.; Toyota, K.; Fukuda, R.; Hasegawa, J.; Ishida, M.; Nakajima, T.; Honda, Y.; Kitao, O.; Nakai, H.; Vreven, T.; Montgomery, Jr., J. A.; Peralta, J. E.; Ogliaro, F.; Bearpark, M.; Heyd, J. J.; Brothers, E.; Kudin, K. N.; Staroverov, V. N.; Kobayashi, R.; Normand, J.; Raghavachari, K.; Rendell, A.; Burant, J. C.; Iyengar, S. S.; Tomasi, J.; Cossi, M.; Rega, N.; Millam, N. J.; Klene, M.; Knox, J. E.; Cross, J. B.; Bakken, V.; Adamo, C.; Jaramillo, J.; Gomperts, R.; Stratmann, R. E.; Yazyev, O.; Austin, A. J.; Cammi, R.; Pomelli, C.; Ochterski, J. W.; Martin, R. L.; Morokuma, K.; Zakrzewski, V. G.; Voth, G. A.; Salvador, P.; Dannenberg, J. J.; Dapprich, S.; Daniels, A. D.; Farkas, Ö.; Foresman, J. B.; Ortiz, J. V.; Cioslowski, J.; Fox, D. J. *Gaussian 09*; 2010.

(20) Yoshihara, K.; Kearns, D. R. *J. Chem. Phys.* **1966**, *45*, 1991–1999.

(21) Dilling, W. L. *J. Org. Chem.* **1966**, *31*, 1045–1050.

(22) Dennington, R.; Keith, T.; Millam, J. *GaussView*; Semichem Inc.: Shawnee Mission KS, 2009.

(23) Cordero, B.; Gomez, V.; Platero-Prats, A. E.; Reves, M.; Echeverria, J.; Cremades, E.; Barragan, F.; Alvarez, S. *Dalton Trans.* **2008**, 2832–2838.

Chapter IV


(1) Harvey, R. G. *Polycyclic Aromatic Hydrocarbons*; Wiley-VCH, Weinheim, Germany, 1997.

(2) *Introduction to Organic Electronic and Optoelectronic Materials and Devices*; Sun, S.-S.; Dalton, L. R., Eds.; CRC Press, 2008.

(3) Anthony, J. E. *Angew. Chem. Int. Ed.* **2008**, *47*, 452–483.

(4) Seyler, H.; Purushothaman, B.; Jones, D. J.; Holmes, A. B.; Wong, W. W. H. *Pure Appl. Chem.* **2012**, *84*, 1047–1067.

(5) Bunz, U. H. F.; Engelhart, J. U.; Lindner, B. D.; Schaffroth, M. *Angew. Chem. Int. Ed.* **2013**, *52*, 3810–3821.

(6) Niimi, K.; Shinamura, S.; Osaka, I.; Miyazaki, E.; Takimiya, K. *J. Am. Chem. Soc.* **2011**, *133*, 8732–8739.

(7) Kawase, T.; Fujiwara, T.; Kitamura, C.; Konishi, A.; Hirao, Y.; Matsumoto, K.; Kurata, H.; Kubo, T.; Shinamura, S.; Mori, H.; Miyazaki, E.; Takimiya, K. *Angew. Chem. Int. Ed.* **2010**, *49*, 7728–7732.

(8) Fix, A. G.; Chase, D. T.; Haley, M. M. *Top. Curr. Chem.* **2012** (DOI: 10.1007/128_2012_376).

(9) Zhou, Q.; Carroll, P. J.; Swager, T. M. *J. Org. Chem.* **1994**, *59*, 1294–1301.

(10) Reisch, H.; Wiesler, U.; Scherf, U.; Tuytuylkov, N. *Macromolecules* **1996**, *29*, 8204–8210.

(11) Hafner, K.; Stowasser, B.; Krimmer, H.-P.; Fischer, S.; Böhm, M. C.; Lindner, H. J. *Angew. Chem. Int. Ed.* **1986**, *25*, 630–632.

(12) Chase, D. T.; Rose, B. D.; McClintock, S. P.; Zakharov, L. N.; Haley, M. M. *Angew. Chem. Int. Ed.* **2011**, *50*, 1127–1130.

(13) Chase, D. T.; Fix, A. G.; Rose, B. D.; Weber, C. D.; Nobusue, S.; Stockwell, C. E.; Zakharov, L. N.; Lonergan, M. C.; Haley, M. M. *Angew. Chem. Int. Ed.* **2011**, *50*, 11103–11106.

(14) Kendrick, M. J.; Neunzert, A.; Payne, M. M.; Purushothaman, B.; Rose, B. D.; Anthony, J. E.; Haley, M. M.; Ostroverkhova, O. *J. Phys. Chem. C* **2012**, *116*, 18108–18116.

(15) Chase, D. T.; Fix, A. G.; Kang, S. J.; Rose, B. D.; Weber, C. D.; Zhong, Y.; Zakharov, L. N.; Lonergan, M. C.; Nuckolls, C.; Haley, M. M. *J. Am. Chem. Soc.* **2012**, *134*, 10349–10352.

(16) Nishida, J.; Tsukaguchi, S.; Yamashita, Y. *Chem. Eur. J.* **2012**, *18*, 8964–8970.

(17) Bachmann, R.; Gerson, F.; Gescheidt, G.; Hafner, K. *Magn. Reson. Chem.* **1995**, *33*, S60–S65.

(18) Cary, D. R.; Green, J. C.; O'Hare, D. *Angew. Chem., Int. Ed. Engl.* **1997**, *36*, 2618–2620.

(19) Coropceanu, V.; Cornil, J.; Da, S. F.; Olivier, Y.; Silbey, R.; Bredas, J.-L. *Chem. Rev.* **2007**, *107*, 926–952.

(20) Hachmann, J.; Olivares-Amaya, R.; Atahan-Evrenk, S.; Amador-Bedolla, C.; Sanchez-Carrera, R. S.; Gold-Parker, A.; Vogt, L.; Brockway, A. M.; Aspuru-Guzik, A. *J. Phys. Chem. Lett.* **2011**, *2*, 2241–2251.

(21) Cramer, C. J. In *Essentials of Computational Chemistry: Theories and Models*; John Wiley & Sons Ltd: Chichester, UK, 2002; pp. 249–303.

(22) Staroverov, V. N.; Scuseria, G. E.; Tao, J.; Perdew, J. P. *J. Chem. Phys.* **2003**, *119*, 12129–12137.

(23) Schreckenbach, G.; Ziegler, T. *Theor. Chem. Acc.* **1998**, *99*, 71–82.

(24) Helgaker, T.; Jaszunski, M.; Ruud, K. *Chem. Rev.* **1999**, *99*, 293–352.

(25) Filatov, A. S.; Zabula, A. V.; Spisak, S. N.; Rogachev, A. Yu.; Petrukhina, M. A. *Angew. Chem. Int. Ed.* **2014**, *53*, 140–145.

(26) Hermosilla, L.; Calle, P.; Garcia, de la V.; Sieiro, C. *J. Phys. Chem. A* **2005**, *109*, 1114–1124.

(27) Barone, V.; Crescenzi, O.; Improta, R. *Quant. Struct.-Act. Relat.* **2002**, *21*, 105–118.

(28) Jacquemin, D.; Wathelet, V.; Perpete, E. A.; Adamo, C. *J. Chem. Theory Comput.* **2009**, *5*, 2420–2435.

(29) Adamo, C.; Jacquemin, D. *Chem. Soc. Rev.* **2013**, *42*, 845–856.

(30) Coulson, C. A. *Tetrahedron* **1961**, *12*, 193–195.

(31) Marcel Swart's Website. *DFT2012*. http://www.marcelswart.eu/ (accessed April 7, 2014)

(32) Becke, A. D. *Phys. Rev. A: Gen. Phys.* **1988**, *38*, 3098–3100.

(33) Perdew, J. P. *Phys. Rev. B* **1986**, *33*, 8822–8824.

(34) Perdew, J. P.; Burke, K.; Ernzerhof, M. *Phys. Rev. Lett.* **1996**, *77*, 3865–3868.

(35) Perdew, J. P.; Chevary, J. A.; Vosko, S. H.; Jackson, K. A.; Pederson, M. R.; Singh, D. J.; Fiolhais, C. *Phys. Rev. B: Condens. Matter* **1992**, *46*, 6671–6687.

(36) Becke, A. D. *J. Chem. Phys.* **1993**, *98*, 1372–1377.

(37) Becke, A. D. *J. Chem. Phys.* **1993**, *98*, 5648–5652.

(38) Stephens, P. J.; Devlin, F. J.; Chabalowski, C. F.; Frisch, M. J. *J. Chem. Phys.* **1994**, *98*, 11623–11627.

(39) Heyd, J.; Scuseria, G. E.; Ernzerhof, M. *J. Chem. Phys.* **2003**, *118*, 8207–8215.

(40) Paier, J.; Marsman, M.; Hummer, K.; Kresse, G.; Gerber, I. C.; Angyan, J. G. *J. Chem. Phys.* **2006**, *125*, 249901/1–249901/2.

(41) Heyd, J.; Scuseria, G. E.; Ernzerhof, M. *J. Chem. Phys.* **2006**, *124*, 219906/1.

(42) Perdew, J. P.; Ernzerhof, M.; Burke, K. *J. Chem. Phys.* **1996**, *105*, 9982–9985.

(43) Ernzerhof, M.; Scuseria, G. E. *J. Chem. Phys.* **1999**, *110*, 5029–5036.

(44) Adamo, C.; Barone, V. *J. Chem. Phys.* **1999**, *110*, 6158–6170.

(45) Adamo, C.; Barone, V. *J. Chem. Phys.* **1998**, *108*, 664–675.

(46) Zhao, Y.; Truhlar, D. G. *Theor. Chem. Acc.* **2008**, *120*, 215–241.

(47) Zhao, Y.; Truhlar, D. G. *J. Chem. Phys.* **2006**, *125*, 194101/1–194101/18.

(48) Zhao, Y.; Schultz, N. E.; Truhlar, D. G. *J. Chem. Phys.* **2005**, *123*, 161103/1–161103/4.

(49) Zhao, Y.; Schultz, N. E.; Truhlar, D. G. *J. Chem. Theory Comput.* **2006**, *2*, 364–382.

(50) Boese, A. D.; Handy, N. C. *J. Chem. Phys.* **2002**, *116*, 9559–9569.

(51) Grimme, S. *J. Comput. Chem.* **2006**, *27*, 1787–1799.

(52) Chai, J.-D.; Head-Gordon, M. *J. Chem. Phys.* **2008**, *128*, 084106/1–084106/15.

(53) Chai, J.-D.; Head-Gordon, M. *Phys. Chem. Chem. Phys.* **2008**, *10*, 6615–6620.

(54) Vydrov, O. A.; Scuseria, G. E. *J. Chem. Phys.* **2006**, *125*, 234109/1–234109/9.

(55) Vydrov, O. A.; Heyd, J.; Krukau, A. V.; Scuseria, G. E. *J. Chem. Phys.* **2006**, *125*, 074106/1–074106/9.

(56) Vydrov, O. A.; Scuseria, G. E.; Perdew, J. P. *J. Chem. Phys.* **2007**, *126*, 154109/1–154109/9.

(57) Yanai, T.; Tew, D. P.; Handy, N. C. *Chem. Phys. Lett.* **2004**, *393*, 51–57.

(58) Frisch, M. J.; Trucks, G. W.; Schlegel, H. B.; Scuseria, G. E.; Robb, M. A.; Cheeseman, J. R.; Scalmani, G.; Barone, V.; Mennucci, B.; Petersson, G. A.; Nakatsuji, H.; Caricato, M.; Li, X.; Hratchian, H. P.; Izmaylov, A. F.; Bloino, J.; Zheng, G.; Sonnenberg, J. L.; Hada, M.; Ehara, M.; Toyota, K.; Fukuda, R.; Hasegawa, J.; Ishida, M.; Nakajima, T.; Honda, Y.; Kitao, O.; Nakai, H.; Vreven, T.; Montgomery, Jr., J. A.; Peralta, J. E.; Ogliaro, F.; Bearpark, M.; Heyd, J. J.; Brothers, E.; Kudin, K. N.; Staroverov, V. N.; Kobayashi, R.; Normand, J.; Raghavachari, K.; Rendell, A.; Burant, J. C.; Iyengar, S. S.; Tomasi, J.; Cossi, M.; Rega, N.; Millam, N. J.; Klene, M.; Knox, J. E.; Cross, J. B.; Bakken, V.; Adamo, C.; Jaramillo, J.; Gomperts, R.; Stratmann, R. E.; Yazyev, O.; Austin, A. J.; Cammi, R.; Pomelli, C.; Ochterski, J. W.; Martin, R. L.; Morokuma, K.; Zakrzewski, V. G.; Voth, G. A.; Salvador, P.; Dannenberg, J. J.; Dapprich, S.; Daniels, A. D.; Farkas, Ö.; Foresman, J. B.; Ortiz, J. V.; Cioslowski, J.; Fox, D. J. *Gaussian 09*; 2010.

(59) Rose, B. D.; Chase, D. T.; Weber, C. D.; Zakharov, L. N.; Lonergan, M. C.; Haley, M. M. *Org. Lett.* **2011**, *13*, 2106–2109.

(60) Rose, B. D.; Zakharov, L. N.; Haley, M. M. *Acta Crystallogr., Sect. E: Struct. Rep. Online* **2013**, *69*, o890.

(61) Zabula, A. V.; Sumner, N. J.; Filatov, A. S.; Spisak, S. N.; Grigoryants, V. M.; Petrukhina, M. A. *Eur. J. Inorg. Chem*. **2012**, 4675–4683.

(62) Spisak, S. N.; Sumner, N. J.; Zabula, A. V.; Filatov, A. S.; Rogachev, A. Yu.; Petrukhina, M. A. *Organometallics* **2013**, *32*, 3773–3779.

(63) Zabula, A. V.; Spisak, S. N.; Filatov, A. S.; Grigoryants, V. M.; Petrukhina, M. A. *Chem. Eur. J.* **2012**, *18*, 6476–6484.

(64) Green, J. R.; Dunbar, R. C. *J. Phys. Chem. A* **2011**, *115*, 4968–4975.

(65) Rellan-Pineiro, M.; Rodriguez-Otero, J.; Cabaleiro-Lago, E. M.; Josa, D. *J. Mol. Modeling* **2013**, *19*, 2049–2055.

(66) Hassan, A.; Dinadayalane, T C.; Grabowski, S. J.; Leszczynski, J. *Phys. Chem Chem. Phys.* **2013**, *15*, 20839–20856.

(67) Spisak, S. N.; Zabula, A. V.; Filatov, A. S.; Rogachev, A. Yu.; Petrukhina, M. A. *Angew. Chem. Int. Ed.* **2011**, *50*, 8090–8094.

(68) Dunitz, J. D.; Kruger, C.; Irngartinger, H.; Wang, M.; Nixdorf, M. *Angew. Chem. Int. Ed.* **1988**, *27*, 387–389.

(69) Stoll, S.; Schweiger, A. *J. Magn. Reson.* **2006**, *178*, 42–55.

(70) *MATLAB*; The MathWorks, Inc.

(71) Barone, V. In *Recent Advances in Density Functional Methods*; Chong, D., Ed.; World Scientific: Singapore; pp. 287–334.

(72) Liu, T.; Troisi, A. *Adv. Mater.* **2013**, *25*, 1038–1041.

(73) Klessinger, M.; Michl, J. In *Excited States and Photochemistry of Organic Molecules*; VCH: New York, 1995; pp. 34–36.

(74) Charaf-Eddin, A.; Planchat, A.; Mennucci, B.; Adamo, C.; Jacquemin, D. *J. Chem. Theory Comput.* **2013**, *9*, 2749–2760.

Chapter V

(1) *Introduction to Organic Electronic and Optoelectronic Materials and Devices*; Sun, S.-S.; Dalton, L. R., Eds.; CRC Press, 2008.

(2) Forrest, S. R. *Nature* **2004**, *428*, 911–918.

(3) Wang, E.; Mammo, W.; Andersson, M. R. *Adv. Mater.* **2014**, *26*, 1801–1826.

(4) Dimitrakopoulos, C. D.; Malenfant, P. R. L. *Adv. Mater.* **2002**, *14*, 99–117.

(5) Bendikov, M.; Wudl, F.; Perepichka, D. F. *Chem. Rev.* **2004**, *104*, 4891–4945.

(6) Huang, J.; Su, J.-H.; Tian, H. *J. Mater. Chem.* **2012**, *22*, 10977–10989.

(7) Chen, D.; Zhou, H.; Li, X.; Liu, M.; Ye, H.; Su, S.-J.; Cao, Y. *Org. Electron.* **2014**, *15*, 1197–1204.

(8) Karak, S.; Reddy, V. S.; Ray, S. K.; Dhar, A. *Org. Electron.* **2009**, *10*, 1006–1010.

(9) Heeney, M.; Bailey, C.; Giles, M.; Shkunov, M.; Sparrowe, D.; Tierney, S.; Zhang, W.; McCulloch, I. *Macromolecules* **2004**, *37*, 5250–5256.

(10) Rose, B. D.; Vonnegut, C. L.; Zakharov, L. N.; Haley, M. M. *Org. Lett.* **2012**, *14*, 2426–2429.

(11) Fix, A. G.; Deal, P. E.; Vonnegut, C. L.; Rose, B. D.; Zakharov, L. N.; Haley, M. M. *Org. Lett.* **2013**, *15*, 1362–1365.

(12) Chase, D. T.; Fix, A. G.; Kang, S. J.; Rose, B. D.; Weber, C. D.; Zhong, Y.; Zakharov, L. N.; Lonergan, M. C.; Nuckolls, C.; Haley, M. M. *J. Am. Chem. Soc.* **2012**, *134*, 10349–10352.

(13) Chase, D. T.; Fix, A. G.; Rose, B. D.; Weber, C. D.; Nobusue, S.; Stockwell, C. E.; Zakharov, L. N.; Lonergan, M. C.; Haley, M. M. *Angew. Chem. Int. Ed.* **2011**, *50*, 11103–11106.

(14) Shimizu, A.; Tobe, Y. *Angew. Chem. Int. Ed.* **2011**, *50*, 6906–6910.

(15) Kendrick, M. J.; Neunzert, A.; Payne, M. M.; Purushothaman, B.; Rose, B. D.; Anthony, J. E.; Haley, M. M.; Ostroverkhova, O. *J. Phys. Chem. C* **2012**, *116*, 18108–18116.

(16) Nishida, J.; Tsukaguchi, S.; Yamashita, Y. *Chem. Eur. J.* **2012**, *18*, 8964–8970.

(17) Ito, S.; Minami, T.; Nakano, M. *J. Phys. Chem. C* **2012**, *116*, 19729–19736.

(18) Eaton, S. W.; Shoer, L. E.; Karlen, S. D.; Dyar, S. M.; Margulies, E. A.; Veldkamp, B. S.; Ramanan, C.; Hartzler, D. A.; Savikhin, S.; Marks, T. J.; Wasielewski, M. R. *J. Am. Chem. Soc.* **2013**, *135*, 14701–14712.

(19) Hanna, M. C.; Nozik, A. J. *J. Appl. Phys.* **2006**, *100*, 074510/1–074510/8.

(20) Bearpark, M. J.; Celani, P.; Jolibois, F.; Olivucci, M.; Robb, M. A.; Bernardi, F. *Mol. Phys.* **1999**, *96*, 645–652.

(21) Pigliucci, A.; Duvanel, G.; Daku, L. M. L.; Vauthey, E. *J. Phys. Chem. A* **2007**, *111*, 6135–6145.

(22) Schwarzer, D.; Hanisch, C.; Kutne, P.; Troe, J. *J. Phys. Chem. A* **2002**, *106*, 8019–8028.

(23) Elsaesser, T.; Kaiser, W. *Annu. Rev. Phys. Chem.* **1991**, *42*, 83–107.

(24) Klann, R.; Bäuerle, R. J.; Laermer, F.; Elsaesser, T.; Niemeyer, M.; Lüttke, W. *Chem. Phys. Lett.* **1990**, *169*, 172–178.

(25) Gellini, C.; Salvi, P. R.; Hafner, K. *J. Phys. Chem.* **1993**, *97*, 8152–8157.

(26) Gellini, C.; Angeloni, L.; Salvi, P. R.; Marconi, G. *J. Phys. Chem.* **1995**, *99*, 85–93.

(27) Turro, N.; Ramamurthy, V.; Scaiano, J. *Modern Molecular Photochemistry of Organic Molecules*; University Science Books, 2010.

(28) Schmidt, M. W.; Baldridge, K. K.; Boatz, J. A.; Elbert, S. T.; Gordon, M. S.; Jensen, J. H.; Koseki, S.; Matsunaga, N.; Nguyen, K. A.; et, al. *J. Comput. Chem.* **1993**, *14*, 1347–1363.

(29) Dunning, T. H., Jr. *J. Chem. Phys.* **1989**, *90*, 1007–1023.

(30) Krishnan, R.; Binkley, J. S.; Seeger, R.; Pople, J. A. *J. Chem. Phys.* **1980**, *72*, 650–654.

(31) Yanai, T.; Tew, D. P.; Handy, N. C. *Chem. Phys. Lett.* **2004**, *393*, 51–57.

(32) Tawada, Y.; Tsuneda, T.; Yanagisawa, S.; Yanai, T.; Hirao, K. *J. Chem. Phys.* **2004**, *120*, 8425–8433.

## Chapter VI

(1) (a) Balaban, A. T.; Banciu, M.; Ciorba, V. *Annulenes, Benzo-, Hetero-, Homo-Derivatives and their Valence Isomers*; CRC Press: Boca Raton, FL., 1987. (b) Hopf, H. *Classics in Hydrocarbon Chemistry: Syntheses, Concepts, Perspectives*; Wiley-VCH: Weinheim, 2000.

(2) (a) Müeller, T. J. J.; Bunz, U. H. F. *Functional Organic Materials: Syntheses, Strategies and Applications*; Wiley-VCH: Weinheim, 2007. (b) Müllen, K.; Scherf, U. *Organic Light Emitting Devices: Synthesis, Properties and Applications*; Wiley-VCH: Weinheim, 2006. (c) Haley, M. M.; Tykwinski, R. R. *Carbon-Rich Compounds: From Molecules to Materials*; Wiley-VCH: Weinheim, 2006.

(3) Anthony, J. E. *Chem. Rev*. **2006**, *106*, 5028–5048.

(4) Shimizu, A.; Tobe, Y. *Angew. Chem., Int. Ed.* **2011**, *50*, 6906–6910.

(5) (a) Chase, D. T.; Rose, B. D.; McClintock, S. P.; Zakharov, L. N.; Haley, M. M. *Angew. Chem., Int. Ed.* **2011**, *50*, 1127–1130. (b) Chase, D. T.; Fix, A. G.; Rose, B. D.; Weber, C. D.; Nobusue, S.; Stockwell, C. E.; Zakharov, L. N.; Lonergan, M. C.; Haley, M. M. *Angew. Chem., Int. Ed.* **2011**, *50*, 11103–11106. (c) Chase, D. T.; Fix, A. G.; Kang, S. J.; Rose, B. D.; Weber, C. D.; Zhong, Y.; Zakharov, L. N.; Lonergan, M. C.; Nuckolls, C.; Haley, M. M., submitted.

(6) Anthony, J. E.; Facchetti, A.; Heeney, M.; Marder, S. R.; Zhan, X. *Adv. Mater.* **2010**, *22*, 3876–3892.

(7) Cramer, C. J. *Essentials of Computational Chemistry: Theories and Models*; John Wiley & Sons Ltd: Chichester, UK, 2002; pp 335–338.

(8) (a) Becke, A. D. *J. Chem. Phys.* **1993**, *98*, 5648–5652. (b) Lee, C.; Yang, W.; Parr, R. G. *Phys. Rev. B: Condens. Matter* **1988**, *37*, 785–789. (c) Stephens, P. J.; Devlin, F. J.; Chabalowski, C. F.; Frisch, M. J. *J. Phys. Chem.* **1994**, *98*, 11623–11627.

(9) M. J. Frisch, G. W. Trucks, H. B. Schlegel, G. E. Scuseria, M. A. Robb, J. R. Cheeseman, J. A. Montgomery, Jr., T. Vreven, K. N. Kudin, J. C. Burant, J. M. Millam, S. S. Iyengar, J. Tomasi, V. Barone, B. Mennucci, M. Cossi, G. Scalmani, N. Rega, G. A. Petersson, H. Nakatsuji, M. Hada, M. Ehara, K. Toyota, R. Fukuda, J. Hasegawa, M. Ishida, T. Nakajima, Y. Honda, O. Kitao, H. Nakai, M. Klene, X. Li, J. E. Knox, H. P. Hratchian, J. B. Cross, C. Adamo, J. Jaramillo, R. Gomperts, R. E. Stratmann, O. Yazyev, A. J. Austin, R. Cammi, C. Pomelli, J. W. Ochterski, P. Y. Ayala, K. Morokuma, G. A. Voth, P. Salvador, J. J. Dannenberg, V. G. Zakrzewski, S. Dapprich, A. D. Daniels, M. C. Strain, O. Farkas, D. K. Malick, A. D. Rabuck, K. Raghavachari, J. B. Foresman, J. V. Ortiz, Q. Cui, A. G. Baboul, S. Clifford, J. Cioslowski, B. B. Stefanov, G. Liu, A. Liashenko, P. Piskorz, I. Komaromi, R. L. Martin, D. J. Fox, T. Keith, M. A. Al-Laham, C. Y. Peng, A. Nanayakkara, M. Challacombe, P. M. W. Gill, B. Johnson, W. Chen, M. W. Wong, C. Gonzalez, and J. A. Pople, *Gaussian 03*, Revision B.04, Gaussian, Inc., Pittsburgh PA, 2003.

(10) Pedley, J. B.; Naylor, R. D.; Kirby, S. P. *Thermochemical Data of Organic Compounds*, 2nd Ed; Chapman and Hall: New York, 1986.

(11) Fallah-Bagher-Shaidaei, H.; Wannere, C. S.; Corminboeuf, C.; Puchta, R.; Schleyer, P. v R. *Org. Lett.* **2006**, *8*, 863–866.

(12) (a) Kubo, T.; Shimizu, A.; Uruichi, M.; Yakushi, K.; Nakano, M.; Shiomi, D.; Sato, K.; Takui, T.; Morita, Y.; Nakasuji, K. *Org. Lett.* **2007**, *9*, 81–84. (b) Sun, Z.; Huang, K.-W.; Wu, J. *J. Am. Chem. Soc.* **2011**, *133*, 11896–11899. (c) Purushothaman, B.; Bruzek, M.; Parkin, S. R.; Miller, A.-F.; Anthony, J. E. *Angew. Chem., Int. Ed.* **2011**, *50*, 7013–7017.

(13) (a) Gao, X.; Hodgson, J. L.; Jiang, D.; Zhang, S. B.; Nagase, S.; Miller, G. P.; Chen, Z. *Org. Lett.* **2011**, *13*, 3316–3319. (b) Takano, Y.; Taniguchi, T.; Isobe, H.; Kubo, T.; Morita, Y.; Yamamoto, K.; Nakasuji, K.; Takui, T.; Yamaguchi, K. *J. Am. Chem. Soc.* **2002**, *124*, 11122–11130.

(14) Wittig, G.; Wiemer, W. *Liebigs Ann. Chem.* **1930**, *483*, 144–156.

(15) Brauer, H. D.; Reinsch, E. A. *Ber. Bunsenges. Phys. Chem.* **1973**, *77*, 348–353.

(16) Preis, E.; Scherf, U. *Macromol. Rapid Commun.* **2006**, *27*, 1105–1109.

(17) Connelly, N. G.; Geiger, W. E. *Chem. Rev.* **1996**, *96*, 877–910.

(18) Reiss, H.; Heller, A. *J. Phys. Chem.* **1985**, *89*, 4207-4213.

(19) Sanz, F.; Daly, J. J. *J. Chem. Soc., Perkin Trans. 2* **1975**, 1141–1145.

## Appendix A

[1] Q. Zhou, P. J. Carroll, T. M. Swager, *J. Org. Chem.* **1994**, *59*, 1294-1301.

[2] M. J. Frisch, G. W. Trucks, H. B. Schlegel, G. E. Scuseria, M. A. Robb, J. R. Cheeseman, J. A. Montgomery, Jr., T. Vreven, K. N. Kudin, J. C. Burant, J. M. Millam, S. S. Iyengar, J. Tomasi, V. Barone, B. Mennucci, M. Cossi, G. Scalmani, N. Rega, G. A. Petersson, H. Nakatsuji, M. Hada, M. Ehara, K. Toyota, R. Fukuda, J. Hasegawa, M. Ishida, T. Nakajima, Y. Honda, O. Kitao, H. Nakai, M. Klene, X. Li, J. E. Knox, H. P. Hratchian, J. B. Cross, C. Adamo, J. Jaramillo, R. Gomperts, R. E. Stratmann, O. Yazyev, A. J. Austin, R. Cammi, C. Pomelli, J. W. Ochterski, P. Y. Ayala, K. Morokuma, G. A. Voth, P. Salvador, J. J. Dannenberg, V. G. Zakrzewski, S. Dapprich, A. D. Daniels, M. C. Strain, O. Farkas, D. K. Malick, A. D. Rabuck, K. Raghavachari, J. B. Foresman, J. V. Ortiz, Q. Cui, A. G. Baboul, S. Clifford, J. Cioslowski, B. B. Stefanov, G. Liu, A. Liashenko, P. Piskorz, I. Komaromi, R. L. Martin, D. J. Fox, T. Keith, M. A. Al-Laham, C. Y. Peng, A. Nanayakkara, M. Challacombe, P. M. W. Gill, B. Johnson, W. Chen, M. W. Wong, C. Gonzalez, and J. A. Pople, *Gaussian 03*, Revision B.04, Gaussian, Inc., Pittsburgh PA, 2003.

## Appendix B

(1) Zhou, Q.; Carroll, P. J.; Swager, T. M. *J. Org. Chem.* **1994**, *59*, 1294–1301.

(2) Lehnherr, D.; Murray, A. H.; McDonald, R.; Tykwinski, R. R. *Angew. Chem. Int. Ed.* **2010**, *9999*, NA.

(3) Anthony, J. E.; Eaton, D. L.; Parkin, S. R. *Org. Lett.* **2002**, *4*, 15–18.

(4) Reiss, H.; Heller, A. *J. Phys. Chem.* **1985**, *89*, 4207–13.

(5) Frisch, M. J.; Trucks, G. W.; Schlegel, H. B.; Scuseria, G. E.; Robb, M. A.; Cheeseman, J. R.; Scalmani, G.; Barone, V.; Mennucci, B.; Petersson, G. A.; Nakatsuji, H.; Caricato, M.; Li, X.; Hratchian, H. P.; Izmaylov, A. F.; Bloino, J.; Zheng, G.; Sonnenberg, J. L.; Hada, M.; Ehara, M.; Toyota, K.; Fukuda, R.; Hasegawa, J.; Ishida, M.; Nakajima, T.; Honda, Y.; Kitao, O.; Nakai, H.; Vreven, T.; Montgomery, Jr., J. A.; Peralta, J. E.; Ogliaro, F.; Bearpark, M.; Heyd, J. J.; Brothers, E.; Kudin, K. N.; Staroverov, V. N.; Kobayashi, R.; Normand, J.; Raghavachari, K.; Rendell, A.; Burant, J. C.; Iyengar, S. S.; Tomasi, J.; Cossi, M.; Rega, N.; Millam, N. J.; Klene, M.; Knox, J. E.; Cross, J. B.; Bakken, V.; Adamo, C.; Jaramillo, J.; Gomperts, R.; Stratmann, R. E.; Yazyev, O.; Austin, A. J.; Cammi, R.; Pomelli, C.; Ochterski, J. W.; Martin, R. L.; Morokuma, K.; Zakrzewski, V. G.; Voth, G. A.; Salvador, P.; Dannenberg, J. J.; Dapprich, S.; Daniels, A. D.; Farkas, Ö.; Foresman, J. B.; Ortiz, J. V.; Cioslowski, J.; Fox, D. J. *Gaussian 09*; 2010.

(6) Dennington, R.; Keith, T.; Millam, J. *GaussView*; Semichem Inc.: Shawnee Mission KS, 2009.

(7) Becke, A. D. *J. Chem. Phys.* **1993**, *98*, 5648–5652.

(8) Lee, C.; Yang, W.; Parr, R. G. *Phys Rev B Condens Matter* **1988**, *37*, 785–789.

(9) Stephens, P. J.; Devlin, F. J.; Chabalowski, C. F.; Frisch, M. J. *J. Phys. Chem.* **1994**, *98*, 11623–11627.

Appendix C

(1) Chase, D. T.; Fix, A. G.; Rose, B. D.; Weber, C. D.; Nobusue, S.; Stockwell, C. E.; Zakharov, L. N.; Lonergan, M. C.; Haley, M. M. *Angew. Chem. Int. Ed.* **2011**, *50*, 11103–11106.

(2) Rose, B. D.; Vonnegut, C. L.; Zakharov, L. N.; Haley, M. M. *Org. Lett.* **2012**, *14*, 2426–2429.

(3) Fix, A. G.; Deal, P. E.; Vonnegut, C. L.; Rose, B. D.; Zakharov, L. N.; Haley, M. M. *Org. Lett.* **2013**, *15*, 1362–1365.

(4) Kelley, R. F.; Goldsmith, R. H.; Wasielewski, M. R. *J. Am. Chem. Soc.* **2007**, *129*, 6384–6385.

(5) Bullock, J. E.; Vagnini, M. T.; Ramanan, C.; Co, D. T.; Wilson, T. M.; Dicke, J. W.; Marks, T. J.; Wasielewski, M. R. *J. Phys. Chem. B* **2010**, *114*, 1794–1802.

(6) Lukas, A. S.; Miller, S. E.; Wasielewski, M. R. *J. Phys. Chem. B* **2000**, *104*, 931–940.

(7) Bode, B. M.; Gordon, M. S. *J. Mol. Graphics Modell.* **1998**, *16*, 133–138.

(8) Zhurko, G. *Chemcraft*; http://www.chemcraftprog.com.

(9) Legault, C. *CYLview*; Université de Sherbrooke: http://www.cylview.org, 2009.

Appendix E

(S1) Preis, E.; Scherf, U. *Macromol. Rapid Commun.* **2006**, *27*, 1105–1109.

(S2) Sheldrick, G. M. *Bruker/Siemens Area Detector Absorption Correction Program*, Bruker AXS, Madison, WI, 1998.

(S3) SHELXTL-6.10 "Program for Structure Solution, Refinement and Presentation" BRUKER AXS Inc., 5465 East Cheryl Parkway, Madison, WI 53711-5373 USA.

(S4) Frisch, M. J.; Trucks, G. W.; Schlegel, H. B.; Scuseria, G. E.; Robb, M. A.; Cheeseman, J. R.; Scalmani, G.; Barone, V.; Mennucci, B.; Petersson, G. A.; Nakatsuji, H.; Caricato, M.; Li, X.; Hratchian, H. P.; Izmaylov, A. F.; Bloino, J.; Zheng, G.; Sonnenberg, J. L.; Hada, M.; Ehara, M.; Toyota, K.; Fukuda, R.; Hasegawa, J.; Ishida, M.; Nakajima, T.; Honda, Y.; Kitao, O.; Nakai, H.; Vreven, T.; Montgomery, Jr., J. A.; Peralta, J. E.; Ogliaro, F.; Bearpark, M.; Heyd, J. J.; Brothers, E.; Kudin, K. N.; Staroverov, V. N.; Kobayashi, R.; Normand, J.; Raghavachari, K.; Rendell, A.; Burant, J. C.; Iyengar, S. S.; Tomasi, J.; Cossi, M.; Rega, N.; Millam, N. J.; Klene, M.; Knox, J. E.; Cross, J. B.; Bakken, V.; Adamo, C.; Jaramillo, J.; Gomperts, R.; Stratmann, R. E.; Yazyev, O.; Austin, A. J.; Cammi, R.; Pomelli, C.; Ochterski, J. W.; Martin, R. L.; Morokuma, K.; Zakrzewski, V. G.; Voth, G. A.; Salvador, P.; Dannenberg, J. J.; Dapprich, S.; Daniels, A. D.; Farkas, Ö.; Foresman, J. B.; Ortiz, J. V.; Cioslowski, J.; Fox, D. J. *Gaussian 09, Revision A.02*; 2009.

(S5) Andersson M. P.; Uvdal, P. *J. Phys. Chem. A* **2005**, *109,* 2937–2941.

(S6) (a) Gao, X.; Hodgson, J. L.; Jiang, D.; Zhang, S. B.; Nagase, S.; Miller, G. P.; Chen, Z. *Org. Lett.* **2011**, *13*, 3316–3319. (b) Takano, Y.; Taniguchi, T.; Isobe, H.; Kubo, T.; Morita, Y.; Yamamoto, K.; Nakasuji, K.; Takui, T.; Yamaguchi, K. *J. Am. Chem. Soc.* **2002**, *124*, 11122–11130.